République Algérienne Démocratique et Populaire
Ministère de l'Enseignement Supérieur et de la Recherche Scientifique

المدرسة الوطنية المتعددة التقنيات
Ecole Nationale Polytechnique

Ecole Nationale Polytechnique
Département de Génie Civil
Laboratoire de Génie Sismique
et de Dynamique des Structures

LGSDS
مخبر هندسة الزلازل و ديناميكا الهياكل
Laboratoire de Génie Sismique
et de Dynamique des Structures

Thèse de Doctorat en Sciences en Génie Civil

Option : Structures

Présentée par :

AFIF CHAOUCH KARIM

Magister en Génie Civil

Titre

ESTIMATION D'ACCELEROGRAMMES SPATIALEMENT VARIABLES SUR PROFILS DE SOLS STOCHASTIQUES : APPLICATION AU SEISME D'EL ASNAM de 1980

Présentée et soutenue publiquement le 27/04/2017 devant le jury composé de :

Président	BERRAH Mounir Khaled	Professeur	E.N.P
Directeur de thèse	TILIOUINE Boualem	Professeur	E.N.P
Co-Directeurs de thèse	HAMMOUTENE Malek	Professeur	E.N.P
	RUPAKHETY Rajesh	Professeur	U.Islande
Examinateurs	BRANCI Taïeb	Professeur	U.Chlef
	HADID Mohamed	Professeur	E.N.S.T.P
	ZENDAGUI Djawad	Professeur	U.Tlemcen

ENP 2017

République Algérienne Démocratique et Populaire
Ministère de l'Enseignement Supérieur et de la Recherche Scientifique

المدرسة الوطنية المتعددة التقنيات
Ecole Nationale Polytechnique

Ecole Nationale Polytechnique
Département de Génie Civil
Laboratoire de Génie Sismique
et de Dynamique des Structures

LGSDS
مخبر هندسة الزلازل و ديناميكا الهياكل
Laboratoire de Génie Sismique
et de Dynamique des Structures

Thèse de Doctorat en Sciences en Génie Civil

Option : Structures

Présentée par :

AFIF CHAOUCH KARIM

Magister en Génie Civil

Titre

ESTIMATION D'ACCELEROGRAMMES SPATIALEMENT VARIABLES SUR PROFILS DE SOLS STOCHASTIQUES : APPLICATION AU SEISME D'EL ASNAM de 1980

Présentée et soutenue publiquement le 27/04/2017 devant le jury composé de :

Président	BERRAH Mounir Khaled	Professeur	E.N.P
Directeur de thèse	TILIOUINE Boualem	Professeur	E.N.P
Co-Directeurs de thèse	HAMMOUTENE Malek	Professeur	E.N.P
	RUPAKHETY Rajesh	Professeur	U.Islande
Examinateurs	BRANCI Taïeb	Professeur	U.Chlef
	HADID Mohamed	Professeur	E.N.S.T.P
	ZENDAGUI Djawad	Professeur	U.Tlemcen

ENP 2017

DEDICATED TO MY PARENTS

ACKNOWLEDGMENTS

I would like to express my sincere gratitude to my supervisor, Professor Boualem TILIOUINE and my co-supervisor, Professor Malek HAMMOUTENE, at the Ecole Nationale Polytechnique for their advice, insights and suggestions, support and encouragement throughout this research.

My special thanks go also to Professor Rajesh RUPAKHETY, who was my co-supervisor at the University of Iceland, and Professor Ragnar SIGBJÖRNSSON, who facilitated my stay at the EERC and supported my research work, for their assistance during my internship, for their valuable support, guidance, and feedback on this research. I would like to express my sincerest gratitude especially to Professor Rajesh RUPAKHETY, for his invaluable supervision, constructive suggestions, patience, and kindness throughout the internship. His active guidance, being always there to help me get over the difficulties, and continuous motivation kept me engaged with my research and enabled successful completion of the doctoral studies.

I would like to thank the thesis committee members, Professors Taïeb BRANCI, Mohamed HADID and Djawad ZENDAGUI, for their in-depth review of the present doctoral thesis. I express my special gratitude to Professor Mounir Khaled BERRAH, who agreed to review the thesis and to chair the doctoral committee.

I also would like to extend my appreciation to the Ministry of Higher Education and Scientific Research of Algeria for the financial support during my stay in Iceland, and to my colleagues at the Laboratoire de Génie Sismique et de Dynamique de Structures (LGSDS, Algeria) and the Earthquake Engineering Research Center (EERC, Iceland) for their availability and helpfulness.

Finally, I am grateful to my family, for always supporting me and being my source of inspiration.

ملخص: التباين المكاني للحركات الأرضية له تأثير كبير على الاستجابة الديناميكية للهياكل الموسعة مثل الجسور و الأنفاق. عند تنفيذ التصميم الزلزالي للهياكل، التعريف المعقول للحركات الأرضية الزلزالية أمر حاسم لتحليل الاستجابة الهيكلية .على الرغم من أن عددا كبيرا من الزلازل المسجلة تم جمعها خلال العقود الماضية، ظروف الموقع اين تم تسجيل هذه الزلازل قد تكون مختلفة كثيرا عن تلك تحت الهياكل. في هذه الدراسة، طريقة دوال غرين الميدانية (EGF) لشق زلزالي ممتد، المستخدمة على نطاق واسع ، مددت لتجميع الحركات الزلزالية عبر مجموعة من المحطات الزلزالية التي تقع على صخر الأساس في منطقة مركز زلزال الاصنام 1980(شمال-غرب الجزائر). نموذج وسائطي للتجانس تمت تقديمه لصخر الأساس بناء على نتائج. وأجريت دراسة وسائطية تبحث حساسية التجانس، لمنبع الزلزال، مسار الانتشار و ظروف الموقع، اجريت باستخدام تمديد طريقة دوال غرين الهجينة (HGF). دوال التجانس المكاني الموافقة للحركات الزلزالية السطحية في موقع Sogedia بالاصنام تم حسابها باستخدام نموذج تحليلي لموقع محدد، المطور في مقاربة Zerva وHarada لموقع ترابي عشوائي الطبقات . توليد عشوائي للتسارعات في مواقع مختلفة على سطح الأرض من الموقع، متوافقة مع تقديراتنا للكثافات الطيفية للطاقة ودوال التجانس المكاني، تم تقديمها. النتائج المتحصل عليها بينت ان تأثير الشق الزلزالي الممتد يمكن أن يسبب انخفاض محسوس في التجانس على صخر الأساس في الحقل القريب. عشوائية الطبقة يمكنها تقليل بشكل محسوس، و الى حد كبير عند مسافة الفصل المتوسطة الى الكبيرة، التجانس قرب تردد رنين المواقع، حتى لظروف تربة ثابتة ذات القيم المنخفضة من نسبة التخميد. من اجل ضروف التربة هذه، عشوائية الطبقة تسيطر على تشوهات الزلزالية للأرض.
الكلمات المفتاحية: محاكاة الحركة الأرضية، دالة غرين، شق زلزالي ممتد، التجانس، تربة عشوائية.

Résumé : La variabilité spatiale des mouvements du sol a une influence notable sur la réponse dynamique des structures étendues telles que les pipelines et les ponts. Lors de la réalisation de la conception sismique des structures, la définition raisonnable des mouvements du sol de tremblement de terre est cruciale pour l'analyse de la réponse structurelle. Bien qu'un grand nombre de séismes enregistrés aient été recueillis au cours des dernières décennies, les conditions du site où ces tremblements de terre sont enregistrés peuvent être très différentes de celles des structures. Dans cette étude, la méthode des Fonctions de Green Empiriques (EGF) pour source finie, la plus utilisée, a été étendue pour synthétiser les mouvements sismiques à travers un réseau de stations localisées au substratum rocheux en champs proche du séisme de 1980 d'El-Asnam (Nord-ouest Algérie). Un modèle paramétrique de la cohérence au rocher est présenté sur la base des résultats de la simulation. Une étude paramétrique investiguant la sensibilité de la cohérence à la source sismique, trajet de propagation et les conditions de site, est réalisée en simulant l'accélération du sol pour différents scénarios en utilisant l'extension de la méthode Hybride de Fonctions de Green (HGF). Les fonctions de cohérence spatiale correspondantes des mouvements sismiques de surface sur le site Sogedia d'El-Asnam sont calculées en utilisant le modèle spécifique de site analytique développé dans l'approche de Zerva et Harada pour un site de sol aléatoire stratifié. Une génération stochastique d'accélérogrammes à divers endroits sur la surface du sol du site, compatibles avec nos estimations des densités spectrales de puissance et des fonctions spatiales de cohérence cibles, est présentée. Les résultats obtenus montrent que l'effet de la source étendue peut entraîner une perte significative de cohérence au substrat rocheux dans le champ proche. La stochasticité de la couche peut réduire de manière significative, et grandement pour la moyenne à grande distance de séparation, la cohérence des sites à proximité de la fréquence de résonance, même pour les conditions de sol ferme lorsque son taux d'amortissement est faible. Pour ces conditions de sol, la stochasticité de la couche contrôle les déformations sismiques du sol.

Mots clés: Simulation de mouvements du sol, fonction de Green, source étendue, cohérence, sol aléatoire.

Abstract: Spatial variability of ground motions has significant influence on dynamic response of extended structures such as pipelines and bridges. When carrying out seismic design of structures, reasonable definition of earthquake ground motions is crucial to structural response analysis. Although a large number of earthquakes have been recorded in the past decades, the site conditions where these earthquakes occured may be much different from those of the structures. In this study, the widely used finite-source empirical Green's function (EGF) method is extended to synthesize seismic motions across an array of stations located at bedrock in the epicentral region of the 1980 El-Asnam earthquake (North-west Algeria). A parametric model of coherency is presented for base rock based on the simulation results. A Parametric study investigating the sensitivity of coherency to seismic source, propagation path and site conditions, is conducted by using the extended hybrid Green's function method. The corresponding spatial coherency functions of surface seismic motions at the El-Asnam Sogedia site are calculated using the analytic site specific model developed in the Zerva and Harada approach for a layered, random soil site. A stochastic generation of time histories at various locations on the ground surface of the site, compatible with our estimations of the target power spectral densities and the spatial coherency functions, is presented. The obtained results show that finite-source effects can cause significant loss of coherency at bedrock in the near-field. The layer stochasticity can significantly reduce, or greatly reduce for medium to large separation distances, the coherency near the sites resonant frequency, even for firm soil conditions when its damping ratio is low. For these soil conditions, the layer stochasticity controls the seismic ground strains.

Keywords: Ground motion simulation, Green's function, finite-source, coherency, random soil.

Table of Contents

List of Tables

List of Figures

CHAPTER 1

GENERAL INTRODUCTION

General introduction:

Lifeline systems, such as gas mains, oil pipelines, bridges, and dams, that are supported on ground over large horizontal distances experience differential seismic movement of their supports during earthquakes. This differential motion of the supports results in displacement and stress distribution in the structural elements that is different from what is caused by uniform motion of all the supports. In many cases, the outcome is additional strains (or stresses) on the elements, which can result in damage to the elements of the structures (e.g., Lupoi *et al*., 2005; Walling and Abrahamson, 2007; Karmakar *et al*. 2012; Soyluk and Sicacik 2012; Shrestha *et al*. 2014). The most definite outcome that can be drawn from all past studies on the effect of spatial variations of seismic ground motions (SVGMs) on the response of lifelines is that the use of identical motions as excitations at the structures' supports will not always yield a conservative response. Indeed, in some cases, the response induced by identical motions can be grossly unconservative. Spatial variations of ground motion result from different physical processes related to the seismic source, the wave propagation path, and local site conditions. Attenuation effects result in the reduction of ground motion amplitudes with distance from the source. At a local spatial scale, for example within a few hundred meters, attenuation effects are not critical, and spatial variation is due to the physical processes such as (1) wave passage effects, which refer to the difference in arrival times of seismic waves at different locations; (2) incoherence effects, which refer to the differences in amplitudes and phases due to multiple reflections and refractions of seismic waves in inhomogeneous medium, as well as complex superposition of waves radiated from different parts of the source; and (3) local site effects, which refer to the change in amplitude and frequency content of ground motion due to local variations of soil conditions (Der Kiureghian, 1996).

When the soil medium is locally uniform, variability in amplitude and frequency content is less significant than variations in phase caused by wave passage and incoherence effects. In such situations, ground motion variability is locally modelled as realizations of random processes with a spatially uniform amplitude and frequency content (Hao e*t al*., 1989; Der Kiureghian, 1996). Engineering models of such processes are often calibrated from strong-motion array data from past earthquakes. This includes estimations of apparent wave propagation velocity, coherency function, and site-dependent power spectral density function (PSD) of seismic waves. These coherency functions usually consist of two parts, the modulus or lagged coherency, which measures the similarity of the seismic motions between two stations, and the phase, which describes the wave passage and local site effects. Several models of coherency and correlation functions: theoretical, empirical and semi-empirical, are reported in the literature (e.g., Der Kiureghian, 1996; Harichandran and Vanmarcke, 1986;

Abrahamson *et al*., 1991a; Luco and Wong, 1986). Such models are needed for simulating time series of spatially variable ground motions that are crucial for seismic response analysis of horizontally extended structures.

It is well known that coherency functions are characteristics of the local site, source, and wave propagation path. Therefore, models calibrated from data collected in one region may not be suitable for use in other areas (Somerville *et al*., 1988, 1991; Zerva, 2009). Due to lack of local data, coherency models calibrated for one region are often used to simulate ground motion in other regions, sometimes with different tectonic and geological settings. Many studies recognize the need for a single expression for the description of the spatial variability of the seismic motions to be used in engineering applications. However, the results of the study of Zerva (1994) on the effects of choosing of spatial incoherence models suggest that the response of lifelines is sensitive to the details of the spatial incoherence model (partial or full correlation at low frequencies, degree of exponential decay as frequency and separation distance increase). This leads to the suggestion that a single generic expression for the spatial incoherence of the motions may not, for the time being, be appropriate for the seismic response analysis of critical engineering structures, but that further research on the physical modeling of the spatial variability is necessary. A conclusion as to which model is better than the others will be reached when we have a complete physical understanding of the causes and the significance of the causes that produce the spatial incoherence in the motions.

On the other hand, almost all the work in ground motion simulation used for structural response history analysis are based on the empirical Kanai–Tajimi spectrum or Clough–Penzien spectrum, which are approximate ground motion power models that fail to accurately account for wave motions transmitted from the earthquake source through the medium. A physically consistent and refined model using a seismological source model that can account for effects of the fault rupture and the transmission of waves from the fault through the media to the ground surface is desired.

1.1 Literature review on numerical simulations of spatially variable ground motions

Although strong motion networks are expanding in many countries, dense arrays are required to record local variability are still rare. An alternative method, in the face of a lack of recorded data, to simulate spatially variable ground motion could be numerical simulation of ground motion. In this context, stochastic simulation methods based on the random vibration approach (Hao *et al*., 1989; Deodatis, 1996; Gao *et al*. 2012) that require pre-specified coherency functions are not applicable, and one needs to resort to simulation based on modelling of the physics of the seismic source and propagation of waves in an elastic medium. The choice of an appropriate simulation method depends on the availability of data

on the wave propagation path and seismic source. The simulation method should be capable of incorporating the physical effects (e.g., finite-source effects) that lead to spatial variability at a local scale that confirm to the current empirical and theoretical understandings of the spatial and spectral nature of coherency functions (e.g., Ding and Song, 2010; Menke *et al*., 1990).

The two widely-used ground motion simulation approaches rely on point-source and finite-source modelling. The point-source method (Boore, 1983, 2003) lacks the ability to model incoherence effects due to seismic waves radiating from different parts of a finite source. Such effects can be at least partially incorporated into finite-source ground motion simulation methods. Such methods rely on modelling an extended earthquake source and the wave propagation medium. Numerical simulations of ground motions incorporating the effects of three-dimensional seismic source, wave propagation in complex media, and the influence of the local site - such as, topographic effects and basin responses -have gained popularity in recent years (e.g., Smerzini and Villani, 2012). Such simulations are often semi-deterministic numerical methods based on finite elements (Bielak *et al*., 2005), finite differences (Pitarka, 1999) or spectral elements (Mazzieri *et al*., 2013). Such extensive simulation methods are very attractive due to their ability to model complex source, path, and site effects in generation and propagation of three-dimensional seismic wave fields. These methods are, however, computationally expensive and require great detail about the source, as well as the geological and geotechnical properties of the area. The results of such simulations are accurate to the same degree that the input data are accurate, as in all simulations.

In other words, detailed information on the fault geometry and slip distribution, as well as geological structure of the site, is required. While such information can be compiled for recent, large earthquakes, it is not easily predicted for future earthquakes. Although such methods have been very successful in reproducing ground-motion records from well-studied, past earthquakes, their reliability in predicting ground motion due to future earthquakes depends on the level of confidence with which various source, path, and site parameters are predicted. Through detailed geological and geotechnical studies, uncertainties in the path and site parameters can potentially be reduced, but inherent uncertainties in source parameters such as slip distribution are still significant, and it is not yet possible to predict the source model of a future earthquake based on past experience.

Most importantly, these physics-based, numerical methods can simulate low-frequency (to about 2.5 Hz; e.g., Smerzini and Villani, 2012) motion. For engineering applications, and especially for incoherence effects, larger frequency components (~2-9 Hz) are more relevant. Hybrid methods of simulation, where low-frequency motion obtained from physics-based models, are combined with high-frequency motion obtained from stochastic models are also

being developed in the recent years (e.g., Graves and Pitarka, 2010). Due to computational costs and lack of detailed information about the source, path, and site, these models have limited use in routine work.

An alternative for modelling the wave propagation effect is provided by the use of the empirical Green's functions (EGF). These functions are calibrated from ground motion time series recorded during small events and, in this sense, incorporate, at least partially, the effect of the wave propagation path. The small events must correspond to the same seismogenic source as the target event being simulated. Hartzell (1978) first utilized observed records from small events (e.g., aftershocks and foreshocks) as Green's functions to a simulate ground motion time series corresponding to a mainshock. Since then, his original idea has been applied, developed, and improved upon by numerous researchers (e.g., Irikura, 1983, 1986; Irikura *et al*., 1997). Sometimes, EGF in the form of recorded time series from small earthquakes are not available. In these cases, the EGF method, as conceived originally, is not applicable.

To overcome this problem, hybrid methods for broadband-frequency ground motion simulations have been developed combining deterministic and stochastic approaches. One such method is the hybrid Green's function (HGF) proposed by Kamae *et al*. (1998a). In this semi-empirical method, ground motion time histories corresponding to small earthquake events are calculated using the stochastic point-source model (Boore, 1983), or using a hybrid scheme combining deterministic and stochastic approaches. The long-period motions $\left(f \prec 1\,\mathrm{Hz}\right)$ from the small events are deterministically calculated using the 3D finite-difference method (Pitarka, 1999) (i.e., assuming a point source and adopting a 3D velocity model of the heterogeneous structure). High-frequency $\left(f \succ 1\,\mathrm{Hz}\right)$ motions from these are stochastically simulated using Boore's 1983 method. The resulting small events are then used as EGF to simulate ground motion corresponding to large earthquakes. The HGF method, in its former version, has been widely used, due to its relative simplicity, in simulating strong motion time series in regions where recorded data is not available (Joshi and Midorikawa, 2004; Joshi and Mohan, 2008).

1.2 Literature review on site conditions effects on coherency

The strong influence of site conditions on strong ground motion characteristics has been widely investigated and extensively documented. This strong influence is due to the fact that the shallow region surrounding the site is usually the most heterogeneous portion of the propagation path between the source and the site. This leads us to expect that the complex wave propagation phenomena that give rise to variability in site response will also give rise to variability in spatial incoherence due to differences in site conditions (Somerville *et al*.,

1991). Therefore, this will influence the response of spatially extended structures. The majority of spatial coherency models were developed from recorded data at relatively uniform (rock or soil) site conditions during the strong-motion, shear-wave window and decay exponentially with separation distance and frequency (Luco and Wong, 1986; Abrahamson *et al*., 1991a). It is generally assumed that a single coherency model evaluated from the data at a uniform site can describe the coherency of the motions between pairs of stations located either both on stiff soil conditions, both on soft soil conditions, or one on stiff and one on soft soil conditions.

This assumption is contradicted by following observations from recorded data. Somerville *et al*. (1991) investigated the coherency function of ground motions of horizontal shear waves on a site located on folded sedimentary rocks, such as the Coalinga anticline in California, and they found that the lagged coherency does not show a strong dependence on station separation and wave frequency. The incoherence is generally higher than on the flat alluvial sites of the El Centro differential array and the SMART-1 array where, in contrast, coherency had uniform (similar) behavior with its own pattern for each soil array (Somerville, 1991). Incoherency decreased smoothly with frequency and separation distance, which Somerville *et al*. (1991) attributed to wave scattering in a laterally homogeneous, horizontally layered sediment. Somerville *et al*. (1991) related the chaotic behavior to the wave propagation in a medium having strong lateral heterogeneities in seismic velocity.

Liao *et al*. (2007) used the seismic data recorded at the Parkway array in Wainuiomata Valley, New Zealand, to study the effect of variable site conditions and irregular subsurface topography on coherency estimates from horizontal S-wave windows. They compared the lagged coherency functions of different station combinations: four groups with station pairs located on the sediments, one group with one sedimentary station, and one rock station (Liao *et al*., 2007). They concluded that the lagged coherency between the sediment and rock stations exhibits large variability and follows no consistent pattern in comparison to the uniform soil sites coherencies (Liao *et al*., 2007).

Schneider *et al*. (1992) conducted an extensive study of spatial, lagged coherency estimates evaluated from data at a number of dense arrays at various sites, classified broadly as soil and rock sites. The coherency estimates evaluated at the rock sites show significant variability, which has been attributed to topographic effects at the rock sites (Schneider *et al*., 1992). The comparison suggests that coherencies estimated at rock sites are lower at low frequencies than coherencies at soil sites (Schneider *et al*., 1992). Also, the decay with frequency of the rock-site coherencies is flatter and slower than the decay of the coherencies at the soil sites, which they explained by the fact that scattering at rock and soil sites differs so the exponential decay of the lagged coherency at these different site conditions will also be different (Schneider *et al*., 1992). These observations suggest that the spatial coherency function measured on flat-lying sedimentary sites may not provide a good description of spatial ground motion

coherencies on sites with variable conditions and irregular subsurface topography (Schneider *et al*., 1992). These include folded sedimentary rocks exposed at the surface, basins generated by the folding of sedimentary rocks, and alluviated river valleys.

In reality, it is hard to obtain a theoretically accurate coherency model that can be extrapolated to other sites, because of the difficulty in studying wave propagation through highly variable and complex soil media. It is well known that a more accurate model can be obtained through a more advanced analysis of wave motion transmitting through an accurately modeled medium. However, most of this work fails to obtain an explicit analytical expression of the coherency function that is needed for the synthesis of SVGMs at a particular site. Furthermore, in the theoretical wave coherency model by Der Kiureghian (1996) in which variability in local site conditions was represented by a one-dimensional, S-wave propagating vertically through two soil columns with different properties, only the randomness of rock was accounted for approximately in the incoherence effect, which is assumed to affect the lagged coherency value only, and the local site effects are assumed to have an influence on the phase only. The advantages of the model is that it can consider different soil properties at different support locations, and it is straightforward to use. However, the local soil properties exhibit greater randomness and spatial variation than the rock, which can also affect the lagged coherency value, as shown by the above observations. Unfortunately, how the local soil profile influences the lagged coherency value, besides affecting the phase part of coherency model, is unknown.

Another point worth noting regarding the difficulty in reliably predicting the local site effects is that uncertainties always exist in defining the properties of soils. This results from the natural heterogeneity or variability of soils, the limited availability of information about internal conditions and sometimes the measurement errors. These uncertainties associated with system parameters are also likely to influence the lagged coherency loss function. Research on uncertain soil properties on the ground motion coherency is relatively rare. Zerva and Harada (1997) presented a semi-empirical, site-specific coherency model that approximated the site topography by a horizontally extended, stochastic layer overlaying a half space (bedrock). They simplified horizontal stochastic layers at a site with no dramatic changes in its topography as a single-degree-of-freedom (1-DOF) system with the soil layer thickness and with soil material properties as random functions of the horizontal coordinate to study the effect of soil stochasticity on the coherency function. They pointed out that the effect of soil layer stochasticity should also be incorporated in spatial variation models because the variability in the soil characteristics will reduce the lagged coherency function at the stochastic layer predominant frequency. This drop in lagged coherency behavior has been noted by Kanasewich (1981), who suggested that site resonances can be identified from holes

in the coherency spectra of motions at adjacent locations. Their analysis is also in concord with the coherency-hole phenomena observed by Cranswick (1988) in his geophysics research. It should be noted, that a 1-DOF system cannot realistically represent local site conditions due to the fact that multiple predominate frequencies exist corresponding to different modes of the site.

Liao and Li (2002) analytically evaluated the spatial coherency in their stochastic methodology to study the effects of uncertain soil properties and irregular topography on the coherency function, where it is shown that the surface layer irregularity of a site with deterministic soil properties subjected to non-identical random input excitation can reduce the lagged coherency function values in the vicinity of the resonant frequencies of the site. Furthermore, the stochasticity in the soil layer also tends to cause diminution of the lagged coherency function values near the site's resonant frequencies. The latter result is in agreement with that of Zerva and Harada (1997) and Cranswick (1988). However, this method is difficult to implement, sometimes a bit arbitrary in selecting the absorbing boundary conditions, and it is difficult to explain why the coherency function varies significantly over a relatively short distance (Bi and Hao, 2011).

Kanda (2000), using two dimensional finite element modeling of a layered medium with irregular interfaces (fully deterministic concave and convex sine-shaped interfaces are assumed between the layers) and random spatially variable incident motions, analyzed coherency and amplitude variability on the free surface of the site. The analytical results showed that interface irregularities between layers significantly change the frequency characteristics of ground motions at the soil surface. Although the spatial lagged coherency of ground motion is near unity at frequencies lower than the first predominant frequency of the soil, it fluctuates and depends on the types of irregular interfaces at high frequencies.

As a result, the effects of irregular surface and subsurface topography and uncertain soil properties of a site on the coherency function of spatial ground motions cannot be neglected. At the present, only very limited recorded spatial ground motion data on sites of different conditions are available. They are not sufficient to determine the general spatial incoherence characteristics of ground motions. Whereas analytical studies can provide insight into various aspects underlying the spatial variability in the seismic motions, the forward, purely analytical modeling of coherency, will be limited by the assumptions that are necessarily to simplify this complex problem.

1.3 Methodology

The research carried out in this thesis concentrates on modeling and simulation of spatially varying earthquake ground motions at the free surface of layered stochastic soil sites in the

epicentral region of the 1980 El-Asnam Earthquake (N.W Algeria), where recorded seismic data from dense arrays are not available. In the first step, based on an extension of the widely used finite-source ground motion simulation approach, the so-called empirical Green's function (EGF) method and given by Irikura *et al*. (1997), shear horizontal (SH) wave seismic motions (out-of-plane) at increasing separation distances at the bedrock (around El-Asnam Sogedia Factory site) in the near field were synthesized using geophysical parameters corresponding to the scenario of the El-Asnam mainshoc event (October 10, 1980, Ms=7.2) and its recorded aftershock (November 8, 1980, M_L=5.6). Power and cross spectral densities are computed, and lagged coherency functions are then estimated for the stationary segment of the strong motion S-wave window. The latter functions are compared to those obtained using the widely referred parametric plane wave coherency models in order to model the incident base rock ground motion spatial variation. To be able to study and understand the effects of the seismological input simulation parameters of source, propagation path and site on the spatial lagged coherency function, in particular, the ranges of magnitude, uniform rock basement and epicentral distance, we synthesized ground motions at various stations from hypothetical earthquakes by using a hybrid Green's function method (HGF) given by Joshi and Mohan (2008). The results are compared with published literature, and they are interpreted in light of the physics of ground motion generation incorporated in the simulation methods.

In the second step, the corresponding power and cross spatial densities of total surface seismic motions at the El-Asnam Sogedia Factory soil site with multiple soil layers are determined using the analytic site specific model developed in the Zerva and Harada (1997) approach for a layered random soil site, which directly relates the local soil conditions and base rock motion characteristics with the surface ground motions. The previously synthetized incident motions by the EGF method at different locations in the base rock, i.e. at the bedrock-layer interface, are assumed herein to have the same power spectral density. Site conditions consist of a vertical transmission of an SH wave with soil proprieties considered as varying randomly along the horizontal direction. Due to the absence of sufficient information to describe the variability of soil properties in the horizontal direction of the present site example, the layer thickness and soil material properties are regarded herein as random variables with the Gaussian distribution accounted for by a given coefficient of variation. The damping ratios adopted in this study are based on iterative equivalent nonlinear site response analysis of the soil layers when subjected to bedrock motion and are, therefore, considered to model hysteretic energy dissipation in the soil layers. The site contribution to the lagged coherency and, using the parametric model idealizing bedrock lagged coherency, the resulting total lagged coherency is then derived. The contribution of the various factors (the spatial correlation function of the predominant ground frequency varying in the horizontal direction,

the mean value of the equivalent damping ratio of the ground, mean value of the predominant ground frequency, and the wave propagation speed in the horizontal direction of the incident motion) to the spatial variation of the surface motions and the resulting seismic ground strains on the surface of the stochastic layer evaluated from the model are examined for the present site. Parametric models of the ground motion coherency and power spectral density at the surface of the study area are presented. Such models are useful in random vibration analysis of lifeline structures under the action of earthquake excitation or in simulation of spatially variable ground-motion time histories to be used in nonlinear time history analysis of such structures.

For such nonlinear analysis, the spectral representation method of unconditional simulation given by Hao *et al*. (1989) is used to generate non-stationary, spatially varying ground motion time histories at various locations on the ground surface of the El-Asnam Sogedia site, compatible with the properties of the target (predictive) random field, e.g. power spectral density and the spatial coherency functions at the surface.

1.4 Thesis Organization

The thesis contains six chapters; the subsequent five chapters are summarized here. In Chapter 2, basic concepts of random processes are first given. The general properties of stochastic coherency function and the coherency estimation procedure based on conventional spectral analysis are then presented.

Chapter 3 provides the methodology of the two widely-used, finite-source ground motion simulation approaches at a single location, the EGF and HGF methods, and their extension to simulate spatially correlated excitations at multiple locations on bedrock. A case study is proposed using the extended EGF method and non-parametric lagged coherency of ground motion is presented for the bedrock in the epicentral area of the 1980 El-Asnam Earthquake in northwest Algeria. Estimated coherency functions are compared with several parametric models proposed by various investigators.

Chapter 4 gives the results of a parametric study investigating the sensitivity of lagged coherency to the engineer parameters of simulation using the extended HGF method.

Chapter 5 deals, first, with a model of accounting for local site effect in the spatial coherency of surface ground motion, including consideration of spatial-random-variable soil profiles, and the resulting seismic ground strains on the surface of a stochastic layer evaluated from the spatial incoherence expression of the model. Next, the contributions of the various factors to the spatial variation of the surface motions and the resulting seismic ground strains

are examined for an example of the El-Asnam Sogedia Factory soil site. The simulated, spatially variable surface ground motions that match the predictive spatial coherency and power spectral density models close the Chapter.

Finally, Chapter 6 summarizes the concluding remarks of the thesis and provides suggestions for future research.

CHAPTER 2

BASIC CONCEPTS OF RANDOM PROCESSES

Basic concepts of random processes:

Structures are subjected to loading that is mostly time dependent in a weak or strong fashion. Response histories under weakly time-dependent loading may be calculated by using the quasi-static analysis procedure. For moderately or strongly time-dependent loading, calculation of response quantities requires a full dynamic analysis procedure, assuming that the structure is deterministic and the loading history is fully determined or known. This means that it obeys a specific rule or a definite function of time, such as constant, linear, or harmonic. time functions with known properties. Under such a structural and loading scenario, the corresponding analysis called the deterministic dynamic analysis, since all necessary parameters of the analysis can be uniquely determined or known. However, the difficulty in the structural dynamic analysis is to determine the loading functions and their properties correctly, such as frequencies, durations, amplitudes, and phases. Due to the lack of sufficient knowledge of dynamic excitations in nature, we possess limited information on loading parameters which that are usually obtained from recorded data or observations of occurrences, such as earthquakes and sea waves, that occur in an arbitrary fashion. Other examples can be wind loading on high-rise buildings and towers and traffic loading on bridges and viaducts, which do not follow specific rules.

Earthquakes occur periodically in seismic areas with unknown information and sea waves occur continuously with random fluctuations of the sea surface. The only information that we have is based on experiences of past occurrences from which we can predict structural response in a probabilistic manner. When the excitation loading varies arbitrarily with time, the corresponding response will also be arbitrary with time. Such a response process deals with the random vibration, and its characteristic properties can be determined by using statistical and probabilistic methods. The basis for probability modelling, processing and simulation of spatial variations of ground motion, is the theory of random processes. Basic concepts and numerical processing methods of random processes are presented in this chapter (Newland, 1984; Jenkins and Watts, 1969).

2.1 Moments

The moment, or expected value functions, of random processes can be obtained using the equations:

$$E\left[x_1(t)\right] = \int_{-\infty}^{+\infty} x_1 f(x_1, t)\, dx_1 \tag{2.1}$$

$$E\left[x_1(t)x_2(s)\right] = \int_{-\infty}^{+\infty} x_1 x_2 f(x_1, x_2, t, s)\, dx_1 dx_2 \tag{2.2}$$

where $x_1(t)$ and $x_2(s)$ are random processes and $f(x_1,t)$, $f(x_1,x_2,t,s)$ are their probability density function (called the first order probability density function) and joint probability density function (called the second order joint probability density function) at any time, respectively.

Using Equations (2.1) and (2.2), any order of moment can be calculated.
Mean value function of $x(t)$ (first order moment):

$$m_x(t) = E\left[x(t)\right] = \int_{-\infty}^{+\infty} x\, f(x,t)\, dx \tag{2.3}$$

autocorrelation function of $x(t)$ (second order moment):

$$R_{xx}(t_1,t_2) = E\left[x(t_1)x(t_2)\right] = \int_{-\infty}^{+\infty} x^2\, f(x,t_1,t_2)\, dxdx \tag{2.4}$$

autocovariance function of $x(t)$ (second order moment):

$$B_{xx}(t_1,t_2) = E\left(\left[x(t_1)-m_x(t_1)\right]\left[x(t_2)-m_x(t_2)\right]\right) = \int_{-\infty}^{+\infty}\int_{-\infty}^{+\infty} \left[x-m_x(t_1)\right]\left[x-m_x(t_2)\right] f(x,t_1,t_2)\, dxdx \tag{2.5}$$

other useful functions are the variance function of $x(t)$:

$$\sigma_x^2(t) = B_{xx}(t) \tag{2.6}$$

and the autocorrelation coefficient function of $x(t)$:

$$\rho_{xx}(t_1,t_2) = \frac{B_{xx}(t_1,t_2)}{\sigma_x(t_1)\sigma_x(t_2)} \tag{2.7}$$

where σ_x is the standard deviation of $x(t)$.

The above formulas can be extended to two random processes, $x_1(t)$ and $x_2(t)$. Instead of using the same $x_1(t_1)$ and $x_1(t_2)$, $x_1(t_1)$ and $x_2(t_2)$ are used to derive the corresponding definition for cross terms, which are called the cross correlation, the cross covariance, and the cross correlation coefficient. For example, the cross covariance function of $x_1(t)$ and $x_2(t)$ is:

$$B_{x_1x_2}(t_1,t_2) = E\left(\left[x_1(t_1) - m_{x_1}(t_1)\right]\left[x_2(t_2) - m_{x_2}(t_2)\right]\right) = \int_{-\infty}^{+\infty}\int_{-\infty}^{+\infty}\left[x_1(t_1) - m_{x_1}(t_1)\right]\left[x_2(t_2) - m_{x_2}(t_2)\right] f(x_1,t_1,x_2,t_2)\, dx_1 dx_2 \tag{2.8}$$

and their cross correlation coefficient function is:

$$\rho_{x_1x_2}(t_1,t_2) = \frac{B_{x_1x_2}(t_1,t_2)}{\sigma_{x_1}(t_1)\sigma_{x_2}(t_2)} \tag{2.9}$$

The correlation and covariance information of stochastic processes is important and frequently used in the spectral analysis of structures. The above mentioned equations for the correlation and covariance functions are general. For special processes, such as stationary and ergodic processes, they are simplified.

If $x(t)$ is a stationary process, then the above-defined first moment, or mean value, in Eq. (2.3) becomes a constant and is independent of time, *t*. For processed acceleration time histories, this mean value is generally zero, and, if it is not, the time histories are demeaned: the mean value is subtracted from the process. Also, the above second-moment functions depend only on the time lag, $\tau = t_2 - t_1$. For example, the autocovariance function can be expressed as :

$$B_{xx}(t_1,t_2) = B_{xx}(t_2 - t_1) = B_{xx}(\tau) \tag{2.10}$$

where $B_{xx}(\tau)$ is an even function, $B_{xx}(\tau) = B_{xx}(-\tau)$.

The stationarity assumption carries a peculiar characteristic. Since the moments do not depend on absolute time, but only on time lag, the time histories have neither a beginning nor an end and maintain the same stochastic characteristics throughout their (infinite) duration. This characteristic is unrealistic as, obviously, seismic ground motions have an absolute starting and ending time. For ease of derivation, one may still argue is valid for the following reason. Generally, the stochastic characteristics of seismic ground motions for engineering applications are evaluated from the strong motion shear S-wave window (Harichandran and Vanmarcke, 1986), that is a segment of the actual seismic time history, that, however, maintains the same properties throughout its duration. This strong motion window can be viewed as a segment of an infinite series with uniform characteristics through time, or a stationary process (Harichandran and Vanmarcke, 1986). For a stationary process, the amplitude and phase of the motions are not functions of time. It is noted that the assumption

of stationarity is relaxed in the simulation of random processes and fields for their subsequent use in engineering applications (see Chapter 5, Sec. 5.2).

The mathematical process of frequency analysis assumes that the limited-duration segment will immediately repeat. This is not completely true. It is often the case that the end of the segment does not smoothly mesh with the start of the segment. The consideration of a finite segment of the time history in the evaluations can be treated as one of infinite duration multiplied by a rectangular window time function. In the frequency domain, the results of this multiplication is equal to a convolution of the Fourier transform of the real time series and the Fourier transform of the rectangular time window. Hence, the results obtained after applying the FFT on the finite segment are distorted by the convolution with the spectral rectangular window at every discrete frequency value. This is an effect of data truncation and is related to the large discontinuity which may occur between the values between the edges of the finite segment.

Generally, instead of the rectangular window, a cosine-tapered window is utilized, with cosine functions at both its ends. The duration of the cosine functions is a small percentage of the overall duration, T, of the segment and results in a smooth transition region in the analyzed segment from zero acceleration values to finite ones at the beginning of the segment, and from finite ones to zero at its end. The role of the taper window is to prevent discontinuities and the resulting spurious high frequency during the Fourier transform to compute the frequency content of the analyzed segment (Ancheta and Stewart., 2015). Many suggestions exist for how to smoothly taper a signal at its edges. Well-known and widely used windows include the Hanning, Hamming, Tukey, and Blackman windows. They differ slightly in how they taper near the edges and are available for direct use in Matlab code. The Tukey window, which is a rectangular window with the edges equal to parts of a cosine, will be used in this research.

It is also assumed that the stationary time histories at the recording stations are ergodic (Newland, 1984). A stationary process is ergodic if averages taken along any realization of the process over its infinite duration are identical to the ensemble averages, i.e., the information contained in each realization is sufficient for the full description of the process. Obviously, the information from the time history is available only for a finite duration window, that presumably represents a segment of the stationary process. The consideration of ergodicity, however, is important, especially in the subsequent parametric modeling of the stochastic descriptors of the motions. The evaluation of these parametric models for the random processes and fields would require, ideally, records at the same site from many earthquakes with similar characteristics so that an ensemble of data can be analyzed and averages of the ensemble evaluated. In reality, there is only one realization of the random process or the random field, i.e., one time history at each recording station or one set of

recorded data at an array for an earthquake with specific characteristics. The assumption of ergodicity permits the use of the characteristics of a single realization over its duration to represent the ensemble characteristics, to which parametric models for the description of the spatial variation of seismic ground motions can be fitted, as will be the case in this research (see Chapter 3). These models are necessary for random vibration analyses or for the generation of artificial time histories. It is obvious that reality does not fully conform to these assumptions, but actual data recorded at dense instrument arrays during the strong motion S-wave window may be viewed as homogeneous, stationary, and ergodic in a limited or weak sense (Zerva and Zervas, 2002).

2.2 Spectral properties of random processes

Since the fast Fourier transform (FFT) algorithm was introduced, harmonic analysis has provided a very effective tool for dealing with many problems. This frequency domain approach is particularly useful and suitable for vibration problems in which frequency is a very important parameter. To carry out a harmonic analysis, it is necessary to determine the spectral properties of the processes involved.

Assume $x_1(t)$ and $x_2(t)$ are two, jointly stationary and zero mean random processes. Their power spectral density (PSD) functions $S_{xx}(\omega)$ ($S_{x_1x_1}(\omega)$ and $S_{x_2x_2}(\omega)$, respectively) and cross power spectral density function $S_{x_1x_2}(\omega)$ can be defined respectively by the Fourier transform of the corresponding covariance functions as given by the Wiener-Khinchine transformation pairs:

$$\begin{cases} S_{xx}(\omega) = (1/2\pi)\int_{-\infty}^{\infty} B_{xx}(\tau)\, e^{-i\omega\tau}\, d\tau \\ B_{xx}(\tau) = \int_{-\infty}^{\infty} S_{xx}(\omega)\, \mathrm{e}^{i\omega\tau}\, d\omega \end{cases} \tag{2.11}$$

where $S_{xx}(\omega)$ is a real-valued even function, $S_{xx}(\omega) = S_{xx}(-\omega)$;

$$\begin{cases} S_{x_1x_2}(i\omega) = (1/2\pi)\int_{-\infty}^{\infty} B_{x_1x_2}(\tau)\, e^{-i\omega\tau}\, d\tau \\ B_{x_1x_2}(\tau) = \int_{-\infty}^{\infty} S_{x_1x_2}(i\omega)\, \mathrm{e}^{i\omega\tau}\, d\omega \end{cases} \tag{2.12}$$

where ω is the circular frequency (in rad/sec). $S_{x_1x_2}(i\omega)$ is, in general complex and has the following properties:

$$S_{x_1x_2}(-i\omega) = S^*_{x_1x_2}(i\omega) = S_{x_2x_1}(i\omega) \tag{2.13}$$

$$\left|S_{x_1x_2}(i\omega)\right|^2 \le S_{x_1x_1}(\omega)S_{x_2x_2}(\omega) \tag{2.14}$$

where $*$ denotes a complex conjugate.

2.3 Estimation of covariances

Assuming that $x_1(t)$ and $x_2(t)$, $0 \le t \le T$ with T is the duration of the strong motion S-wave window, they are two, jointly stationary random processes having zero mean values, or they have been demeaned. An estimation of the theoretical autocovariance function (Eq. 2.5) for $x_1(t)$ is (Jenkins and Watts, 1969; Zerva, 2009):

$$B_{x_1x_1}(\tau) = \begin{cases} \dfrac{1}{T}\displaystyle\int_0^{T-|\tau|} x_1(t)x_1\left(t+|\tau|\right)\,dt & 0 \le |\tau| \le T \\ 0 & |\tau| \succ T \end{cases} \tag{2.15}$$

It can be recognized from the equation that the stationary autocovariance is an even function of the time lag τ, i.e., $B_{xx}(\tau) = B_{xx}(-\tau)$. Equation (2.15) evaluates the stochastic descriptors of the time histories as continuous functions of time. For a discrete data series having N data points at intervals Δt and times $t_k = (k+1)\Delta t$, $k = 1 \ldots N$, so that $(N+1)\Delta t = T$. The autocovariance function is estimated using :

$$B_{x_1x_1}(l) = \begin{cases} \dfrac{1}{N+1}\displaystyle\sum_{n=0}^{N-l} x_1(n)x_1(n+l) & 0 \le l \le N+1 \\ 0 & l \succ N+1 \end{cases} \tag{2.16}$$

The autocovariance estimators of the motions at different seismic stations are evaluated from Eq. (2.16). The estimators are sharply peaked at $\tau = 0$, decay quickly with the time lag τ, and exhibit symmetry around the zero axis.

The estimator of the cross covariance function (Eq. 2.8) for processes $x_1(t)$ and $x_2(t)$ is (Zerva, 2009):

$$B_{x_1x_2}(\tau) = \begin{cases} \dfrac{1}{T}\displaystyle\int_0^{T-|\tau|} x_1(t)x_2\left(t+\tau\right)\,dt & 0 \le |\tau| \le T \\ 0 & |\tau| \succ T \end{cases} \tag{2.17}$$

which can also be written as (Newland, 1984):

$$B_{x_1x_2}(\tau)=\begin{cases}\dfrac{1}{T}\displaystyle\int_0^{T-\tau} x_1(t)x_2\left(t+\tau\right)\,dt & 0\le\tau\le T\\ \dfrac{1}{T}\displaystyle\int_{-\tau}^{T} x_1(t)x_2\left(t-\tau\right)\,dt & -T\le\tau\le 0\\ 0 & \left|\tau\right|\succ T\end{cases} \tag{2.18}$$

For a discrete data series, Eq. (2.18) becomes :

$$B_{x_1x_2}(l)=\begin{cases}\dfrac{1}{N+1}\displaystyle\sum_{n=1}^{-N+l} x_1(n)x_2(n+l) & 0\le l\le N+1\\ \dfrac{1}{N+1}\displaystyle\sum_{n=2+l}^{N} x_1(n)x_2(n-l) & (N+1)\le l\le 0\\ 0 & \left|l\right|\succ N+1\end{cases} \tag{2.19}$$

Contrary to the autocovariance functions of the data (Eqs. 2.15 and 2.16), the cross covariance functions are not peaked $\tau=0$. They decay quickly with the time lag τ and exhibit no symmetry around the zero axis $\tau=0$. An equivalent symmetry property of the cross covariance function can be derived from Eq. (2.18), is $B_{x_1x_2}(\tau)=B_{x_2x_1}(-\tau)$. The peaks of the cross covariance functions between separated stations occur at time lags τ_0, that has values close to $\tau=0$ for short separation distances and that increase with increasing distance. The locations of the peaks, as well as their amplitudes, vary between station pairs. The shift of the peak values of the cross covariance functions from $\tau=0$ is associated with the propagation of the waves and has a significant effect on the bias of the spectral estimates, as the lagged coherency function. The lag τ_0, due to wave-train propagation, is the amount of time by which one of the records must be shifted to look like the other one as much as possible.

The autocorrelation coefficient and cross correlation coefficient functions of the discrete time series $x_1(t)$ and $x_2(t)$ can be easily calculated using:

$$\rho_{x_1x_1}(l)=\frac{B_{x_1x_1}(l)}{B_{x_1x_1}(0)} \tag{2.20}$$

$$\rho_{x_1x_2}(l)=\frac{B_{x_1x_2}(l)}{\sqrt{B_{x_1x_1}(0)B_{x_2x_2}(0)}} \tag{2.21}$$

2.4 Estimation of Spectra

Assume $x_1(t)$ is a series in $0 \le t \le T$ having sample increment Δt. Thus, the total number of data points is $N = T/\Delta t + 1$. The power spectral density function of $x_1(t)$ can be estimated by first tapering $x_1(t)$ and evaluating its Fourier transform:

$$X_1(\omega) = \frac{1}{2\pi} \int_{-\infty}^{+\infty} x_1(t) e^{-i\omega t}\, dt = \bar{X}_1(\omega) \exp\left[i\Phi_1(\omega)\right] \tag{2.22}$$

$$\Leftrightarrow \quad x_1(t) = \int_{-\infty}^{+\infty} X_1(\omega) e^{i\omega t}\, d\omega \tag{2.23}$$

The power spectral estimate of Eq. (2.11) can be alternatively evaluated directly in the frequency domain as follows (Zerva, 2009):

$$S_{11}(\omega) = \frac{2\pi}{T} X_1^*(\omega) X_1(\omega) = \frac{2\pi}{T} \bar{X}_1{}^2(\omega) \tag{2.24}$$

where $S_{11}(\omega)$ is used rather than $S_{x_1x_1}(\omega)$, for simplicity in presentation. Equation (2.24) clearly indicates that the power spectral density is real-valued. It further provides the physical interpretation of the power spectrum, namely that it is a scaled square of the Fourier amplitudes of the time history at the recording station during the analyzed window. An alternative approach to approximation of the PSD of the ground acceleration is by converting a response spectrum to an equivalent PSD, e.g., Tiliouine *et al*. (2003); Zhang *et al*. (2013).

The smoothed spectral estimate can be evaluated directly in the frequency domain through the following convolution expression (Jenkins and Watts, 1969):

$$\bar{S}_{11}(\omega) = \int_{-\infty}^{+\infty} W(u) S_{11}(\omega - u)\, du \tag{2.25}$$

where the spectral window, $W(\omega)$, and the lag window, $\Lambda(\tau)$, are Fourier transforms of each other, i.e.,

$$W(\omega) = \frac{1}{2\pi} \int_{-\infty}^{+\infty} \Lambda(\tau) e^{-i\omega\tau}\, d\tau \tag{2.26}$$

$$\Leftrightarrow \quad \Lambda(\tau) = \int_{-\infty}^{+\infty} W(\omega) e^{i\omega\tau}\, d\omega \tag{2.27}$$

The window $\Lambda(\tau)$ has the properties:

$$\begin{cases} \Lambda(0) = 1 \\ \Lambda(\tau) = \Lambda(-\tau) \\ \Lambda(\tau) = 0 \qquad\qquad |\tau| \prec T \end{cases} \tag{2.28}$$

Analogous to these properties (Eq. 2.28), the spectral window, $W(\omega)$ has the properties:

$$\begin{cases} \int_{-\infty}^{+\infty} W(\omega)\, d\omega = \Lambda(0) = 1 \\ W(\omega) = W(-\omega) \end{cases} \tag{2.29}$$

For discrete frequencies, Eq. (2.25) takes the form:

$$\begin{aligned} \bar{S}_{11}^{M}(\omega_n) &= \sum_{m=-M}^{+M} W(m\Delta\omega) S_{11}(\omega_n + m\Delta\omega) \\ &= \frac{2\pi}{T} \sum_{m=-M}^{+M} W(m\Delta\omega)\, \bar{X}_1{}^2(\omega_n + m\Delta\omega) \end{aligned} \tag{2.30}$$

where $\Delta\omega = 2\pi/T$ is the frequency step, $\omega_n = n\Delta\omega$ is the discrete frequency, $W(m\Delta\omega)$ is the spectral window, $2M+1$ is the number of frequencies over which the averaging is performed, the superscript M indicates the dependence of the estimate on the length of the smoothing window, and the last equality in Eq. (2.30) results from Eq. (2.24). Examples of smoothing windows include the rectangular, Bartlett, Tukey, Parzen, Hanning and Hamming windows (e.g., Jenkins and Watts, 1969). It is noted that different smoothing windows yield similar results, as long as the bandwidth of the windows is the same (Jenkins and Watts, 1969). Equations (2.25) and (2.30) suggest that the smoothed spectral estimate is an average over-frequency of the raw spectral estimate. With the smoothing operation, the variance of the estimate is reduced. The application of smoothing produces a trade-off between resolution and data scattering, as the level of smoothing increases the scattering of the spectral estimate decreases, and the mean value also decreases.

The spectral bandwidth of the window is defined as (e.g., Jenkins and Watts, 1969):

$$\text{Bandwith} = \text{B} = \left[\int_{-\infty}^{+\infty} \Lambda^2(\tau)\, d\tau \right]^{-1} = \left[\int_{-\infty}^{+\infty} W^2(\omega)\, d\omega \right]^{-1} \tag{2.31}$$

From the available smoothing windows, the Hamming window is most commonly used for smoothing seismic spectral estimates (Abrahamson *et al.*, 1991a; Ancheta and Stewart, 2015). Its expression (in samples) is given by:

$$W(m) = 0.54 - 0.46\cos\left(\frac{\pi(m+M)}{M}\right) \qquad m = -M....M \tag{2.32}$$

The area underneath the Hamming window is $1.08M$. If the window is used in the frequency domain, as is most commonly the case in analyzing seismic data, it ought to satisfy the characteristics of spectral windows (Eq. 2.29). Hence, the area underneath the window needs to be equal to unity, i.e., the right-hand side of Eq. (2.32) needs to be divided by $1.80M$.

To compute the cross power spectral density function (or cross spectrum) between $x_1(t)$ and $x_2(t)$, both $x_1(t)$ and $x_2(t)$ need to be tapered. After transforming $x_1(t)$ and $x_2(t)$ to the frequency domain, i.e., $X_1(\omega) = \bar{X}_1(\omega)\exp\left[i\Phi_1(\omega)\right]$ and $X_2(\omega) = \bar{X}_2(\omega)\exp\left[i\Phi_2(\omega)\right]$, the cross power spectral density function can be obtained using Eq. (2.33) as an alternative to Eq. (2.12) (Zerva, 2009):

$$\begin{aligned} S_{12}(\omega) &= \frac{2\pi}{T} X_1^*(\omega) X_2(\omega) \\ &= \frac{2\pi}{T} \bar{X}_1(\omega)\bar{X}_2(\omega)\exp\left[i\left(\Phi_2(\omega) - \Phi_1(\omega)\right)\right] \end{aligned} \tag{2.33}$$

where $S_{12}(\omega)$ is used rather than $S_{x_1x_2}(i\omega)$, for simplicity in presentation. The absolute value of the cross spectral density,

$$\left|S_{12}(\omega)\right| = \frac{2\pi}{T}\bar{X}_1(\omega)\bar{X}_2(\omega) \tag{2.34}$$

is usually termed the cross amplitude spectrum and the phase difference in Eq. (2.33), i.e.,

$$\varphi_{12}(\omega) = \tan^{-1}\frac{\mathrm{Im}\left[S_{12}(\omega)\right]}{\mathrm{Re}\left[S_{12}(\omega)\right]} = \Phi_2(\omega) - \Phi_1(\omega) \tag{2.35}$$

The cross amplitude spectrum is controlled by the Fourier amplitudes of the motions at the two stations, and the phase spectrum indicates whether the frequency component of the time history at one station precedes or follows the other time series at that frequency.

Similar to the power spectrum, cross spectral estimates also need to be smoothed to reduce their variance. The smoothed cross spectrum can be evaluated directly in the frequency domain through the convolution:

$$\bar{S}_{12}(\omega) = \int_{-\infty}^{+\infty} W(u) S_{12}(\omega - u)\, du \tag{2.36}$$

For discrete frequencies, Eq. (2.36) takes the form:

$$\bar{S}_{12}^{M}(\omega_n) = \frac{2\pi}{T} \sum_{m=-M}^{+M} W(m\Delta\omega)\bar{X}_1(\omega_n + m\Delta\omega)\bar{X}_2(\omega_n + m\Delta\omega) \exp\left[i\left(\Phi_2(\omega_n + m\Delta\omega) - \Phi_1(\omega_n + m\Delta\omega)\right)\right] \tag{2.37}$$

Equation (2.37) is derived in a manner similar to the smoothed, discrete power spectral density of Eq. (2.30). An important observation that can be recognized from Eq. (2.37), and also applies to Eq. (2.36), is that the Fourier phases of the individual time series contribute not only to the phase spectrum of the smoothed estimator, but also to its cross spectral amplitude. For the unsmoothed estimates, the cross amplitude spectrum (Eq. 2.34) is not affected by the phases, which contribute only to the phase spectrum (Eq. 2.35). For clarity, the smoothed cross amplitude spectrum is given by:

$$\left|\bar{S}_{12}^{M}(\omega_n)\right| = \frac{2\pi}{T} \left| \sum_{m=-M}^{+M} W(m\Delta\omega)\bar{X}_1(\omega_n + m\Delta\omega)\bar{X}_2(\omega_n + m\Delta\omega) \exp\left[i\left(\Phi_2(\omega_n + m\Delta\omega) - \Phi_1(\omega_n + m\Delta\omega)\right)\right] \right| \tag{2.38}$$

and the smoothed phase spectrum by:

$$\bar{\varphi}_{12}^{M}(\omega_n) = \tan^{-1} \frac{\mathrm{Im}\left[\bar{S}_{12}^{M}(\omega_n)\right]}{\mathrm{Re}\left[\bar{S}_{12}^{M}(\omega_n)\right]} \tag{2.39}$$

It is noted that the last equality of the unsmoothed phase spectrum in Eq. (2.35), i.e., $\varphi_{12}(\omega) = \Phi_2(\omega) - \Phi_1(\omega)$, no longer applies to the smoothed estimate (Eq. 2.39).

2.5 Stochastic and empirical ground motion coherency models

Spatial variability of ground motion at two points (or locations) is caused by a number of factors (Abrahamson *et al*., 1991a; Der Kiureghian 1996; Zerva and Harada 1997; Somerville *et al*., 1988) which can be summarized as follows:

a) Differences in the manner of superposition of waves arriving from an extended finite source and wave scattering by irregularities and inhomogeneity along the wave path and at the site, commonly termed incoherence effects.
b) Traveling-wave or wave passage effects, in which non vertical waves reach different points on the ground surface at different times, producing a time shift between the motions at those points.
c) Site effects due to the variation in filtering effects of overlying soil columns.

Considering motions $x_i(t)$ and $x_j(t)$ at two discrete locations i and j separated by a distance ξ, the complex coherency function in space and circular frequency ω is defined as:

$$\gamma_{ij}(\xi,\omega)=\frac{\bar{S}_{ij}(\xi,\omega)}{\sqrt{\bar{S}_{ii}(\omega)\bar{S}_{jj}(\omega)}} \tag{2.40}$$

where $\bar{S}_{ij}(\xi,\omega)$ is the smoothed cross spectral density function of $x_i(t)$ and $x_j(t)$; and $\bar{S}_{ii}(\omega)$ and $\bar{S}_{jj}(\omega)$ are their smoothed power spectral density functions. Separating $\gamma_{ij}(\xi,\omega)$ into its absolute value and phase, we have:

$$\gamma_{ij}(\xi,\omega)=\left|\gamma_{ij}(\xi,\omega)\right|\exp\left[i\bar{\varphi}_{ij}(\xi,\omega)\right] \tag{2.41}$$

where $0\le\left|\gamma_{ij}(\xi,\omega)\right|\le 1$ is a term commonly referred to as the *lagged* coherency function, and $\varphi_{ij}(\xi,\omega)$ is the smoothed phase spectrum given by:

$$\bar{\varphi}_{ij}(\omega) = \tan^{-1}\frac{\mathrm{Im}\left[\gamma_{ij}(\xi,\omega)\right]}{\mathrm{Re}\left[\gamma_{ij}(\xi,\omega)\right]} = \tan^{-1}\frac{\mathrm{Im}\left[\bar{S}_{ij}(\xi,\omega)\right]}{\mathrm{Re}\left[\bar{S}_{ij}(\xi,\omega)\right]} \tag{2.42}$$

which is the same as the phase spectrum of Eq. (2.39).

The wave passage introduces a deterministic shift in the Fourier phase (or deterministic delay in time) dependent on the wave speed and the separation distance between locations. Stochastic variations of Fourier amplitude and phase, unrelated to wave passage, occur due to wave scattering and interference along the source-to-site ray paths. These random variations in the Fourier phase are represented through the lagged coherency function. Generally, lagged coherency decreases with an increase in separation distance and frequency. The lagged coherency indicates the degree of linear relation between the data at each frequency. The closer the value of the lagged coherency to unity, the higher the indication of the linear trend,

and the closer the value of the lagged coherency to zero, the larger the scattering in the data. Lagged coherency, the most commonly cited coherency, and plane wave coherency, which is also used as a way of describing motion incoherency of the two points and is defined as the real value of complex coherency, are both obtained when the tapered time series are aligned using a single wave speed, i.e., considering that the time histories propagate with constant velocity at all frequencies as if they were a perfect plane wave propagation (Ancheta and Stewart, 2015).

In the alignment process, a reference station is selected. The cross covariance between the reference station time history and the motions at individual stations is evaluated, the time lag τ_0 associated with the peak value of the cross covariance identified, and the time histories are shifted as much as the identified time lag, so that wave propagation effects (i.e. wave passage effects) are partially removed. Indeed, seismic ground motions incorporate random time delay fluctuations around the wave passage delay, that are particular for each recording station. These arrival time perturbations are caused by the upward traveling of the waves through horizontal variations of the geologic structure underneath the array and, also, due to deviations of the propagation pattern of the waves from that of plane wave propagation.

In this study, lagged coherency functions are computed from the numerically simulated time series of ground acceleration at different space locations; the simulation methods are described in Chapters 3 and 5. The stationary part (strong motion S-wave window) of the time series is first extracted by visual inspection of the time evolution of Arias Intensity of the simulated time series. After extraction, a Tukey time window with a tapering length of 15% of the length of the demeaned stationary part is applied. The tapered S-wave signals are aligned to remove wave passage effects (e.g., Rupakhety and Sigbjörnsson, 2012; Zerva, 2009). The alignment is achieved by shifting the time axis of tapered S-wave windows with respect to an arbitrarily selected reference station by an amount corresponding to the time lag where the cross-covariance function of the tapered S-wave window and that at the reference station is maximal. The aligned, tapered windowed signals are then used to estimate power and cross spectral density functions, which are smoothed. We smooth all power spectra using a Hamming spectral window with a parameter of $M = 39$ ($2M+1$ is the width of the window). This level of smoothing is selected in order to reduce the variance in lagged coherency. We note that the window length used here is longer than that reported in Zerva (2009). The fact that the simulated time series in our study have a relatively long duration means that the frequency resolution of the computed spectra is relatively fine. This allows us to use longer windows to effectively reduce the variance of computed spectral estimates without seriously compromising their frequency resolution.

Based on coherency estimates from recorded strong motion array data, several models of parametric lagged coherency functions have been proposed in the literature: empirical, semi-empirical and analytical coherency models (see Zerva, 2009 for a detailed description). In the present study, coherencies estimated from simulated ground motion (Chapter 3) are compared with the models the empirical model of Hindy and Novak (1980) and the semi-empirical models of Luco and Wong (1986) and Somerville *et al*. (1988).

The Hindy and Novak (1980) model is mathematically expressed as (Novak and Hindy, 1979; Hindy and Novak, 1980):

$$\left|\gamma_{ij}\left(\xi,\omega\right)\right| = \exp\left[-(\alpha\omega\xi)^{\beta}\right] \tag{2.43}$$

Where α and β are model parameters. The dimensionless parameter, α, is defined as $\alpha = \eta / v_s$, with $\eta = \mu\left(R / r_o\right)^{1/2}$, where v_s is the shear wave velocity, R is the distance travelled by the wave, r_o the scale length of random inhomogeneities along the path, and μ^2 is a measure of the relative variation of the elastic properties in the medium. It is found that the exponentially decaying spatial incoherence model of Hindy and Novak (1980) is in general agreement with a number of spatial incoherencies when the model parameters are chosen appropriately.

The model of Luco and Wong (1986) is a particular case of Eq. (2.43) with $\beta = 2$. The model has been used extensively by researchers in seismic response analysis of lifelines (e.g. Zerva, 1994; Liao and Li, 2002; Martinellia *et al*., 2016). The model is based on shear wave propagation through a random media, an approximation of which may be valid for the propagation of the waves from the source to the ground surface or from the source to the bedrock-layer interface. Zerva and Harada (1997) and Der Kiureghian (1996) have also used this model for the description of coherency of bedrock motion. It is pointed out that the parameter η has values in the range of 0.02 to 0.5. The model of Hindy and Novak (1980) is more flexible than the Luco and Wong (1986) model, and is therefore adopted in this study. Somerville *et al*. (1988) assumed the following model showing a larger decrease with the frequency than with the separation distance:

$$\left|\gamma_{ij}\left(\xi,\omega\right)\right| = \exp\left[-(a+b\omega^2)\xi\right] \tag{2.44}$$

where a and b are two independent constants.

On the other hand, the wave passage effect is modelled by theorizing that ground motions consist of a waveform that propagates unchanged (unit amplitude, monochromatic) with velocity, $\vec{c}$, on the ground surface along a line connecting two stations. The vector of the

separation distance between the stations is denoted here by $\vec{\xi}_{ij} = \vec{r}_j - \vec{r}_i$. The analytical coherency expression of Eq. (2.40) for this type of motion would be (Zerva and Zervas, 2002):

$$\gamma_{ij}(\xi_{ij}, \omega) = \exp\left[-i \frac{\omega\left(\vec{c}.\vec{\xi}_{ij}\right)}{\left|\vec{c}\right|^2} \right] = \exp\left[-i \frac{\omega \xi_{ij}}{c} \right] \tag{2.45}$$

where $\xi_{ij} = \left|\vec{\xi}_{ij}\right|$, $c = \left|\vec{c}\right|$. It has been implicitly assumed that the waveform propagates from station *i* to station *j*. Equation (2.45) implies that $\left|\gamma_{ij}(\xi_{ij}, \omega)\right| = 1$ and that the complex term in the equation describes the wave passage effect, i.e., the delay in the arrival of the waveforms at the further away station is caused solely by their propagation. The phase spectrum of such motions is a linear function of frequency described as:

$$\varphi_{ij}\left(\xi_{ij}, \omega\right) = \frac{-\omega \xi_{ij}}{c} \tag{2.46}$$

where ξ_{ij}/c reflects the time lag, τ_0, defined earlier in the discussion of the alignment of the time histories. For a single type of wave dominating the window analyzed, as is most commonly the case for the strong motion S-wave window used in spatial variability evaluations, the consideration that the waves propagate with constant velocity on the ground surface is a valid one (Harichandran and Vanmarcke, 1986). Since body waves are non-dispersive, except in highly attenuated media, they have approximately the same velocity over a wide range of frequencies. In reality, the apparent propagation velocity of the motions may vary slightly with frequency, even for the broad-band shear wave window. Equation (2.45) is most commonly used to describe the wave passage part of the phase spectrum in the simulation of spatially variable ground motions (see Chapter 5).

CHAPTER 3

FINITE-FAULT SIMULATION OF MULTIPLE-STATION BEDROCK GROUND MOTIONS

Finite-fault simulation of multiple-station bedrock ground motions:

As indicated in Chapter 1, the spatial variation of seismic ground motion can significantly affect the seismic responses of extended structures, and the characterization of the spatial variation is important for the reliable seismic resistant analysis of lifeline structures. Due to wave scattering arising from the complexity of the earth's structure (inhomogeneity, anisotropy, presence of asperities, etc.), as well as rupture propagation effects along extended faults, strong ground motions at different points in a site would be characterized not only by amplitude and frequency content variability (described by a code-prescribed response spectrum or a power spectral density for the appropriate ground type) and wave propagation effects (deterministic phase variability), but also by coherency decay effects (random phase variability) (Harichandran, 1991).

Selection of the coherency function in modeling the SVGMs or seismic analysis of critical systems is an important task (Zerva, 1994). However, most of these models are different and dependent on specific array data, such as coherency models developed using the strong-motion shear-wave window from recorded array data on uniform local soil sites, rock sites, and some non-uniform sites. Because of the complexity of earthquake wave propagation through the random, heterogenous, nonlinear, spatially variable, and site specific soil profile, it is difficult to ensure that the resulting structural analysis is accurate when using a coherency model obtained at a similar local site as that where the structure is located.

For example, Schneider *et al*. (1992), analyzed the spatial incoherence of the motions recorded at dense arrays in California and Japan and compared the results with the spatial incoherence model of Abrahamson *et al*. (1991) for the site of the SMART-1 array in Lotung, Taiwan. They observed that, for distances of less than 100 m, the spatial incoherence of the motions is consistent at all sites. Coherencies computed on rock were lower than those on alluvium and show large variability, suggesting that the spatial incoherence may be more dependent on path and source effects than on local site geology. This dependence may be explained as follows. The near-receiver scattering is presumed to low enough that it is masked by the scattering from greater distances. Menke *et al*. (1990) analyzed the coherency of data recorded at the ECO and DBM arrays located on hard rock sites in the Adironack Mountains. Their results imply that the heterogeneities are three-dimensional and that scattering from near-receiver heterogeneities controls the incoherence properties of the seismograms. Bi and Hao (2011) analyzed that the coherency function between surface ground motions on a canyon site (irregular subsurface topography) and found that it is different from that between base rock motions. The lagged coherency function on the base rock is the upper bound of that of the ground surface. This shows the effect of lateral heterogeneities in surface soil sites,

which are, in general, site-specific. Therefore, it is unreasonable to apply the coherency function models from records at soil surface to base rock under soil.

It is obvious that the choice of a spatial incoherence model, a conclusion as to which of the models should be preferred in the seismic response analysis of a specific structure, will only be possible when the physical reasons underlying the spatial incoherence of the motions are fully understood. These are as follows: interference of different waves from an extended source that can arrive at the site during the same time window, long path scattering, scattering effects of the local site topography, the variability in the soil properties, etc. All of these factors are, in general, event and site specific estimations (Zerva, 1994). Many researchers have recognized the physical reasons. For example, Somerville *et al*. (1988, 1990) have posited that the spatial variation of ground motion is influenced by earthquake source, propagation path, and site condition. Der Kiureghian (1996) theorized that the spatial variation of ground motion could be attributed to wave passage effects, incoherence effects, attenuation effects, and site response effects. However, it is very difficult to evaluate, distinguish, and quantify the influence of each factor from records.

The ideal method for characterizing the ground motion spatial variation is to develop a geophysical model that can simulate the earthquake process directly. However, this kind of model is still not available because of the complexity of the fault rupture mechanism, the uncertainty of the soil and rock structures, and the seismic wave propagation path (Harichandran 1991). As explained in detail in Chapter1, empirical Green's functions (EGF) are an alternative for modelling the wave propagation effect by the finite-fault methods of ground motions simulation (e.g., Irikura 1983, 1986; Irikura *et al*., 1997). These functions are calibrated from ground motion time series recorded during small events and, in this sense, incorporate, at least partially, the effect of the wave propagation path (i.e., the effects of long path and near source scattering, or the scattering from the source to the site, on coherency properties are included in EGFs), in addition to the finite source effect on coherency incorporated by the using these finite-fault methods. The small event must correspond to the same seismogenic source as the target event being simulated. Sometimes, EGF in the form of a recorded time series from small earthquakes is not available, in which case the EGF method is not applicable as originally conceived.

To overcome this problem, hybrid methods for broadband-frequency ground motion simulation have been developed combining deterministic and stochastic approaches. One such method is the hybrid Green's function (HGF) technique proposed by Kamae *et al*. (1998a). In this semi-empirical method, ground motion time histories corresponding to small earthquake events are calculated theoretically using the stochastic point-source model (Boore, 1983), or using its modified version, which is a hybrid scheme combining deterministic and stochastic

approaches. The long-period motions ($f \succ 1\,\mathrm{Hz}$) from the small events are deterministically calculated using the 3D finite-difference method (Pitarka, 1999), i.e., assuming a point source and adopting a 3D velocity model of the heterogeneous structure, whereas the high-frequency ($f \prec 1\,\mathrm{Hz}$) motions are stochastically simulated using Boore's 1983 method. The resulting small events are then used as EGF to simulate ground motion corresponding to large earthquakes. The HGF method, in its former version, has been widely used due to its simplicity compared to EGF in simulating strong motion time series in regions where recorded data is not available (e.g., Joshi and Midorikawa, 2004; Joshi and Mohan, 2008).

In this chapter, we provides the methodology of the two widely-used, finite-source ground motion simulation approaches at a single location, EGF and HGF, for which we extended to be able to simulate at multiple locations on bedrock. A case study of the 1980 El-Asnam Earthquake (North-West Algeria) in the epicentral region is proposed using the EGF method. Power and cross spectral densities and lagged coherency functions are estimated from the strong motion shear-wave window, and the latter is calibrated to the existing parametric coherency function models. The extended HGF method will be used in Chapter 4 to simulate different earthquake scenarios that are needed for a parametric study investigating sensitivity of lagged coherency to the engineer parameters of simulation.

3.1 Ground motion simulation

3.1.1 The empirical Green's function method

The EGF of Irikura *et al*. (1997) considers a rectangular fault plane (length *L*, width *W*) divided into $l \times m$ elementary, rectangular sub-faults on its surface, as shown in Fig. 3.1. Denoting the Green's function associated with a sub-fault (i_o, j_o) by $u_{e_{i_o j_o}}(\mathbf{x},t)$, the total synthetic signal $U(\mathbf{x},t)$ at point $\mathbf{x}$ due to the whole fault plane is given by:

$$U(\mathbf{x},t) = \sum_{i=1}^{l}\sum_{j=1}^{m} \frac{R_s(\theta_{ij},\varphi_{ij})\, r_{i_o j_o}}{R_s(\theta_{i_o j_o},\varphi_{i_o j_o})\, r_{ij}} F(t) * cu_{e_{i_o j_o}}(\mathbf{x},t) \tag{4.1}$$

where $*$ denotes convolution. The function $F(t)$ is given by:

$$F(t)=\delta\left(t-t_{ij}\right)+\left(\frac{1}{n'}\right)\left\{1-\exp(-1)\right\}\sum_{k=1}^{(n-1)n'}\left[\exp\left\{\frac{-(k-1)}{(n-1)n'}\right\}\right]\times\delta\left(t-t_{ij}-\frac{(k-1)\tau}{(n-1)n'}\right) \quad (4.2)$$

and t_{ij} is given by Eq. (4.3):

$$t_{ij}=\frac{r_{ij}-r_o}{v_s}+\frac{\xi_{ij}}{v_r} \quad (4.3)$$

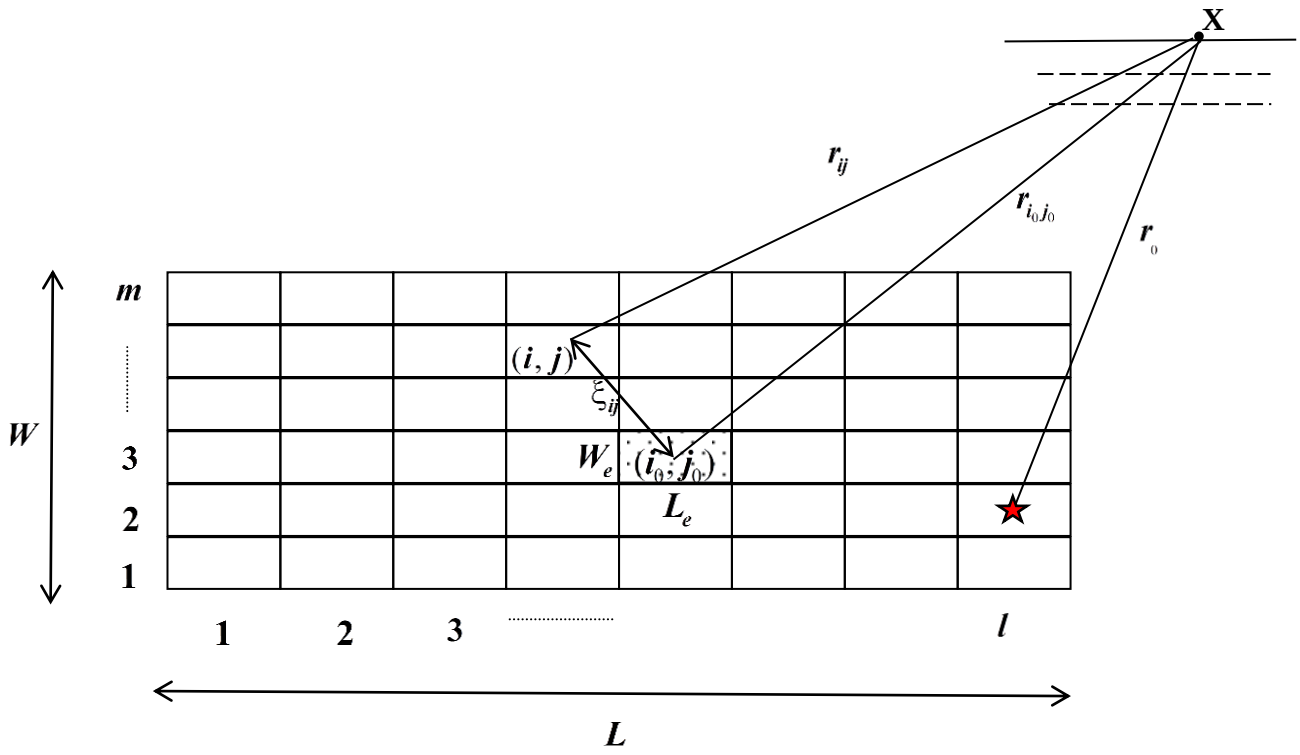

Fig. 3.1 - Schematic source model for synthesis. The start indicates the hypocentre location.

In these equations, t_{ij} is the phase delay, R_s is the radiation pattern (Aki and Richards, 2002), τ is the rise time of the event for which ground motion is being simulated, $r_{i_o j_o}$ is the Euclidean distance between the receiver, $\mathbf{x}$, and the rupture starting point on the elementary sub-fault (i_o, j_o), r_{ij} is the Euclidean distance between the receiver and the centre of the sub-fault (i, j), ξ_{ij} is the distance between the hypocentre and the centre of the sub-fault (i, j), v_s is the shear wave velocity, $v_r = 0.72v_s$ is the rupture velocity, n' is an integer to eliminate spurious periodicity (Irikura, 1983), $F(t)$ is the slip-time filtering function, c is the stress drop ratio, r_0 is the Euclidean distance between hypocentre and the receiver, and $\delta(t-t_{ij})$ represents the Dirac delta function. The parameters l, m, and n are determined from the scaling relations given by Kanamori and Anderson (1975). When the seismic moment ratio of

the target earthquake (the one being simulated) to the elementary one (the one used for empirical Green's function) is N^3, the parameters l, m, and n should each be equal to N (Irikura, 1983), the total number of divisions along the length or width of the fault so that the dimensions of sub-faults are small enough to be treated as point sources.

Kamae *et al*. (1998b) revised the Kanamori and Anderson (1975) relation to allow for a potential difference in stress drop between the target and the small events. The revised relations are:

$$\frac{L}{L_e} = \frac{W}{W_e} = \frac{D}{cD_e} = \frac{\tau}{\tau_e} = \left(\frac{M_0}{cM_{0_e}} \right)^{1/3} = N \tag{4.4}$$

where L and L_e are fault lengths, W and W_e are widths, τ and τ_e are rise times, and D and D_e are average slip, corresponding to the target event and small event, respectively.

The rise time parameter, τ, is given by the following relation in Geller (1976):

$$\tau = \frac{16 S^{\frac{1}{2}}}{7 \pi^{\frac{3}{2}} v_s} \tag{4.5}$$

where $S = L \times W$ is the fault plane area. The rise time of the mainshock can be calculated from the similarity relation (Eq. 4.4) by using a small event rise time determined by picking the frequency of the significant trough of its Fourier spectra (see Irikura, 1983).

Because the frequency content of earthquakes is magnitude dependent, direct application of Green's function as in Irikura (1986), can lead to underestimating the ground motion amplitudes at low frequencies. To overcome this, Irikura *et al*. (1997) introduced the exponential slip function (Eq. 4.2).

3.1.2 The hybrid Green's function method

HGF works in a similar way as the EGF method, except that a synthetic time series, rather than a recorded time series from small earthquakes, is used as the empirical Green's function. As discussed in the beginning of this chapter, the HGF method used by Joshi and Midorikawa (2004) and Joshi and Mohan (2008) is presented here and will be used in the next Chapter 4. In this approach, Boore's (1983) method is used to first simulate ground motion corresponding to an aftershock, which is then used as the Green's function to simulate ground

motion due to main shocks corresponding to different scenarios. To simulate the Green's function, we calibrate the model parameters of a theoretical Fourier amplitude spectrum (FAS) using the available aftershock data in the zone of interest. Only the S-wave portion of the recorded data is used in calibrating the model. More details on the calibration process and the model parameters are presented in subsequent sections and in Chapter 4.

The theoretical FAS of ground acceleration shear waves, $A(f)$, at a distance, r, from a point source with seismic moment, M_o, is given by (Boore, 1983):

$$A(f) = \frac{CM_o S(f, f_c) P(f, f_m)}{r} \exp\left(-\frac{\pi f r}{Q_s v_s}\right) \tag{4.6}$$

where f is the frequency, Q_s is the shear-wave quality factor accounting for inelastic attenuation, $1/r$ models the geometric spreading, and C is the scaling factor given by Eq. (4.7):

$$C = \frac{R_s(\theta,\varphi)(FS)(PJ)}{4\pi\rho v_s^3} \tag{4.7}$$

$R_s(\theta,\varphi)$ is the radiation pattern of shear waves (Aki and Richards, 2002), FS accounts for free surface, PJ is a factor that accounts for the partitioning of total shear-wave energy into two horizontal components, and ρ is the average density of the rock. The source spectrum, $S(f, f_c)$, is the ω-squared model function of the corner frequency which is given by:

$$f_c = 4.9\times10^6 v_s \left(\frac{\Delta\sigma}{M_o}\right)^{\frac{1}{3}} \tag{4.8}$$

where $\Delta\sigma$ is the stress drop. The function, $P(f, f_m)$, is a high-cut filter function with cut-off frequency, f_m and is taken from Boore (1983).

3.2 Case study: Coherency estimated from ground motion simulated using EGF method

The EGF method, which has been used in simulating ground motion at a single location, is extended here to synthesize spatially varying horizontal ground motion at bedrock. The seismic scenario is the October 10, 1980 El-Asnam Earthquake of magnitude $M_s = 7.3$, for which ground motion records are not available. The earthquake occurred at 12:25 GMT, and

the hypocentre was estimated to be at 36°17'N, 1°41'E at a depth of 12 km (Cisternas *et al*., 1982). The ground motion from the $M_L = 5.6$ aftershock of 08 November 1980 recorded at the Sogedia Factory Station (see Fig. 3.2) is used as EGF. We note that only one aftershock from the source of the target event is available at the study site. In a more favourable situation, where multiple aftershocks would be available, it is preferable to use them as Green's functions from different sections of the source to the site. This would allow for a more accurate representation of the path effect, especially for large faults. The epicentral distance of this station is about 5 km. The aftershock event took place in the same rupture zone as the mainschock (target) and had a similar faulting mechanism (Cisternas *et al*., 1982). In the following, the mainshock, for which ground motion is being simulated, is called the target event. The aftershock, from which EGF is obtained, is called as the small event.

In order to simulate ground motion at bedrock, the EGF should also correspond to the bedrock. Since the bedrock is not outcropping at the recording station, deconvoluted motion (Petrovski and Milutinovic, 1981) corresponding to the bedrock is utilized. The time series of the deconvoluted motion is baseline corrected using the method described in Rupakhety *et al*. (2010). The horizontal components of ground acceleration corresponding to the bedrock are shown in Fig. 3.3. The fault plane is assumed to be 40 km x 15 km, with a dip angle of 60° (see Fig. 3.4). Shear wave velocity is equal to 2 km/s (Petrovski and Milutinovic, 1981; Yielding *et al*., 1981), and the corresponding rupture velocity (v_r) is equal to 1.44 km/sec. The stress drop of the mainshock is 100 bars (from Dechamps *et al*., 1982). For the small event, a value of 82.57 bars is calculated by using the relation given by Boore (1983) and a corner frequency of 0.37 Hz obtained from a spectral fitting procedure described in Chapter 4. This gives a stress drop ratio, (c) equal to 1.21. The fault plane is divided equally into seven parts in both directions. The scale factor parameter, N, is equal to 7, and the number n' is taken to be 20. The Fourier spectrum (FAS) of the aftershock (see Fig. 4.1 in Chapter 4) is characterized by a significant trough around 5Hz, which yields a rise time of $\tau_e = 0.2$ sec. Using the similarity condition (Eq. 4.4), rise time for the mainshock is estimated to be $\tau = 1.4$ sec. The latter value is close to the 1 sec adopted by Dechamps *et al*. (1982). Other relevant parameters used in the simulation are given in Table A.1 in the Appendix.

The location of hypocentre is shown with a red star in Fig. 3.4. It lies on cell $(i_0, j_0) = (7, 4)$ from where the rupture is assumed to propagate radially. In the presented methodology, the total seismic moment of the target event is assumed to be uniformly distributed over the entire fault plane. This assumption was invoked due to the lack of information about the actual (or expected) slip distribution of the past (or future) event. If heterogeneous slip distribution models are available, the methodology can be extended to account for non-uniform slip distribution. This can be done by scaling the contribution of each sub-fault in the total motion in proportion to the seismic moment released at the sub-fault,

keeping the total seismic moment unchanged. Horizontal components of ground acceleration are then simulated at five stations at bedrock, namely $S^{(0)}$, $S^{(1)}$, $S^{(2)}$, $S^{(3)}$ and $S^{(4)}$ (see Fig. 3.4). Station $S^{(0)}$ is considered to be reference station, and it lies directly under the Sogedia Factory station. The other stations are separated from it by 40 m, 100 m, 200 m, and 500 m. These are the same distances as those considered by Zerva and Harada (1997) in their shear strains estimation for buried structures. Evaluation of seismic ground strains requires coherency models developed for strong motion shear wave windows that are valid at short separation or epicentral distances. The epicentral distance of the reference station is 5 km. Simulation of ground motion and estimation of lagged coherencies were performed by computer codes developed by us.

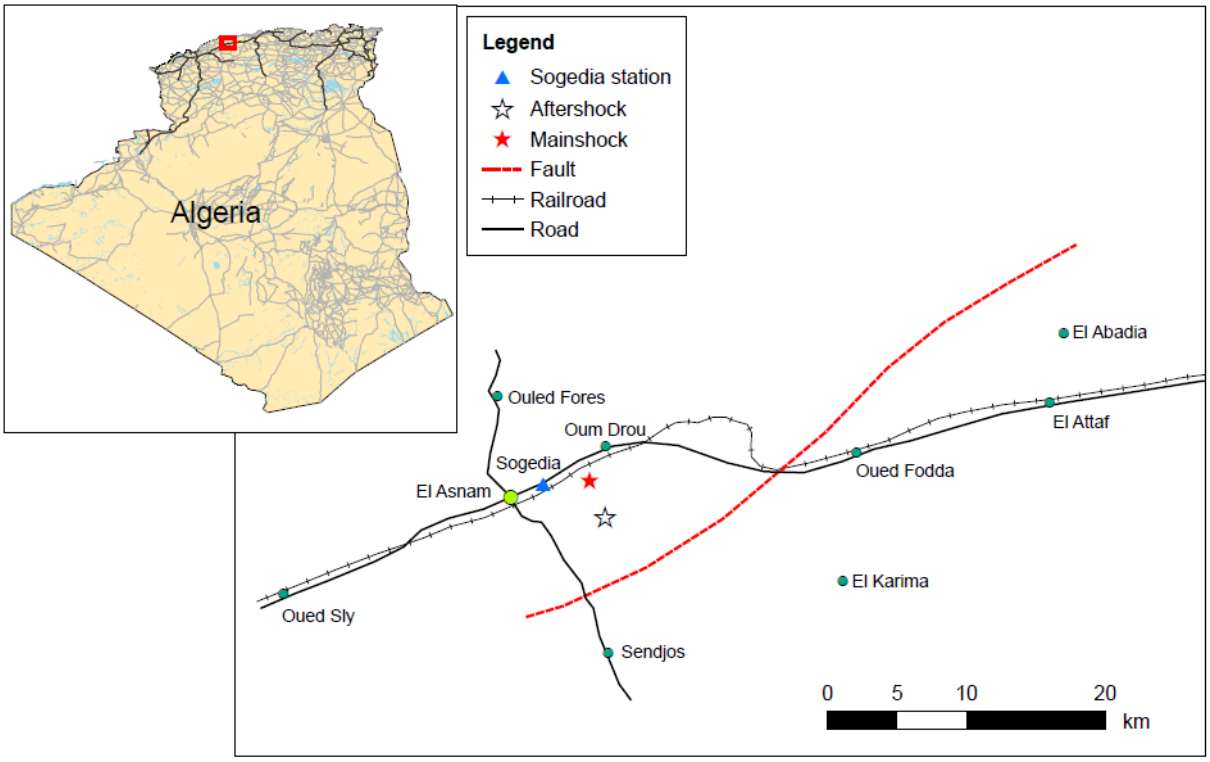

Fig. 3.2 - Map of the epicentral region of the 10 October 1980 El-Asnam Earthquake (simplified from Despeyroux, 1984). Epicentral locations (from Cisternas *et al*., 1982) and the Sogedia Factory station are indicated.

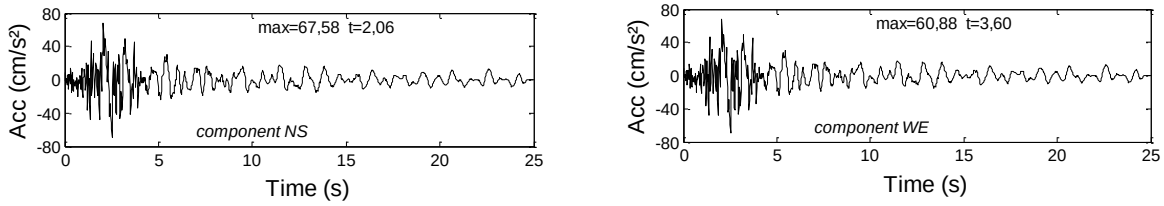

Fig. 3.3 - Acceleration of bedrock (NS and WE components) obtained by deconvolution of ground acceleration due to the 8 November 1980 aftershock recorded at the Sogedia Factory station. The acceleration time series are from Petrovski and Milutinovic (1981).

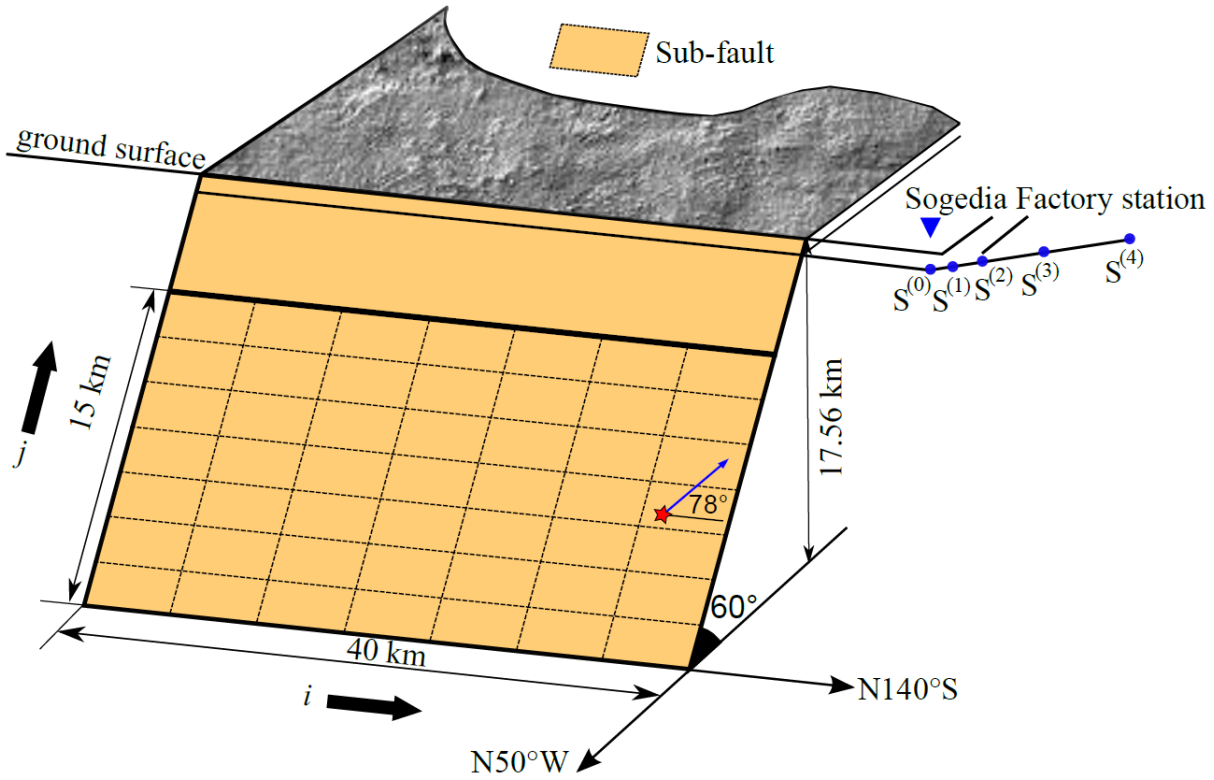

Fig. 3.4 - Schematic representation of the finite-fault model corresponding to the 1980 El-Asnam mainshock; the star indicates the location of the hypocentre, the blue triangle represents the Sogedia Factory Station which recorded the 8 November 1980 aftershock, and the blue dots represent the locations of bedrock stations at which ground motion is simulated (dimensions are not to scale).

Ground acceleration time series simulated at the five stations are shown in Figs. 3.5 and 3.6. Peak ground acceleration (PGA) of the simulated motion is close to 60% of acceleration due to gravity. Figure 3.7 presents the smoothed (with an 39-point Hamming window) power spectral densities of the aligned data at the five stations (Fig. 3.6) and smoothed cross amplitude spectra between reference station $S^{(0)}$ and stations $S^{(1)}$, $S^{(2)}$, $S^{(3)}$ and $S^{(4)}$ at separation distances of 40, 100, 200 and 500m, respectively. It can be clearly seen from Fig. 3.7a that the power spectral density (as a square of the Fourier amplitudes of the data) is a clearer descriptor of the characteristics of the seismic motions than the autocovariance

function. Figure 3.7a suggests that the PSDs at five stations have a fairly similar frequency content, which should be consistent with the shape of their autocovariance functions. The peaks in the spectra occur at the same frequencies, with the highest peak at a low frequency of approximately 1 Hz (the predominant frequency of the rock) and essentially the same amplitude at all stations, except for the station for $S^{(4)}$ at 500 m, where the peak occurs at the high frequency of 7.5 Hz. At a high frequency of 7.5 Hz, i.e., short wavelength, wave energy arrives to all stations from the fault after performing a high number of cycles of propagation in the rock. Therefore, wave energy should be highly attenuated and arrive with low amplitude. At the low frequency of 1 Hz with a long wavelength, they are less attenuated and arrive with high amplitudes. This trend is not observed at the station $S^{(4)}$, which implies that its high peak of 7.5 Hz is not real but is produced artificially by the digital summation in equation (4.1).

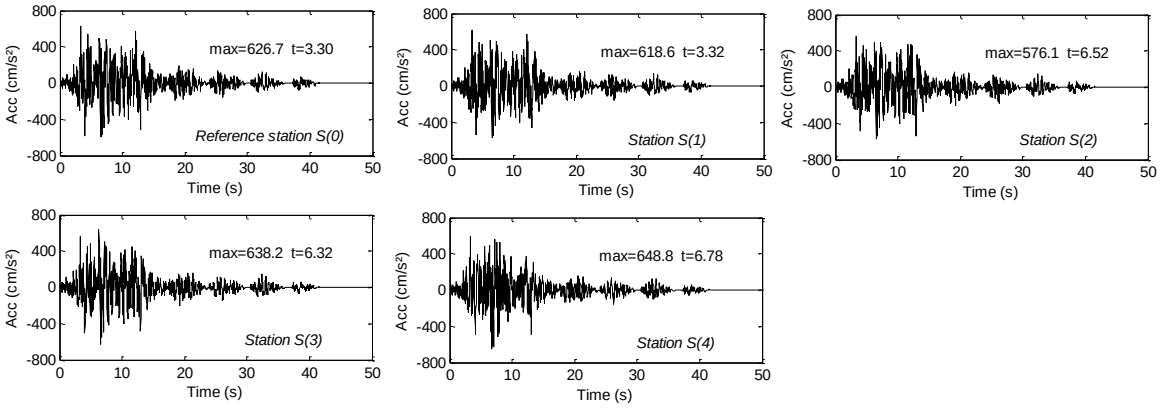

Fig. 3.5 - Transverse (orthogonal to the epicentral direction) component of ground acceleration simulated at the five stations.

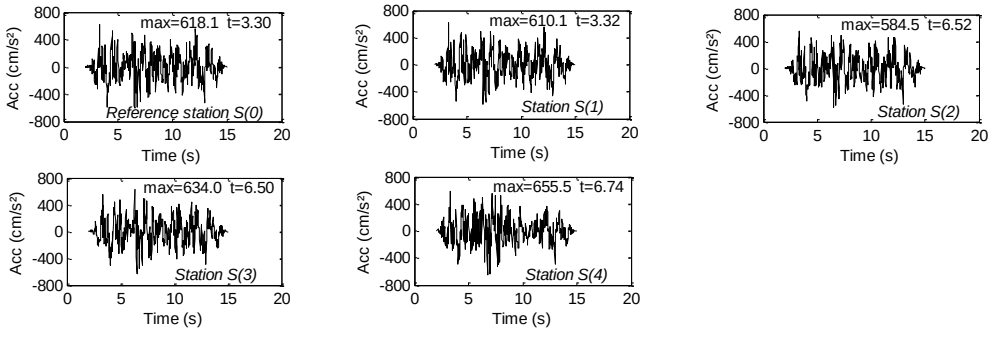

Fig. 3.6 - Transverse component of aligned, tapered time histories corresponding to the non-aligned data at the five stations presented in Fig. 3.5. As described in Chapter 2, Sec. 2.5, first, the stationary part signal (by visual inspection of time evolution of Arias Intensity of time series in Fig. 3.5) is extracted, demeaned and then tapered with Tukey window with the end taper length equal to 15% of the length of the signal. The tapered stationary signals are aligned to eliminate wave passage effects. These aligned tapered signals are used to compute lagged coherencies shown in Fig. 3.8 (left). The duration of the strong S-window is T = 13sec (2.00-15.00sec).

On the other hand, the fairly similar frequencies content and amplitudes in PSDs between stations, i.e., no significant variation with the separation distance, are related to the fact that the stations are considered to be located on the same rock conditions through the use of a single Green function, where the waves propagate over long distances without encountering variability in the rock strata along their path. In addition, 500m is considered as low value for the maximum separation distance between stations. It is not sufficient to have larger differences in radiation $R_s(\theta,\varphi)$ and attenuation $1/r$ in equation (4.1) between stations. These considerations result in a less pronounced difference between the motions at the stations. It is noted that the PSDs of bedrock motions in Fig 3.7a possess several significant modes of vibration. It shows that the point estimates of the motions should be described by seismological models rather than by engineering ones, such as the Kanai-Tijimi (1957, 1960) or the Clough–Penzien spectrum (1975) of ground motions on soil sites, which model only the effect of the local soil conditions, since the bedrock excitation is a white process.

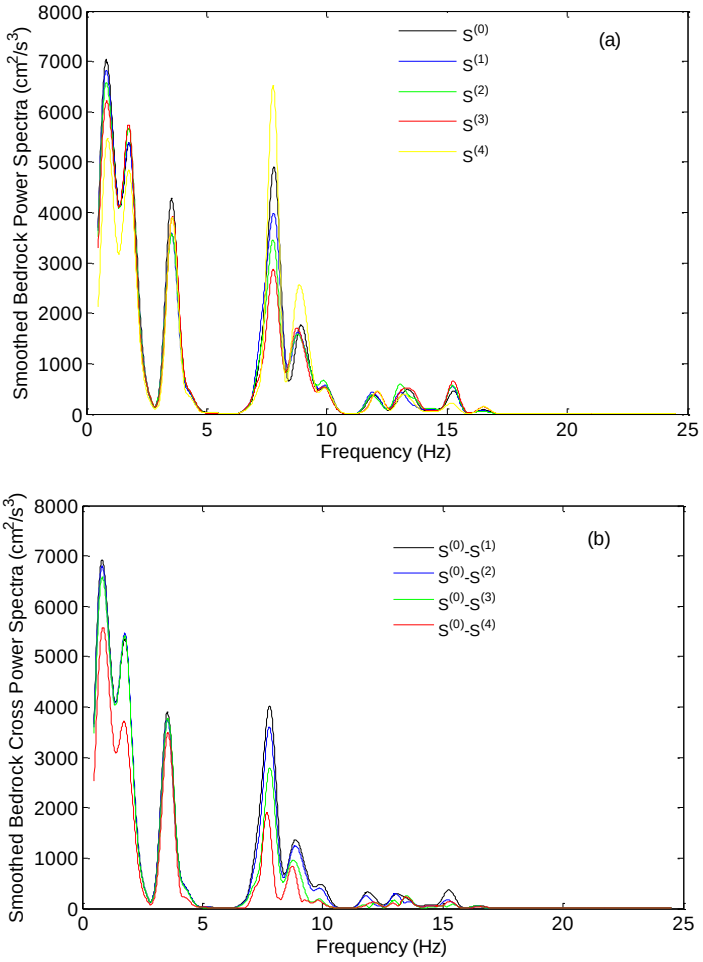

Fig. 3.7 - Smoothed power spectral density functions (a) and smoothed cross amplitude spectra (b) derived as described in Sec. 2.5 and the M = 39 Hamming window of the aligned time histories of Fig. 3.6.

As was the case for the smoothed power spectral densities (Fig. 3.7a), the cross spectra are sharply peaked. It can be clearly seen from the figures 3.7a and 3.7b that the similarity in the frequency content data (Fig. 3.7a), due to the above considerations, leads to similar cross amplitude estimates (Fig. 3.7b). Whereas, the more differentiated PSD stations data (which occur when using multiples Green functions or/and longer separation distances) should yield cross amplitude spectra with significant differences in their frequency content. Figures 3.7a and 3.7b provide the reference figures for the evaluation of the lagged coherency of the present case study following the procedure given in Section 2.5. As the shear waves do not contribute to the motions above the value of around 9 Hz for all stations, the lagged coherency functions will be shown only up to 9 Hz and not up to the cutoff frequency of 25 Hz used in the analysis so that the comparison may be made with the other coherencies presented in the next chapter of the parametric study. The fitting of analytical parametric models to the data will be up to 8Hz.

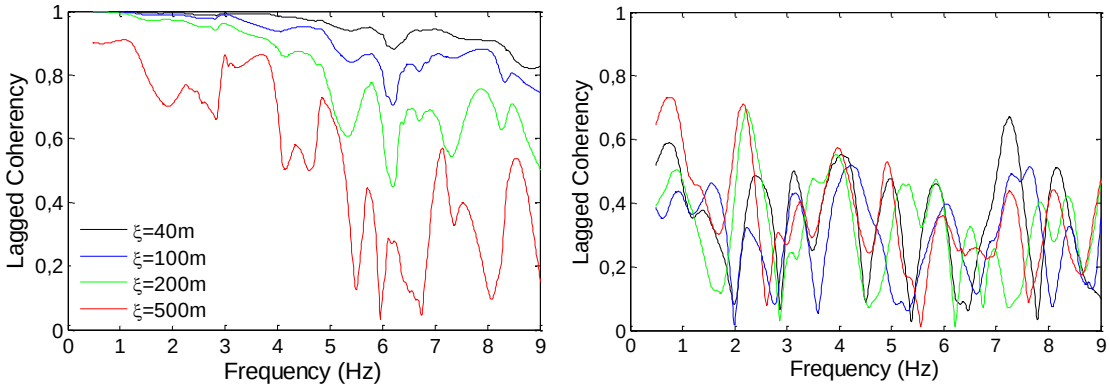

Fig. 3.8 - Lagged coherencies (left) at the four stations obtained from ground acceleration time series shown in Fig. 3.6. Lagged coherencies (right) estimated from the Boore's point source model (Eq. 4.6).

Lagged coherencies computed from the simulated signals (Figs. 3.5 and 3.6) are shown in Fig. 3.8 (left). The spectral and spatial characteristics of the simulated lagged coherencies, as shown in Fig. 3.8 (left), are similar to that reported in the literature (for example, Zerva, 2009). In general, lagged coherency decays in both frequency and space. The lagged coherencies for the short separation distances of 40 and 100m show frequency decay less significant than that for a separation distance of a few hundred meters. It is noted that the coherency estimate for a separation distance of 500m first decreases with frequency, then starts increasing around 7 Hz. Such increase of coherency with frequency is physically not meaningful and is most likely due to uncertainties in the spectral estimation and smoothing operation (e.g., Zerva, 2009 and Rupakhety and Sigbjörnsson, 2012). The coherency is significantly less than 1.0 at low frequencies (1-2 Hz) for the long separation distance of 500 m and at intermediate frequencies (3-5 Hz) for the medium separation distance of 200 m.

Such loss in coherency has been attributed to scattering of waves along the propagation path caused by heterogeneities in the path and near the stations due to heterogeneities near the surface (see, Zerva, 2009).

It is noted that such effects are not fully modelled in the present simulation method because EGF is available at only one station. In this sense, the spatial variation of scattering effects is not captured in the simulation. The relatively low value of incoherence at low frequencies and large separate distance may, therefore, be due to source effects in the near field, which are found to be prominent at low frequencies (Abrahamson *et al*., 1991). This behaviour can also be explained by the fact that the term t_{ij} in (Eq. 4.3) might become nearly random in the near-field region of a rectangular fault plane (Irikura, 1986). Consequently, the phase difference between two stations increases with increasing separation distances. In the far-field, the source to site distance is large compared to the inter-station separation distance of a few hundred meters. Therefore, the loss of coherency with separation distance is less pronounced than in the near-field, as the term t_{ij} is almost the same for the different stations.

The results of the simulation indicate that source effects in coherency are significant; considerable loss in coherency is obtained just by modelling the source effect. On the other hand, the source effects, site effects, and scattering effects may constructively and destructively interfere in coherency decay (see Zerva, 2009 for a detailed discussion). Therefore, isolating these different effects from recorded data is not straightforward. The simulation method presented in this work models coherency decay mainly due to source effect, which seems significant for the case under study.

For comparison, Fig. 3.8 (right) shows the lagged coherencies estimated from the simulated accelerations at the same rock stations by using the Boore's point source model (Eq. 4.6) and the same spectral estimates of coherency. This lagged coherency, which is low, occurs because the stochastic point source model does not contain built-in coherency (Boore, 2003). The low lagged coherency is also typical for any pair of simulated records and is independent of ξ, which is not in agreement with the observed coherency structure from actual records (e.g., Harichandran and Vanmarcke, 1986). Different authors (e.g., AfifChaouch *et al*., 2003) suggested that a finite source produces more incoherent motion than a point source, because, in the near-field of an extended seismic source, ray paths extending from different portions of the ruptured fault give rise to differential ground motion at two points some distance apart because of different azimuths, incidence angles, attenuation, and scattering paths.

3.3 Parametric modelling of spatial coherency

In this section, we calibrate the three selected parametric models (see Sect. 2.5) to the coherency functions computed from simulated ground motion corresponding to the 1980 El-Asnam Earthquake (see Section 3.2, and Fig. 3.8 (left)). The functional form of the models is taken to be the same as that of Hindy and Novak (1980), Luco and Wong (1986) and Somerville *et al*. (1988) and is presented in Eqs. (2.43) and (2.44). These models were selected because they have been extensively used by researchers in seismic response analysis of lifelines. Since these models do not explicitly consider scattering effects and noise, they are often viewed as a plane wave coherency models, and are, therefore, suitable for our analysis. We note that we tried to calibrate Harichandran and Vanmarcke's (1986) model without success, as this model did not seem to be well constrained by the simulated coherency data. To calibrate the parameters of the Hindy and Novak (1980), Luco and Wong (1986) and Somerville *et al*. (1988) models, we use non-linear, least squares regression in the hyperbolic arctangent $\left(\tanh^{-1}\right)$ transformation of lagged coherency. Such a transformation is preferable because the transformed variable has an approximately frequency independent variance (Jenkins and Watts, 1969). The frequency and separation distance ranges used in fitting the model were $\left[0-8\right]$ Hz and $\left[0-500\right]$ m, respectively. The regression parameters and the goodness of fit of the models (i.e., the coefficient of determination R-square and the Root mean squared error RMSE) are found to be:

Hindy and Novak	Luco and Wong	Somerville *et al*.
$\alpha = 5.87\times10^{-5}$ sec m^{-1} rad^{-1}	$\alpha = 9.41\times10^{-5}$ sec m^{-1} rad^{-1}	$a = 7.42\times10^{-6}$ m^{-1}
$\lambda = 1.52$	---	$b = 1.03\times10^{-6}$ sec^2 m^{-1} rad^{-2}
R-squared = 0.88	R-squared = 0.82	R-squared = 0.89
RMSE = 0.30	RMSE = 0.38	RMSE = 0.29

The comparison in Fig. 3.9 shows that the Hindy and Novak, and Somerville *et al*. models are flexible and fit the data well for the four separation distances. At 500m, the Hindy and Novak model fits better in low frequencies, 0-2Hz, than the Somerville *et al*. model. The Luco and Wong model fits the simulated lagged coherencies relatively well for separation distances up to 100 m. For a separation distance of 200 m, the fit is good up to a frequency of 6 Hz. For a separation distance of 500 m, it falls and differs significantly from the estimated coherency function except at low frequencies up to 2Hz.

The quality of fit is also clear from the residuals in the $\tanh^{-1}$ transformation as shown in Fig. 3.10. The mean value of the residuals is generally closest to 0, while it is clearly most biased for a separation distance of 500 m in the Luco and Wong model. Residuals were

calculated as the difference between data and model, which are then normalized by the constant standard deviation. For the lagged coherency, the residual is defined as: $R_{\gamma,ij}(\xi,\omega)=\left(\tanh^{-1}\left|\gamma_{ij}\right|-\tanh^{-1}\left|\gamma_{m,ij}\right|\right)\Big/\sigma_{\gamma}$ with, $\sigma_{\gamma}=1.09$, a value estimated (Jenkins and Watts, 1969) using $B=0.03$ Hz (Eqs. 2.31 and 2.32 with M = 39) as bandwidth and a stationary window duration of T = 13 sec.

The present results indicate that the Hindy and Novak parametric model can be used as a first approximation, or, at the least, an upper bound of the lagged coherency of the motions on the ground surface in the near-field region of the El-Asnam Earthquake scenario. This model, with the PSD functions (Fig. 3.7a), could be useful in a random vibration analysis or the generation of spatially variable ground motion for a time history analysis of lifeline structures in our study area of El-Asnam. Because of the differentiable condition required in seismic strain estimates in Chapter 5, the Luco and Wong model will be used rather than the Hindy and Novak model.

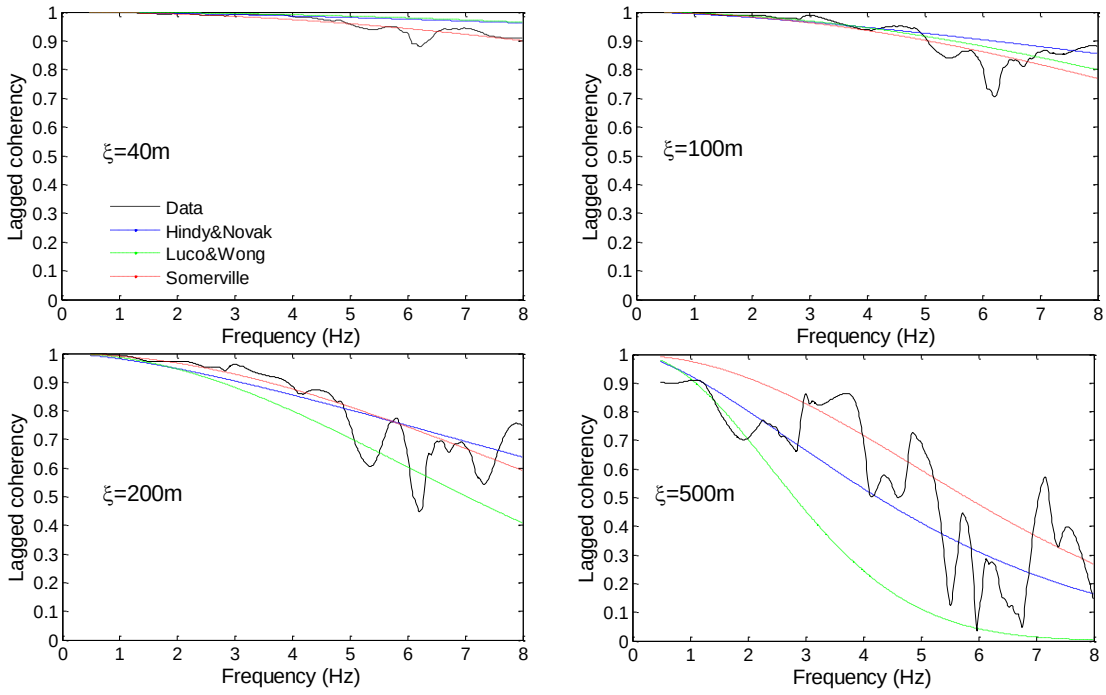

Fig. 3.9 - Lagged coherencies of transverse ground acceleration at bedrock (see Fig. 3.5) due to the 1980 El-Asnam Earthquake (solid lines) and the corresponding parametric models (dashed lines).

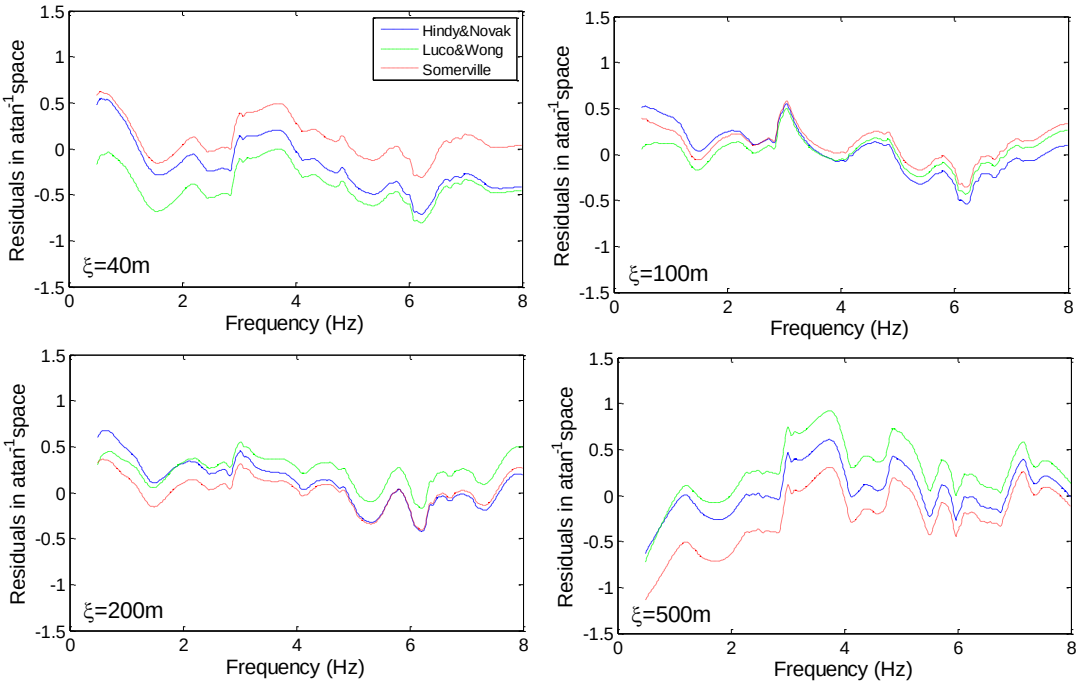

Fig. 3.10 - Residual $\tanh^{-1}$ lagged coherencies corresponding to the simulated results and fitted models shown in Fig. 3.9.

CHAPTER 4

SENSITIVITY ANALYSIS OF SIMULATED COHERENCY

Sensitivity analysis of simulated coherency:

It is well known that the coherency of ground motion is affected by seismic source, propagating medium, site conditions, the relative orientation between the source and the site (directivity), and parameters such as fault orientation and fault depth (Jin *et al*., 2000; Ding and Song, 2010). The sensitivity of ground motion parameters at a station simulated by the EGF method has been already studied. However, the sensitivity of the coherency of the simulated ground motion to the parameters used in simulation has not been studied. In this section, such a sensitivity analysis is presented.

The main objective of this chapter is to identify the simulation parameters which have a large influence on simulated coherency functions and, therefore, need to be well constrained for simulation of the strong ground motion field (Zerva, 1994; Jin *et al*., 2000). The parameters considered in this analysis are magnitude (source parameter), wave velocity (path parameter), and epicentral distance (path parameter). It is noted that other source phenomenon, such as heterogeneous slip distribution, directivity effect, focal mechanism, depth of the epicenter, rupture velocity, numbers of sub-sources, etc., can influence the coherency of resulting ground motions (Zerva and Shinozuka, 1991; Ding and Song, 2010). Parameters such as slip distribution and the directivity effect are not easily modelled (or predicted for future events). In this sense, priority is given to those source parameters that are relatively well understood in the sensitivity analysis presented in this work. The effects of other relevant source parameters are outside the scope of this study, but parametric studies investigating such effects could shed more light on source effects in the coherency of ground motion in the near-fault and are currently underway. Because EGFs corresponding to various scenarios of these parameters are not available, we use the HGF method (Sect. 3.1) for ground motion simulation.

The stress-drop ratio, c, is assumed to be 1. We also investigated the effect of this parameter in coherency estimates and decided that a value equal to 1 was suitable. It was found that, although this parameter has some effects in simulated ground motion amplitudes, lagged coherencies were not very sensitive to this parameter. A direct implication of changing this parameter is the change in number of sub-faults to be used in simulation. If too few sub-faults are used (corresponding to large values of c), the finite-fault effect is not appropriately modelled. Such a situation is not likely because, within reasonable variations of the parameter, the number of sub-faults remains unchanged (see Eq. 4.4) as it is rounded off to the next integer. When a suitable value of number of sub-faults is selected, c needs to be adjusted to conserve the seismic moment. The simulated coherency functions were found to be relatively insensitive to the choice of this parameter as long as a reasonable number of sub-

faults is used in the simulation. In the HGF method, the EGFs are simulated using the stochastic method with a theoretical source spectrum given in Eq. (4.6).

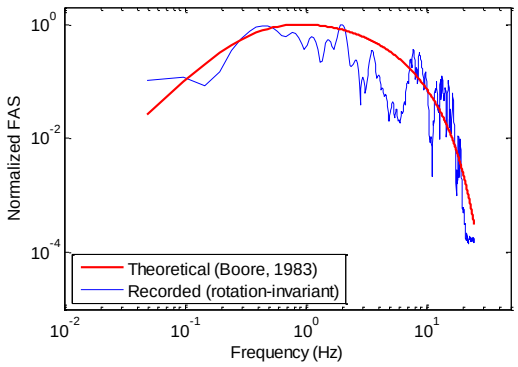

Fig. 4.1 - Comparison between the recorded and theoretical FAS (normalized by its maximum) of ground acceleration at bedrock. The recorded spectrum is obtained from the 8 November 1980 aftershock at Sogedia Factory station deconvoluted at bedrock (see text above for more details). The hypocentral distance is 12.96 km, and an average radiation pattern of 0.868 is used.

Some parameters of the spectrum are kept constant for all scenarios, namely, $FS = 2$, $PJ = 0.71$ and $\Delta\sigma = 100$ bars (from Dechamps *et al.*, 1982). The parameters Q_s , f_c and f_m were obtained by fitting the theoretical source spectral model of Eq. (4.6) to the FAS of the deconvoluted aftershock ground motion time series recorded at the Sogedia Factory station (Fig. 3.3). Only the shear wave parts of the two horizontal components of motion were extracted and windowed. Rotation-invariant estimate of FAS of horizontal motion is then obtained based on the formulation presented in Rupakhety and Sigbjörnsson (2014). The FAS is fitted to the theoretical model yielding $Q_s = 45$, $f_c = 0.368$ Hz and cut-off frequency, $f_m = 20$ Hz. Figure 4.1 shows a comparison between the rotation invariant spectra and the theoretical model fitted to it. The other parameters required for simulating EGF are mentioned in the following sections as they depend on the different scenarios being simulated. Using the FAS spectra and phase spectrum obtained from the aftershock record, EGF are simulated using the stochastic method. These EGFs are then used to simulate ground acceleration at the five bedrock stations. Coherency estimates are obtained from the simulated ground motion using the procedure described in Section 2.5.

4.1 Effect of shear wave velocity

Shear wave velocity, and rupture velocity which are closely related, play an important role in how the seismic waves radiated from the different sections of an extended source superimpose in time at a station. Since the superposition of these waves at nearby stations is expected to affect coherency of motion across the stations, we study the sensitivity of

coherency to shear wave velocity. Three different scenarios of generic rock with $v_s^a = 1500$ m/s, $v_s^b = 2500$ m/s, and $v_s^c = 3500$ m/s are considered to simulate ground acceleration at the five stations using the HGF method. Table A2 in the Appendix lists the others relevant properties of the generic rocks (from Chapellier and Mari, 2011). Transverse component of simulated ground acceleration by using HGF method for the three generic rocks are shown in Fig. 4.2, and their corresponding lagged coherencies are shown in Fig. 4.3.

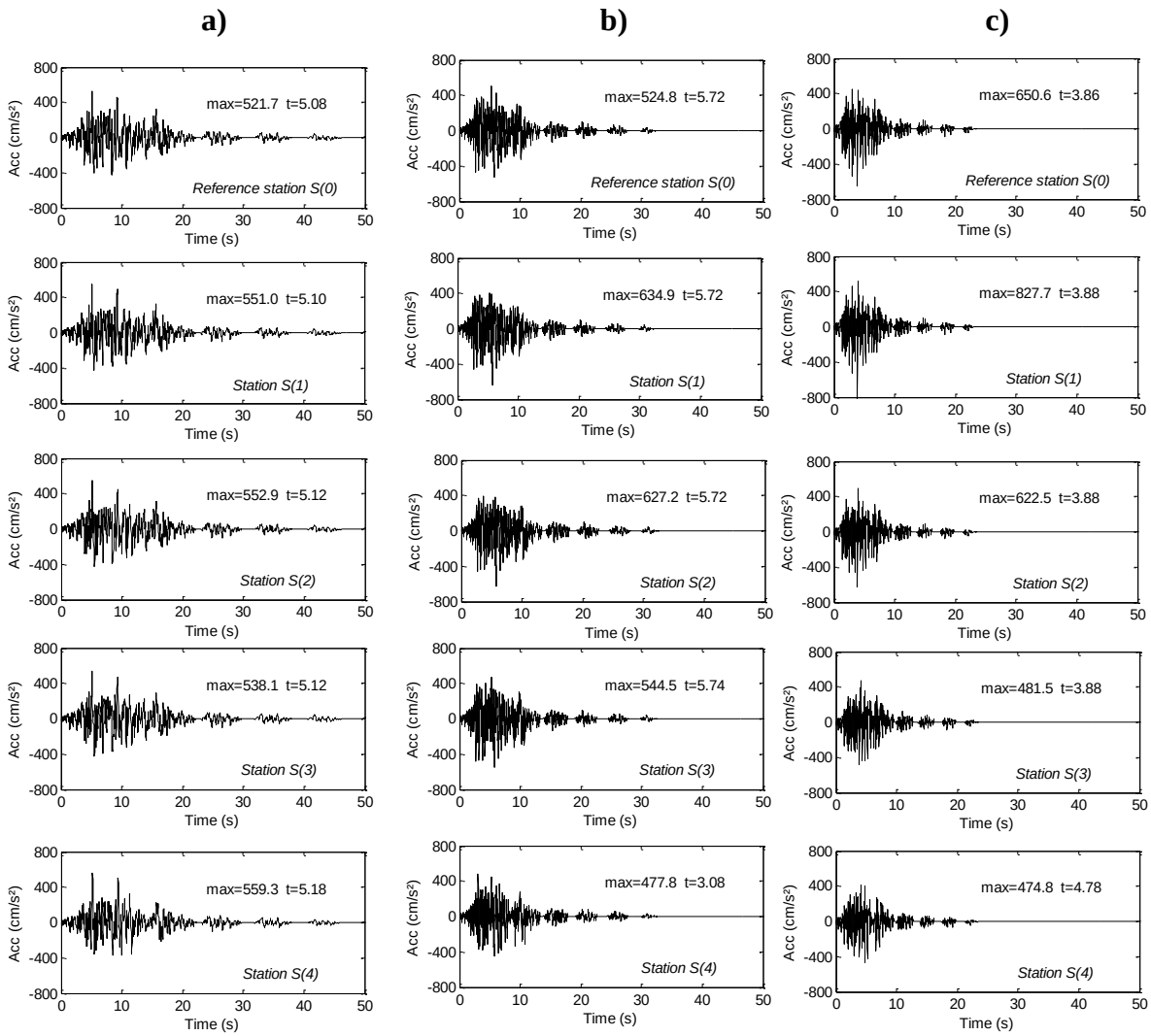

Fig. 4.2 - Transverse ground acceleration simulated at the five stations for three generic rocks: **a)** for $v_s^a = 1500$ m/s, **b)** for $v_s^b = 2500$ m/s, and **c)** for $v_s^c = 3500$ m/s.

The results indicate that at low frequencies (<2 Hz) lagged coherency is not very sensitive to shear wave velocity. At such low frequencies, the wavelengths of shear waves are not as sensitive to variations in wave velocity as they are at high frequencies. High sensitivity of wavelengths might result in high sensitivity of coherency within a small spatial area. It is also observed that the decay of coherency with frequency is faster when the shear wave velocity is

lower. At frequencies above 2 Hz, the coherency seems, in general, to increase with shear wave velocity, except for a separation distance of 500 m, where the increase is not consistent for all frequencies. The overall increase of coherency with shear wave velocity is expected from the fact that the differential arrival time of shear waves radiated from different sections of the fault decreases with increasing wave velocity. Increasing wave velocity also implies smaller time difference in arrival of waves radiated from a sub-fault at different stations, which results in higher coherency. It should be noted that the simulation method used here considers only the source effect in loss of coherency, and does not take into account scattering effects in the propagation medium and near the receiver. Even in lack of these scattering effects, considerable loss in coherency is observed at medium and high frequencies, which implies that source effect alone can have significant effect on coherency. This effect is expected to be more pronounced in the near-field region (e.g., Abrahamson *et al.*, 1991) - which is the case of the present analysis - for the reasons explained in Section 3.2.

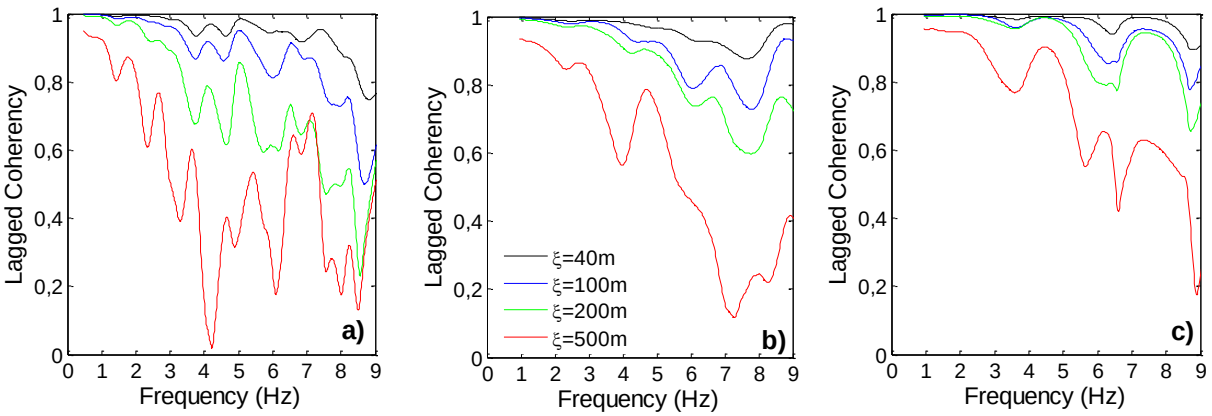

Fig. 4.3 - Lagged coherencies of transverse ground acceleration for three generic rocks: **a)** for $v_s^a = 1500\,\text{m/s}$, **b)** for $v_s^b = 2500\,\text{m/s}$, and **c)** for $v_s^c = 3500\,\text{m/s}$. The black, blue, green, and redlines correspond to separation distance of 40m, 100m, 200m, and 500m, respectively.

4.2. Effect of earthquake magnitude

Abrahamson *et al.* (1991) show some evidence of magnitude dependence of coherency: at frequencies below 5 Hz small magnitude events tend to have lower coherency than large magnitude events while at frequencies of 6 to 10 Hz, the reverse is true. Somerville *et al.* (1988) suggested that coherency for aftershocks is greater at all frequencies than that for mainshock in the near-field.

To study the effect of the magnitude on bedrock coherency, we compute accelerograms which correspond to two earthquake events. One of them corresponds to the 1980 El-Asnam

mainshock with $M_s = 7.3$ $\left(M_0 = 540\times10^{24}\text{ dyne-cm}\right)$ and the other one corresponds to the 13 May 1995 Kozani-Greneva Earthquake with $M_w = 6.5$ $\left(M_0 = 55\times10^{24}\text{ dyne-cm}\right)$ which occurred in North-western Greece. The five receiver stations are placed on bedrock of type b (shear wave velocity equal to 2500 m/s, see Table A2 in the Appendix) for both events. For the larger event, simulations are based on the HGF method using aftershock data from 8 Nov 1980 aftershock. The fault geometry is considered to be the same as that of the El-Asnam Earthquake, with $N=7$ and $(i_0, j_0)=(7,4)$. For the smaller event, hybrid Green's functions are simulated from the recording of the largest aftershock of Kozani-Greneva Earthquake that occurred on 15 May 1995 with $M_w = 5.1$ $\left(M_0 = 0.44\times10^{24}\text{ dyne-cm}\right)$. For this event, a rectangular fault with dimensions $29\text{ km}\times 13\text{ km}$ is divided into 5×5 sub-faults. The strike, dip, and the rake of this event are taken to be the same as that of the El-Asnam mainshock, the cut-off frequency is taken to be 7 Hz and the stress-drop 12.19 bars. The relevant parameters of this event are taken from Roumelioti *et al*. (2000). The rupture is assumed to start at the cell $\left(i_0, j_0\right)=\left(1,2\right)$ with radial propagation. The resulting lagged coherency functions are shown in Fig. 4.5 and their corresponding simulated motions are in Fig. 4.4.

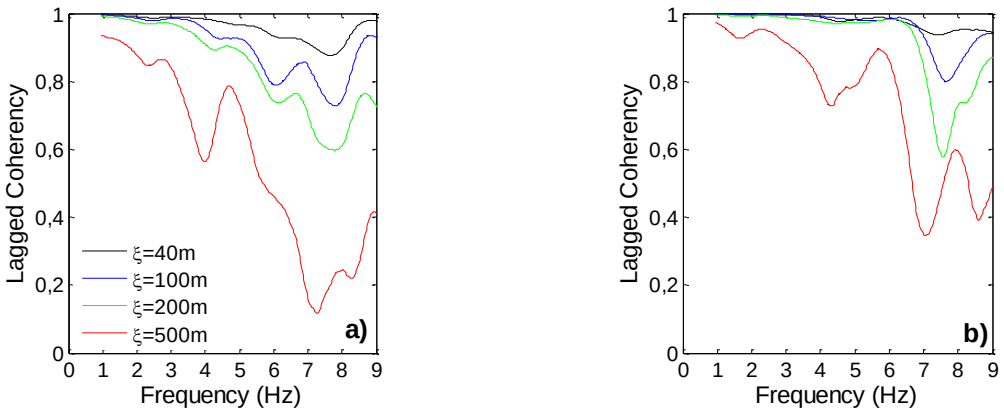

Fig. 4.5 - Lagged coherency at bedrock for **a)** large magnitude and **b)** and small magnitude earthquakes. The black, blue, green, and red lines represent separation distance of 40 m, 100 m, 200 m, and 500 m, respectively.

It is observed that coherency of smaller earthquake is larger than that of the larger one at all frequencies which is consistent with the observations of Somerville *et al*. (1988). For the smaller earthquake, and for separation distance up to 200 m, loss in coherency does not start until about 6 Hz, whereas lagged coherency for 500 m separation distance steadily decreases from about 1 Hz. On the contrary, loss in coherency with frequency starts at much lower frequencies for all separation distance for the larger earthquake. Spatial decay of lagged coherency is more pronounced for the larger earthquake. These results indicate the finite source effect on lagged coherency. As the rupture area increases, seismic waves radiated from

different parts of the fault arrive more asynchronously at nearby stations, resulting in loss of coherency.

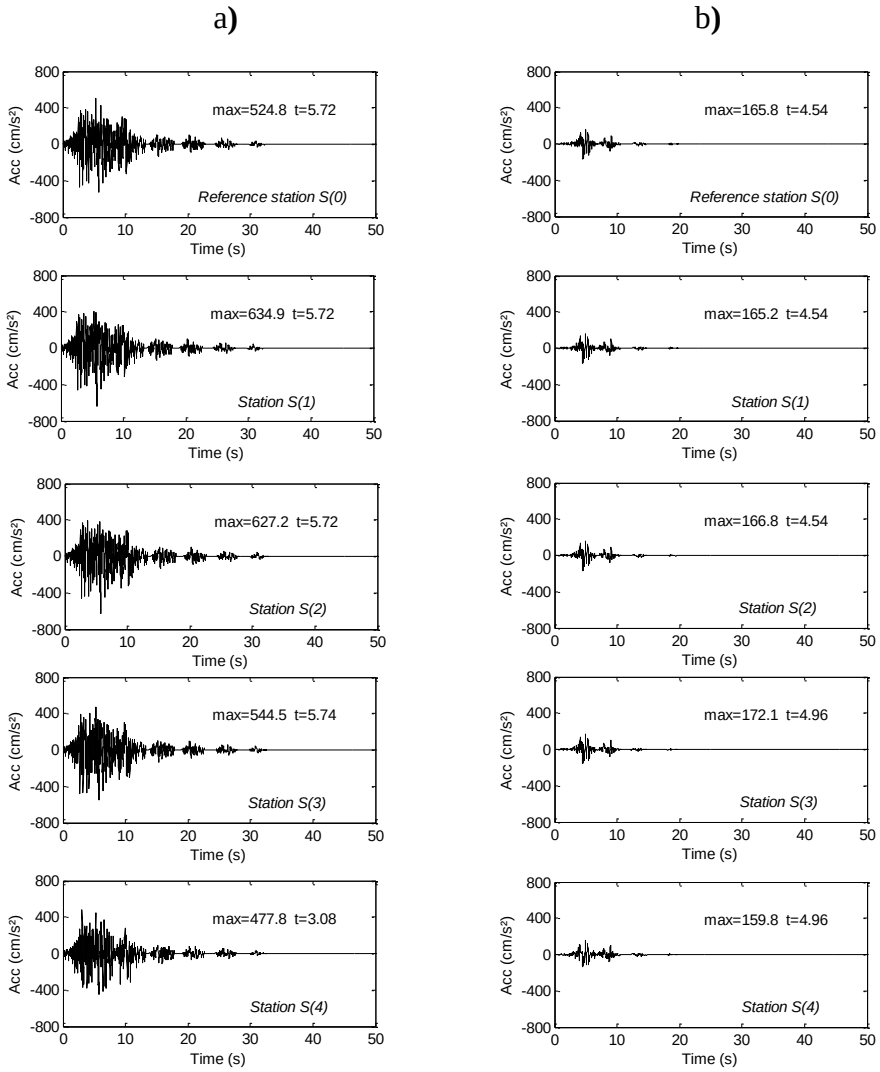

Fig. 4.4 - Transverse ground acceleration simulated at the five stations on the generic medium bedrock ($v_s^b = 2500$ m/s) for **a)** large magnitude and **b)** and small magnitude earthquakes.

4.3. Effect of epicentral distance

Abrahamson *et al*. (1991), using data recorded on soil site at the LSST array in Lotung, Taiwan, observed that coherency in the near-field was lower than that in the far-field at low frequencies, which was interpreted as a source effect, whereas the reverse was true for higher frequencies, which was interpreted as a path effect. Similar results were found by Somerville *et al*. (1988). In the presented simulation method, site effects are not modelled, and thus the loss in coherency is mainly due to source effect. This section investigates the importance of this effect for different epicentral distances.

Three different epicentral distances are considered: $d_1 = 5$ km, $d_2 = 33$ km, and $d_3 = 65$ km, which correspond, respectively, to hypocentral distance of 12.96 km, 35.1 km, and 66.09 km. These three distances are assumed to represent, for the 1980 El-Asnam mainshock, the near-, intermediate-, and far-field (from the Table A3 in the Appendix and given by Hammoutene *et al.*, 1992). By using the HGF method, ground acceleration time series are simulated at three sets of five stations on bedrock of type b. On each set, the reference stations are placed at the epicentral distance mentioned above, and the other stations are separated from it by, 40 m, 100 m, 200 m, and 500 m. All the stations lie on the hanging wall and lie on the radial line from the epicentre of the target event to the Sogedia Factory station. Hybrid Green's functions for the simulation are based on the $M_L = 5.6$ $\left(M_0 = 1.55 \times 10^{24} \text{ dyne-cm}\right)$ event. Figure 4.6 and 4.7 show the generated time histories and the lagged coherency functions at different separation distance, respectively, in the near-, intermediate-, and the far-field.

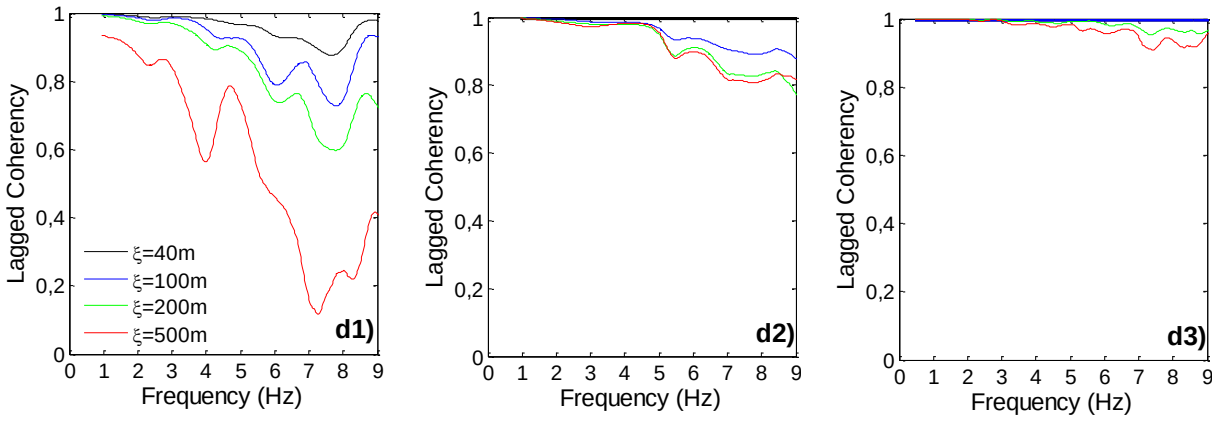

Fig. 4.7 - Lagged coherency functions, from left to right, corresponding to near-, intermediate-, and far-field of the 1980 El-Asnam Earthquake. The black, blue, green, and red lines correspond to separation distance of 40m, 100m, 200m, and 500m, respectively.

It can be observed that lagged coherency increases, at all frequencies, with epicentral distance. In the far-field, and on bedrock, the loss in coherency is negligible up to 8 Hz. This is expected because the simulation method presented here only accounts for the source effect, which is not strong in the far-field. It can be concluded that the effect of finite source in lagged coherency is negligible in the far-field. This implies that scattering and local site effects are the main sources of incoherence. In the near-field, however, considerable loss in coherency is observed, which indicates that source-effects are important. In the near-field, the term t_{ij} in Eq. (4.3) is sensitive to the separation distance between the stations, which implies asynchrony in the arrival of waves radiating from different sub-faults at these stations. This asynchrony results in a loss of coherency. In the far-field, this term is not sensitive to inter-

station separation distance. Therefore waves radiating from different stations arrive almost synchronously at nearby stations. This results in highly coherent motion. The consequence of this differential sensitivity is also apparent from Fig. 4.7, where lagged coherency functions are less sensitive for increasing epicentral distance.

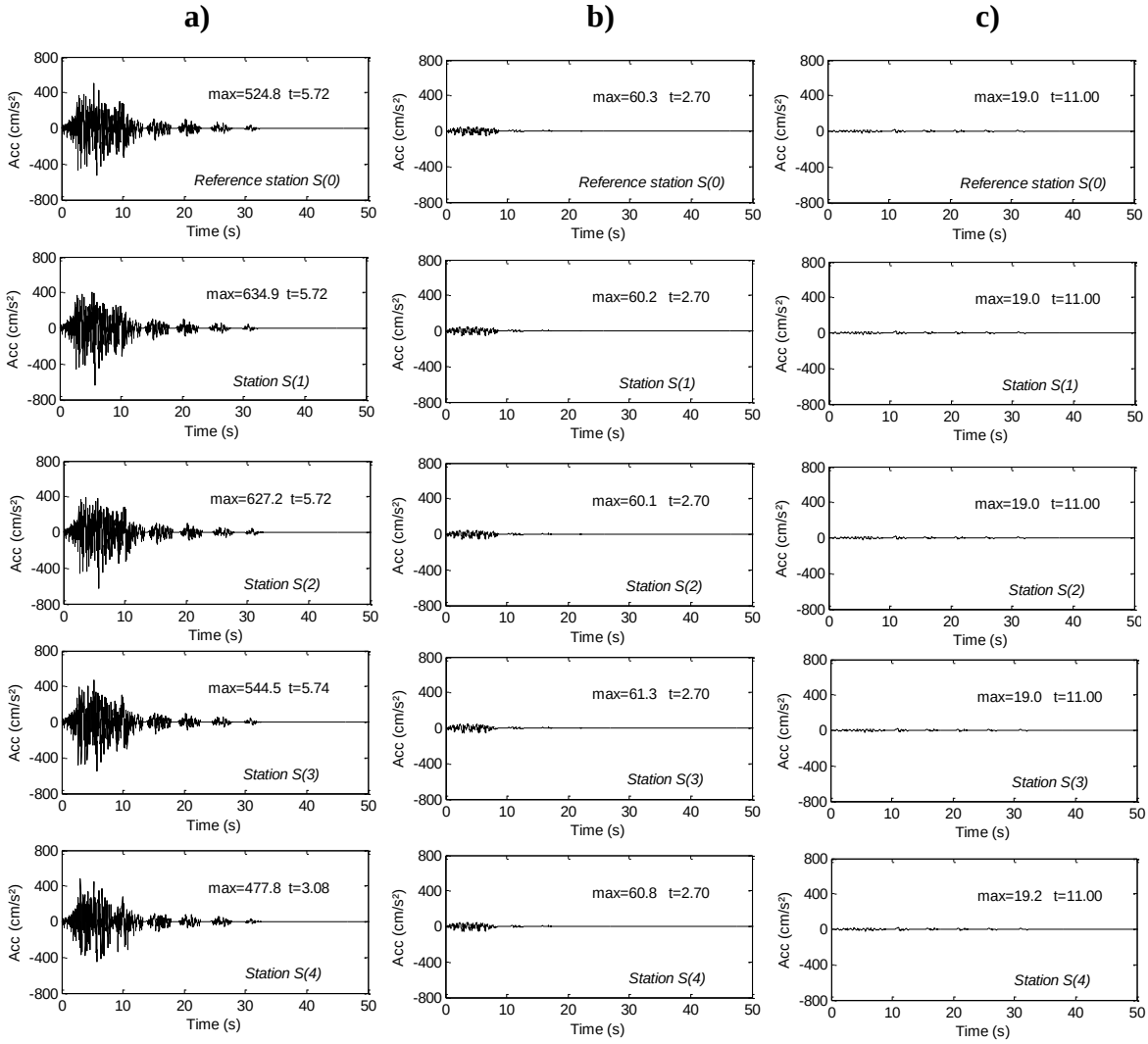

Fig. 4.6 - Transverse ground acceleration simulated at the five stations on the generic medium bedrock ($v_s^b = 2500$ m/s), from left to right, corresponding to near-, intermediate-, and far-field of the 1980 El-Asnam Earthquake.

A word of caution regarding this interpretation is that the presented results account only for finite source effect, and lack modelling of scattering and local site effects. When these effects are present, lagged coherencies in the far-field are expected to be smaller than what is presented in Fig. 4.7.

The present results of the parametric study investigating the sensitivity of lagged coherency showed that shear wave velocity, earthquake magnitude, and epicentral distance are all important factors that contribute to plane wave coherency. Larger shear wave velocity was found to produce more coherent motion in general. Larger earthquakes were found to produce more incoherent motion. In the near-field, the finite source effect seems to be significant, producing incoherent motion. While in the far-field, plane wave coherency was found to be almost equal to one up to a frequency of 8 Hz. Due to the lack of information about ground motions at base rock, there are no statistical coherency function models of base rock. If EGFs with well-known source parameters are not available, the HGF technique seems to be preferable in the sense that it provides at least a first approximation, and possibly an upper bound, on lagged coherencies of any earthquake scenario.

CHAPTER 5

MODELLING AND SIMULATION OF SPATIALLY VARIABLE MOTIONS AT THE SURFACE OF A RANDOM AND SPATIALLY VARIABLE SOIL PROFILE

Modelling and simulation of spatially variable motions at the surface of a random and spatially variable soil profile:

Research on the seismic-resistant design of structures of extended lifeline systems (e.g., Lupoi *et al*., 2005; Walling and Abrahamson, 2007) indicate that the type of response (conservative or unconservative) induced by spatially variable ground motions (SVGMs) compared to that of identical ones depends strongly on the spatial variation models used in the analysis. A realistic characterization of seismic ground motion spatial variation is highly desired. Hence, appropriate modeling of the spatial variation of seismic ground motions, as well as the generation of realistic spatially variable seismic time histories (if time history analysis is considered to deal with material and geometric nonlinearity; its use is recommended in the building codes such as NRCC 2010), becomes important for engineering in the seismic response analysis of extended structures (Zerva and Zervas, 2002; Zerva, 2009).

Coherency and power spectral density functions are commonly used to describe the spatial variation of seismic ground motions at multiple supports of long-span structures. Many coherency function models have been proposed based on theoretical derivation (semi-empirical coherency models) or measured spatial ground motion time histories at dense seismographic arrays (empirical coherency models). Usually, the time window containing the shear wave part of the accelerograms is chosen to estimate the stationary power density and coherency functions. In most cases, the shear wave contains the strongest energy in earthquake recordings and, generally, is the most damaging component from the engineering point of view. The existing empirical coherency models (e.g., Harichandran and Vanmarke, 1986; Menke *et al*., 1990) are dependent on sites/arrays and, even, events (i.e., the fact that they were developed for a particular site and a specific earthquake). They cannot be reliably extrapolated to engineering sites other than those for which the models were developed. In addition to that, there are significant differences in the way the individual investigators apply numerical processing techniques in their spectral estimations, treat the wave passage effect, and select a particular analytical function as a coherency model to fit the data. Researchers have gradually realized that the estimation of a site-specific coherency function that relies solely on an empirical approach is not practical (Der Kiureghian, 1996).

In order to overcome the drawbacks of the empirical approaches, some researchers are resorting to analytical or semi-empirical coherency models (e.g., Luco and Wong, 1986; Somerville *et al*., 1988; Der Kiureghian, 1996). Their techniques rely on combining theoretical derivations and spectral estimation techniques so as to make the coherency models more flexible and adaptable to site-specific characteristics. However, most of them are suitable for modeling spatial ground motions on flat-lying alluvial sites (i.e. laterally

homogeneous and deterministic, horizontally layered sediment site). It has been found that these coherency functions are not appropriate for modeling spatial variations of ground motions at sites with lateral variations in their surface and/or subsurface topography or soil conditions.

In practice, the local soil properties (including layer thickness, shear modulus, density and damping ratio of each soil layer) exhibit greater randomness and spatial variation than the rock, that can also affect the lagged coherency value, as shown by the observations from recorded data investigating the lagged coherency function of ground motions of horizontal shear waves on such irregular sites (see, e.g., researcher's observations described in Chapter 1, Somerville *et al*., 1991, Schneider *et al*., 1992; Liao *et al*., 2007). Unfortunately, how local site conditions with heterogeneous soil profiles influence the lagged coherency value, besides affecting the phase part of coherency model, is unknown.

To account for the effect of local site conditions in the current engineering practice, different ground motion response spectra specified in design codes are incorporated to account for the effects of different local site conditions at different stations, but the coherency models utilized are those for uniform soil conditions (Deodadis, 1996). The above suggests that coherency estimates are significantly affected by topography and inhomogeneous media (random soil properties). The current simulation practice accounting for the effects of different site conditions may not reflect reality. To consider local site effects, Der Kiureghian (1996) proposed a theoretical model describing the coherency function of motions on the ground surface, in which he assumed that site effects influence the phase of the coherency function only, while they do not affect the lagged coherency. This is a simple model for determining site-dependent coherency. For example, it does not account for the effect of incoherency resulting from wave scattering (scattering from near-receiver heterogeneities) within the two soil columns at two stations, that can, in some cases, control the properties of the lagged coherency (Menke, 1990).

On the other hand, the Der Kiureghian (1996) model represents the power spectral density function of ground motion using the site-dependent transfer function and the white noise spectrum. He also posited the corresponding parameters (central frequency and damping ratio) for this model in three typical sites, i.e., stiff site, medium site, and soft site. Although this model takes into account the difference in soil conditions at various support points of lifelines, it over estimates the effects of local site conditions. Deodatis (1996) generated a set of sample functions of a non-stationary, multivariate, stochastic process based on a spectral representation method that could be used to simulate ground motions at spatially correlated points with different power spectral densities modeled by the Clough-Penzien spectrum. Similar to the Der Kiureghian model, this model is a modified power spectral density function

obtained by the filtration process of bedrock white noise when propagating the media with different central frequencies and damping ratios. Hence, it can only approximately represent the local site effects.

All of these models are based on the parametric Kanai–Tajimi spectrum (1957, 1960) or its extension represented by the Clough–Penzien spectrum (1975), which models only the effect of the local soil conditions, since bedrock excitation is a white process. However, seismic ground motions are the result of the rupture at the fault and the transmission of waves through the media from the fault to the ground surface. A physically consistent and refined model, using a seismological source model simulation (e.g., Irikura, 1983) that can account for effects of the finite-fault rupture process and the directivity (which affect intensity and frequency content of base rock motions in the near field, as shown in Fig. 3.7a) and the transmission of waves from the fault through the media to the ground surface, is desired (Zerva, 2009).

Also, it is interesting to note that the damping ratios of soft, intermediate, and firm sites estimated from average Kanai-Tajimi spectra are not consistent with common geotechnical engineering practice. Hence, a suitable model directly connects the local site conditions and the characteristics of bedrock motion with the ground motion using the transfer function that truly reflects the influence of the site amplification effect on the shear waves transferred from bedrock to surface. Moreover, trying to establish an analytical expression for a realistic ground motion power spectrum related to the local site conditions is quite difficult since very limited information is available on the spectral characteristics of propagating seismic waves.

In this context, many studies of site amplifications of seismic waves have also been reported, with various simplifications adopted in the analysis, mainly by reducing the problem to a combination of one-dimensional (1-D) propagation schemes (Wolf, 1985). Taking the site amplification effect into consideration, Hao (1993) developed a numerical method to calculate the site amplification effect on ground motion time histories by assuming seismic waves consisting of SH and combined P and SV waves. Wang and Hao (2002) then extended this method to include the effects of random variation of soil properties on site amplifications of seismic waves. Some computer programs, such as SHAKE91 (by Idriss *et al*., 1992), are also able to calculate site responses to incoming seismic waves and the ground motion time histories on the ground surface by solving the fundamental dynamic equations of motion in the frequency domain.

These approaches are based on a 1-D wave propagation assumption, and the seismic waves are assumed to propagate vertically from the base rock (i.e., from the rock-layer interface) to ground surface. Horizontal wave propagation, wave scattering owing to uneven surface conditions, as in the surface of a canyon site, are neglected. However, these methods have

predicted amplifications well, and the corresponding computer programs, such as SHAKE, are commonly used in engineering practice to calculate earthquake ground motions on the surface of a soft soil site. This one-dimensional site response analysis is perhaps the most used technique in accounting for the local site effect and has been adopted by several design standards. Admittedly, results obtained from 2-D or 3-D analysis with accurate local soil modeling are preferred; however, these results are not readily applicable in reality.

It should be noted that these approaches only simulate ground motion time histories at one point on the ground surface. Ground motion spatial variations are not considered. Studies which consider both the ground motion spatial variation effect and the site amplification effect are limited because of the complexity of earthquake wave propagation through the random, heterogeneous, nonlinear, spatially variable, and site specific soil profile. In reality, spatial variations and uncertainties about soil properties always exist. These are caused by the inherent heterogeneity or variability of soils, the limited availability of information about internal conditions, and, sometimes, measurement errors. Therefore, soil properties cannot be realistically considered to be deterministic. These uncertainties associated with system parameters are also likely to influence the lagged coherency loss function (Zerva and Harada, 1997; Liao and Li, 2002).

For this purpose, Bi and Hao (2011) investigated the coherence loss between simulated spatial ground motions on the surface of a layered soil site induced by the irregular surface topography of a canyon site (non-uniform site) and random soil properties. They based their work on the combined one-dimensional wave propagation theory and spectral representation method of Hao *et al*. (1989). The spatially varying bedrock motions are assumed to consist of out-of-plane SH waves or in-plane, combined P and SV waves that propagate into a random, layered soil site with an assumed incident angle. The shear modulus, density, and damping ratio of each soil layer are considered as random variables in the analysis, are assumed to follow a normal distribution, and are modeled by one-dimensional random fields in the vertical direction. We found that the lagged coherency function between surface ground motions on a canyon site is different from that between base rock motions. At all frequencies, the coherency loss functions on the ground surface are smaller than those on the base rock, even with deterministic soil site properties, i.e., the coherency function on the base rock is the upper bound of the coherency of spatial ground motions on the surface of a canyon site.

For a deterministic canyon site, the lagged coherency function of the spatial surface ground motions oscillates with frequency. The maximum (peaks) and minimum (troughs) coherency values are directly related to the modulus of the site amplification spectral ratios (transfer function ratios) of two local sites or two wave paths. When the spectral ratios of two local sites differ from each other significantly, the spatial ground motions on the ground surface are

weakly correlated. The coherency function models for motions on a flat-lying site cannot be used to model that of motions on a canyon site.

The influence of random soil properties in the vertical direction in all layers of a canyon site, compared with a deterministic case, on the lagged coherency function depends on the amount of variation in soil properties. In general, the more significant the random variations of soil properties are, the larger the local site effects on spatial surface ground motion variations are. However, they could result in larger coherency values at certain frequencies corresponding to smaller mean amplification spectra ratios. This is expected because smaller amplification spectra ratios indicate smaller differences between two local sites at the corresponding frequencies. The random variations of the soil damping ratio and density have an insignificant effect on the lagged coherency as compared to the random variations of shear modulus.

Compared to the work by Deodatis (1996), the power spectral density functions at different locations of a canyon site in this analytical study are derived from the wave propagation theory, that directly relates the local soil conditions and base rock motion characteristics with the surface ground motions, thus local site effects can be realistically considered. Also, this example shows that the site significantly amplifies the motions on the base rock, which makes the energy of surface ground motions concentrate at a few frequencies corresponding to the various vibration modes of the site. This result indicates the importance of considering the multiple modes of a local soil site when estimating the seismic wave propagation and site amplification. The result of this research is an extension of that obtained using a 1-DOF model (Zerva and Harada, 1997). With a 1-DOF model, the influence of the higher vibration modes of the site on site amplification, and hence the spatial ground motion coherency, cannot be included.

Earlier, Liao and Li (2002), Zerva and Harada (1997), and Kanda (2000) performed analytic studies on the influence of local site conditions, including topography and/or spatial-random-variable soil properties, on the wave motion coherency. Liao and Li (2002), in their approach to evaluate the spatial coherency in their stochastic methodology to study the effects of uncertain soil properties and irregular topography at sites on the coherency function, show that the layer irregularity of a site with deterministic soil properties, subjected to non-identical random input excitation, can reduce the lagged coherency function values in the vicinity of the resonant frequencies of the site. Furthermore, the stochasticity of the soil layer tends to cause diminution of the lagged coherency function values near the site's resonant frequencies. The latter result is in agreement with Zerva and Harada (1997) and Cranswick (1988). However, this method is difficult to implement and sometimes a bit arbitrary selecting the

absorbing boundary conditions. Furthermore, it is difficult to explain why the coherency function varies significantly over relatively short distances (Bi and Hao, 2011).

Zerva and Harada (1997) modeled horizontal soil layers at a site with no dramatic changes in their topography (uniform site with only subsurface soil variability) as a 1-DOF system with horizontally random, variable characteristics to study the effect of uncertain soil properties on the coherency function. They pointed out that the spatial coherency of motions on the ground surface is similar to that of the incident motion at the base rock except at the predominant frequency of the layer, where it decreases considerably. The effect of uncertain soil properties should also be incorporated in spatial variation models of ground motions.

Their explanation for this phenomenon was that for input motion frequencies close to the mean natural frequency of the 1-DOF oscillators, the response of the systems was affected by the variability in the value of this natural frequency and resulted in the loss of correlation. However, it should be noted that a 1-DOF system cannot realistically represent the multiple, predominate frequencies that may exist at a site with multiple layers and multiple modes, but one should not discard this simple model too soon, since there are many structures, e.g., log-span bridges, for which the high frequency component of ground motions are not significant, and even this simple model may be adequate if it captures the first resonant frequency well.

Kanda (2000), using two-dimensional, finite element modeling of a layered medium with irregular interfaces (fully deterministic concave and convex sine-shaped interfaces are assumed between the layers) and random, spatially variable incident motions, analyzed coherency and amplitude variability on the free surface of the site. The analytic results showed that interface irregularities between layers significantly change the frequency characteristics of ground motions at the soil surface and alter its spatial incoherence function.

It is obvious from these examples, and the early observations, that the effects of irregular surface topography and random soil properties of a site on the lagged coherency function of spatial ground motions cannot be neglected. It should be noted that, whereas analytical studies can provide insight into various aspects underlying the spatial variability in the seismic motions, the forward, purely analytical modeling of coherency will be limited by the necessary assumptions made to simplify this complex problem.

In this chapter, the significance of stochasticity in the characteristics of the surface layers of a site to the spatial variation of seismic ground motions and the resulting seismic ground strains is investigated for the case of El-Asnam Sogedia Factory soil site located in the epicentral region of the 1980 El-Asnam Earthquake (N.W Algeria). For this purpose, we use the analytic site specific model developed in Zerva and Harada (1997) and Harada and

Shinouzuka (1987), in which they approximate the site topography by homogeneous, horizontally extended soil layers with random thicknesses and soil material properties overlying a half-space (bedrock). The methodology is applicable to sites without dramatic changes in their topography and for the strong motion S-wave window.

The incident motions at different locations at the bedrock-layer interface, consisting of stationary out-of-plane SH waves with an incident angle and synthetized by the EGF method (Section 3.2), are assumed to have the same intensity and frequency content and represented by the average of their unsmoothed power spectral density functions. The spatial variation of ground motions on the base rock is accounted for by means of the two, selected parametric models of lagged coherency (Section 3.3) and the commonly used complex term to describe the wave passage effect (Eq. 2.45) with a specified constant apparent propagation velocity. The incident shear waves at the bedrock-layer interface were then assumed to propagate vertically through the stochastic soil layer, and the site response was approximated by that of one-degree-of-freedom oscillators with random properties.

The power and cross spatial densities of total surface seismic motions on a spatially random variable site with multiple soil layers are analytically derived using the Zerva and Harada (1997) approach, which directly relates the local soil conditions and base rock motion characteristics with the surface ground motions. The expression of the total coherency function is then obtained, and the total lagged coherency and its site contribution part are deducted. Due to the absence of sufficient information to describe the variability of soil properties in the horizontal direction at the Sogedia Factory site, the layer thickness and soil material properties are regarded as random variable with Gaussian distributions. The damping ratios adopted in this study are based on iterative equivalent nonlinear site response analysis of the soil layers when subjected to bedrock motion and are considered to model hysteretic energy dissipation in the soil layers. The contribution of the various factors (spatial correlation function of the predominant ground frequency varying in the horizontal direction, mean value of the equivalent damping ratio of the ground, mean value of the predominant ground frequency, and wave propagation speed in the horizontal direction of the incident motion) to the spatial variation of the surface motions and the resulting seismic ground strains on the surface of the stochastic layer evaluated from the model are examined for the present site.

Parametric models of ground motion coherency and power spectral density at the surface of the study area have been presented. Such models are useful in random vibration analysis of lifeline structures under the action of earthquake excitation or in simulation of spatially variable ground-motion time histories to be used in nonlinear time history analysis of such structures. For such nonlinear analysis, the spectral representation method of unconditional simulation given by Hao *et al*. (1989) is used to generate non-stationary, spatially varying ground motion time histories at various locations on the ground surface of the El-Asnam

Sogedia site, compatible with the properties of the target (predictive) random field, i.e. power spectral density and the spatial coherency functions at the surface.

5.1 Stochastic modeling of seismic surface ground motion

5.1.1 Homogeneous stochastic horizontal ground

The necessarily limited number of soil tests and their inherent lack of representativeness are significant sources of uncertainty in the evaluation of site response analyses. The uncertainty of the accuracy of analytical or numerical models used for the analysis is, in general, less significant. Moreover, uncertainty in field data is increased by the inherent soil heterogeneity, namely spatial variability of soil properties within so-called homogeneous soil layers. Therefore, deterministic descriptions of spatial variability of soil properties are not always feasible, and the sufficiently large degree of disorder, leads to the use of statistical methods in describing their distribution within a statistically homogeneous soil zone. While the natural variability of soil properties is known to affect the soil system behavior, the consequences of spatial variability are not well understood yet, and their exploration requires the use of stochastic, field-based techniques of data analysis.

In this context, and as schematically shown in Fig. 5.1 where X and Z represent the horizontal and vertical space coordinates, respectively, the soil thickness $H_j(x)$ of the *j*-th layer may vary randomly in the X-direction. Similarly, a representative soil property, $q(x,z)$, which can be attributed to, e.g., shear modulus, $G(x,z)$, mass density, $\rho(x,z)$, and damping ratio, $\zeta(x,z)$, may be a random function of x and z. As in the Zerva and Harada (1997) study, it is assumed, for the first approximation, that the soil layer thickness, $H_j(x)$, and soil property, $q(x,z)$, are random functions of x only :

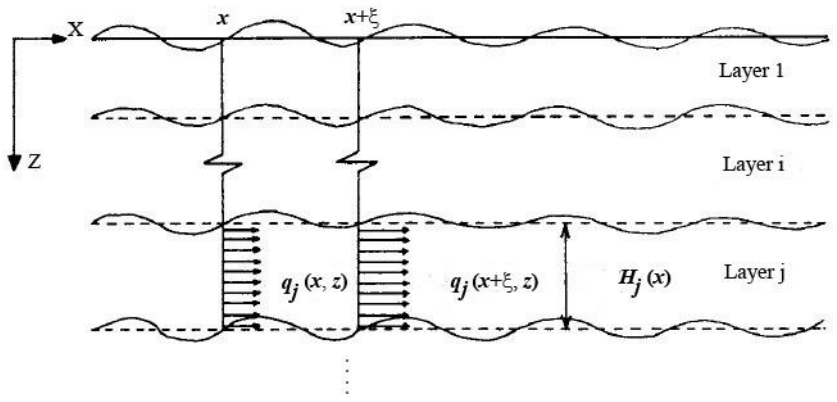

Fig. 5.1 - Horizontal soil layers showing layer depth, $H_j(x)$, and soil property, $q_j(x,z)$

$$H_j(x) = H_j\left[1 + f_{H_j}(x)\right] \tag{5.1}$$

$$q(x,z) = q_z(z)\left[1 + f_q(x)\right] \tag{5.2}$$

where H_j and $q(z)$ are the expected values of $H_j(x)$ and $q(x,z)$ with respect to x:

$$\mathrm{E}\left[H_j(x)\right] = H_j \qquad \text{(constant)} \tag{5.3}$$

$$\mathrm{E}\left[q(x,z)\right] = q_z(z) \qquad \text{(deterministic function of z)} \tag{5.4}$$

The quantities $f_{H_j}(x)$ and $f_{q(x)}$ in Eqs. (5.1) and (5.2) represent the stochastic fluctuations of $H_j(x)$ and $q(x,z)$ with respect to x and have a mean of zero: $\mathrm{E}\left[f_{H_j}(x)\right] = 0$ and $\mathrm{E}\left[f_q(x)\right] = 0$. It is noted here that the layer thickness is a nominally constant value and the soil layers are almost statistically homogeneous in the sense that $\mathrm{E}\left[\left(f_{H_j}(x)\right)^2\right] \prec\prec 1$ (i.e., the coefficient of variation $(cov_{H_j})^2 \prec\prec 1$) and $\mathrm{E}\left[\left(f_q(x)\right)^2\right] \prec\prec 1$ (i.e., $(cov_q)^2 \prec\prec 1$), in equations (5.1) and (5.2).

5.1.2 Equations of seismic ground motion

Consider ground layers resting on elastic rigid bedrock and subjected to earthquake ground motion as shown in Fig. 5.1. The total soil depth is assumed to be a constant, H. The input earthquake ground motion at the bedrock is assumed to be a stationary random shear wave (SH) propagating with speed, c, in the X-direction and represented by $u_b(x,t)$. The displacement time history at any location (x,z) within the layer is the superposition of the incident displacement at the bedrock-layer interface, $u_b(x,t)$, and the relative displacement between the bedrock and the location under consideration, $u_r(x,z,t)$:

$$u(x,z,t) = u_b(x,t) + u_r(x,z,t) \tag{5.5}$$

The following assumptions are made at this point regarding the layer response to the random incident motion.

First, the incident random waves impinge the bedrock layer interface at such an angle that their propagation within the layers can be assumed to be vertical. This assumption serves as a first approximation, since it simplifies the wave propagation patterns in layered media, and is commonly used in the consideration of the effects of layers on seismic ground motions (e.g., Bi and Hao, 2011). Furthermore, it can be reasoned that, because the angle of transmission of body waves from the bedrock to the surface layer can be as steep as 90°, i.e., a nearly vertical direction, (O'Rouke *et al*., 1980, 1982), the propagation of the waveforms within the layer can be considered vertical. This one-dimensional ground response analysis is also based on the assumption that all boundaries are horizontal, and, the soil and bedrock surface extends infinitely in the horizontal direction.

Second, the relative displacement, $u_r(x,z,t)$, can be represented by the product of the generalized coordinate, $u^*(x,t)$, and an assumed single mode shape, $\psi(z)$, that satisfies the normalization and the geometric boundary conditions expressed as, respectively, $\psi(o)=1$ (at the ground surface) and $\psi(H)=0$ ($u_r(x,z,t)=0$ at the bedrock-layer interface $z=H$):

$$u_r(x,z,t)=\psi(z)\,u^*(x,t) \tag{5.6}$$

The assumed mode shape takes, for simplicity, the following form (Harada and Shinouzuka, 1987), and corresponds to the first mode shape of a single, homogeneous, infinite horizontal layer lying on elastic rigid bedrock and under vertically propagating seismic shear waves:

$$\psi(z)=\cos\left(\frac{\pi z}{2H}\right) \tag{5.7}$$

This consideration approximates the layer or soil column response by that of a single-degree-of-freedom oscillator with random characteristics. It is noted that this simplification eliminates the effects of higher modes present in a layered half-space, but captures the dominant layer response. It is generally acceptable that the site responds with a dominant frequency to seismic excitations, since the maximum amplification at the homogeneous horizontal soil profile under shear waves that travel up and down occurs, in general, at the fundamental-mode frequency. For this reason, the fundamental period of a site is widely used in the calculation of seismic soil amplification factors for the evaluation of the base shear force for building design (Motazedian *et al*., 2011).

It is also noted that, with the enforcement of the boundary condition, $\psi(H)=0$, the model does not properly consider the effect of the soil layers (waves propagate with refraction and reflection at the layer-layer irregular interfaces) on the total motion at the bedrock-layer interface. Thus, the present approach is valid only for the estimation of surface ground motion

characteristics. The layer characteristics and the parameters affecting the incident motion at the bedrock-layer interface, such as source effects and random inhomogeneities along the path of the waves in the bedrock, are statistically independent quantities.

Through the principle of virtual work, the differential equation of motion for the generalized displacement coordinate, $u^*(x,t)$, is given by (Zerva and Harada, 1997):

$$\ddot{u}^*(x,t)+\left(2\zeta^*(x)\,\omega^*(x)\right)\dot{u}^*(x,t)+\left(\omega^*(x)\right)^2 u^*(x,t) \;=\; -\beta\,\ddot{u}_b(x,t) \tag{5.8}$$

where $\omega^*(x)$ is the ground predominant natural frequency and β is the participation factor. They are given as:

$$\omega^*(x)=\sqrt{\frac{(1+f_G(x))\int_0^H G_z(z)\,\left[\psi'(z)\right]^2\,\mathrm{dz}}{(1+f_\rho(x))\int_0^H \rho_z(z)\,\left[\psi(z)\right]^2\,\mathrm{dz}}} \tag{5.9}$$

$$\beta=\frac{\int_0^H \rho(x,z)\;\psi(z)\;\mathrm{dz}}{\int_0^H \rho(x,z)\;\left[\psi(z)\right]^2\,\mathrm{dz}}=\frac{\int_0^H \rho_z(z)\;\psi(z)\;\mathrm{dz}}{\int_0^H \rho_z(z)\;\left[\psi(z)\right]^2\,\mathrm{dz}} \tag{5.10}$$

where, $\rho_z(z)$ and $G_z(z)$ are the means values of the random quantities, $\rho(x,z)$ and $G\left(x,z\right)$, respectively.

$\zeta^*(x)$ is an approximate, equivalent damping ratio for shear waves to account for the energy loss. Alternatively, the (natural) predominant ground frequency, $\omega^*(x)$, and the equivalent damping ratio, $\zeta^*(x)$, may also be expressed according to Eq. (5.2):

$$\omega^*(x)=\omega_0\left[1+\omega(x)\right] \tag{5.11}$$

$$\zeta^*(x)=\zeta_0\left[1+\zeta(x)\right] \tag{5.12}$$

in which, ω_0 and ζ_0 are the mean values of $\omega^*(x)$ and $\zeta^*(x)$, respectively, and $\omega(x)$ and $\zeta(x)$ are homogeneous stochastic fields with zero mean and corresponding standard deviations, $\sigma_{\omega\omega}$ and $\sigma_{\zeta\zeta}$. It is easy to show that $\sigma_{\omega\omega}=cov_{\omega^*}$ and $\sigma_{\zeta\zeta}=cov_{\zeta^*}$.

Once $u^*(x,t)$ is determined, the seismic motions on the ground surface $u(x,t) = u(x, z = 0, t)$ can be evaluated from Eq. (5.5) with $\psi(o) = 1$. For this, Zerva and Harada conducted a random vibration analysis to evaluate first the solution to Eq. (5.8), where the cross-spectral density function, $S_{u^*u^*}(\xi,\omega)$, was developed and expressed in the term $S_{u_b u_b}(\xi,\omega)$ and the soil layer transfer function, $H(\omega_0,\zeta_0,\omega)$, as:

$$S_{u^*u^*}(\xi,\omega) = \left(\beta^2\omega^4 \cdot \left|H(\omega_0,\zeta_0,\omega)\right|^2 + 4\omega_0^4\omega^4 R_{\omega\omega}(\xi)\cdot\left|H(\omega_0,\zeta_0,\omega)\right|^4\right) S_{u_b u_b}(\xi,\omega) \qquad (5.13)$$

and then from Eqs. (5.13) and (5.5), they deducted a similar relation for the ground surface response $u(x, z = 0, t)$, as :

$$S_{uu}(\xi,\omega) = \begin{pmatrix} (\omega_0^4 + (2\beta + 4\zeta_0^4 - 2)\omega_0^2\omega^2 + (\beta-1)^2\omega^4)\cdot\left|H(\omega_0,\zeta_0,\omega)\right|^2 \\ +4\beta^2\omega_0^4\omega^4 R_{\omega\omega}(\xi)\cdot\left|H(\omega_0,\zeta_0,\omega)\right|^4 \end{pmatrix} S_{u_b u_b}(\xi,\omega) \qquad (5.14)$$

in which, $R_{\omega\omega}(\xi)$ is the autocorrelation of the $\omega(x)$ field (Eq. 5.11) and the complex frequency response function $H(\omega_0,\zeta_0,\omega)$ is given as:

$$H(\omega_0,\zeta_0,\omega) = \frac{1}{\omega_0^2 - \omega^2 + 2i\zeta_0\omega_0\omega} \qquad (5.15)$$

This spatial correlation function, $R_{\omega\omega}(\xi)$, of the predominant circular frequency, $\omega(x)$, of the ground results from the spatial variability of the soil material as well as the soil layer thickness. Equation (5.14) is useful for estimating the site-specific spatial variability of the ground displacement $u(x,t)$, which is of primary importance for the seismic analysis and design of buried lifeline structures.

The corresponding power spectral density of the motions is obtained from Eq. (5.14) by setting the separation distance equal to zero, $(\xi = 0)$, as:

$$S_{uu}(\omega) = \begin{pmatrix} (\omega_0^4 + (2\beta + 4\zeta_0^4 - 2)\omega_0^2\omega^2 + (\beta-1)^2\omega^4)\cdot\left|H(\omega_0,\zeta_0,\omega)\right|^2 \\ +4\beta^2\omega_0^4\omega^4\sigma_{\omega\omega}^2\cdot\left|H(\omega_0,\zeta_0,\omega)\right|^4 \end{pmatrix} S_{u_b u_b}(\omega) \qquad (5.16)$$

in which $S_{u_b u_b}(\omega) = S_{u_b u_b}(\xi = 0, \omega)$ is the power spectrum of the incident motion. It is noted that, for a participation factor equal to unity ($\beta = 1$, i.e. simple, single-degree-of freedom oscillator) and for deterministic values of the soil properties, Eq. (5.16) reduces to the well-known KanaiTajimi spectrum (Kanai, 1957; Tajimi, 1960). The surface motions are assumed to be spatially homogeneous, which implies that their power spectrum, which is proportional to the square of their amplitude (see Eq. 2.24), is assumed to be the same at all locations. An assumption also made implicitly in Eq. (5.16) to the bedrock motions. This assumption is reasonable since the source to site distance is much larger than the site dimension and stations are situated on a Sogedia site considered to have approximately the same local soil profile (or local soil conditions) without dramatic changes in topography (Zerva and Zervas, 2002).

5.1.3 Spatial variability of surface motion

The total spatial variability of surface motion is composed of terms corresponding to wave passage effects, bedrock motion loss of coherency effects, and site response contributions (Der kiureghian, 1996). In this approach, coherency function of surface motion is expressed as follows:

$$\begin{aligned} \gamma(\xi, \omega) &= \frac{S_{uu}(\xi, \omega)}{S_{uu}(\omega)} \\ &= \gamma_{b,coh}(\xi, \omega) \cdot \gamma_{b,prop}(\xi, \omega) \cdot \gamma_{l,coh}(\xi, \omega) \end{aligned} \tag{5.17}$$

where: $\gamma_{b,coh}(\xi, \omega)$ is the loss of coherency of the incident base rock motion, it is often described by the existing lagged coherency models from the literature. In this study we will idealized $\gamma_{b,coh}(\xi, \omega)$ by using a parametric coherency model, calibrated to coherency functions estimated in the Sec. 3.2 from ground motion simulations using the extension of the EGF method at the bedrock of the epicentral region of the 1980 El-Asnam Earthquake. As well, $\gamma_{b,prop}(\xi, \omega) = \exp\{-i\omega\xi/c\}$ is a term describing the wave passage effect in the incident motion (Eq. 2.45), and $\gamma_{l,coh}(\xi, \omega)$ is a term representing the contribution of the layer stochasticity to the spatial variation of coherency. $\gamma_{l,coh}(\xi, \omega)$ can be extracted by substituting Eqs. (5.15) and (5.16) for the first equality in Eq. (5.17), followed by identifying the result of the last equality in Eq. (5.17), taking into account the relation in Eq. (5.18):

$$\begin{aligned} \gamma_b(\xi, \omega) &= \frac{S_{u_b u_b}(\xi, \omega)}{S_{u_b u_b}(\omega)} \\ &= \gamma_{b,coh}(\xi, \omega) \cdot \gamma_{b,prop}(\xi, \omega) \end{aligned} \tag{5.18}$$

the result takes the form:

$$\gamma_{l,coh} = \frac{\left[H_1(\beta,\omega_0,\zeta_0,\omega) + R_{\omega\omega}(\xi)\cdot H_2(\beta,\omega_0,\zeta_0,\omega)\right]}{\left[H_1(\beta,\omega_0,\zeta_0,\omega) + \sigma^2_{\omega\omega}\cdot H_2(\beta,\omega_0,\zeta_0,\omega)\right]} \tag{5.19}$$

in which,

$$\begin{aligned} H_1(\beta,\omega_0,\zeta_0,\omega) &= (\omega_0^4 + (2\beta + 4\zeta_0^4 - 2)\omega_0^2\omega^2 + (\beta-1)^2\omega^4)\cdot\left|H(\omega_0,\zeta_0,\omega)\right|^2 \\ H_2(\beta,\omega_0,\zeta_0,\omega) &= 4\beta^2\omega_0^4\omega^4\cdot\left|H(\omega_0,\zeta_0,\omega)\right|^4 \end{aligned} \tag{5.20}$$

It is noted that c (in $\gamma_{b,prop}(\xi,\omega) = \exp\{-\mathrm{i}\omega\xi/c\}$) is the apparent propagation velocity of the incident motion at the bedrock-layer interface. This is a function of the shear wave velocity in the bedrock v_s and the angle of incidence of waves at the interface.

The overall incoherence (incident motion incoherence and layer stochasticity) in the spatial variation of the surface motions is given by taking the modulus of the complex function in Eq. (5.17) and expressing it as the following equation:

$$\gamma_{coh}(\xi,\omega) = \gamma_{b,coh}(\xi,\omega)\cdot\gamma_{l,coh}(\xi,\omega) \tag{5.21}$$

5.1.4 Analytical evaluation of seismic ground strains

The relative significance of the effects of the incoherence evaluated from the present model and the apparent propagation of the seismic ground motions on the response of buried lifelines is evaluated in this section. The spatial incoherence model of the motions is described by the Eq. (5.21) (i.e., the modulus of the complex function in Eq. (5.17)), and a wide range of apparent propagation velocities is considered in the wave passage effect.

The analysis and design of buried pipelines to resist seismic motions differs fundamentally from that of conventional structures. One of the basic differences is that, because of their extended length, pipelines are subjected to spatially variable seismic ground motions. Furthermore, it has been postulated, both from recorded data and from analytical evaluations, that inertia effects for buried pipelines may be neglected, that their movement during earthquakes is similar to that of the ground, and that the maximum axial strain along a straight buried pipeline coincides with the maximum ground strain (e.g., O'Rourke *et al*., 1984). Generally, the seismic design of buried structures (pipelines and tunnels) relies directly on the characterization of the seismic ground deformations and strains (e.g., Hashash *et al*. 2001,

Newmark and Roesenblueth, 1971) that are imposed on the structure due to its interactions with the surrounding soil and constitute, essentially, their seismic loads. Axial deformations in these structures are induced by the seismic wave components with motions parallel to the axis of the structure, and bending deformations are caused by the seismic wave components with motions perpendicular to the axis of the structure. Axial strains are considered to be more important in the seismic design of straight, buried, small diameter pipelines (O'Rourke *et al*., 1982). As the radius of the pipeline increases, however, axial stresses decrease, and the structure becomes sensitive to bending stresses as well. For tunnels, shear waves propagating in a direction normal or nearly normal to the structure's axis can lead to deformations of the cross section of the tunnel lining (ovaling or racking deformations). Larger strains ought to be expected in soft and deep soils, due to smaller shear wave velocity in the layer, and smaller strains ought to be expected in the basement rock.

Simplified guidelines for the design of pipelines to resist seismic motions determine the ground strain through the assumption of a plane, sinusoidal wave that propagates along the structure's axis with a constant velocity, without interference from other waves, and without changing shape (Newmark and Rosenblueth, 1971). Newmark and Roesenblueth (1971), in their empirical estimation of seismic ground strains, noted that horizontal, straight buried pipelines follow the motion of the ground, and that maximum axial strains induced in buried pipelines can be adequately approximated by the maximum ground strains, which are given by:

$$\varepsilon_{max} = \frac{(\upsilon_L)_{max}}{c} \tag{5.22}$$

in which, $(\upsilon_L)_{max}$ is the maximum horizontal (particle) velocity in the longitudinal direction of the pipeline at a location on the ground surface and c is the component of the apparent velocity of the waves with respect to the ground surface in the same direction. The rotational ground deformation for the evaluation of the torsional response in structures was also approximated by a similar expression (Newmark and Roesenblueth, 1971). In this case, the maximum angle of rotation of the ground about the vertical axis, θ_{max}, is approximated by:

$$\theta_{max} = \frac{(\upsilon_T)_{max}}{c} \tag{5.23}$$

in which, $(\upsilon_T)_{max}$ is the maximum horizontal (particle) velocity in the transverse direction.

The strain estimates of Eqs. (5.22) and (5.23), as well as comparative ones for radial, tangential and shear strains, rely on the following assumptions: (i) the seismic energy travels as a sinusoidal, single plane wave with a known azimuth and constant horizontal velocity; (ii)

the surface deformation is caused solely by the propagation of the motions; and (iii) the medium is laterally homogeneous.

Recent evaluations of strains still rely on the traveling-wave assumption of Eqs. (5.22) and (5.23) and consider seismic ground motions as being dominated by body or surface waves for the estimation of the apparent propagation velocity. Strain estimates based on these expressions are commonly referred to as single-station strain estimates, and their evaluation requires knowledge of the particle velocity and a representative propagation velocity of the motions. The particle velocity may be available from recorded data at a single station and/or attenuation relations, while the appropriate estimates for the apparent propagation velocity of the motions are difficult to obtain. Indeed, near field ground motions are caused by interference a number of different types of waves during the same time window, each with its own propagation velocity. The propagation velocity of P-waves is larger than the propagation velocity of S-waves, which, in turn, travel faster than surface waves. In reality, the apparent propagation velocity of the motions may vary slightly with frequency even for the broad-band shear wave window. In addition, surface waves for realistic soil profiles are dispersive, which means that the phase or propagation velocity is a function of frequency. A common rule is that surface waves become significant and tend to govern only in shallow structures and at sites located more than about five focal depths from the epicenter (O'Rourke *et al*., 1984). Surface waves are generated by the reflection and refraction of body waves at the ground surface. Surface waves can be more destructive to buried pipelines than body waves by generating larger ground strain caused by their low phase velocity. Therefore their omission will lead to discrepancies between the actual strains and the single-station strain estimates. These observations contradict the validity of the first assumption in (i).

At the sites of dense instrument arrays, frequency-wavenumber techniques can be utilized for the estimation of the propagation characteristics (the azimuth and apparent propagation velocity of the contributing waves imping upon the array during different time windows and at different frequencies for each component of the motions and each event. All techniques evaluate, in different forms, the frequency-wavenumber (F-K) spectrum of the motions, i.e., the triple Fourier transform of the recorded time histories, and identify the average propagation velocity of the motions from the peak of the spectrum (Zerva and Zevra, 2002). However, that such estimates reflect only the average propagation velocity of the waves but do not capture the arrival time perturbations at individual stations caused by horizontal variations in the geologic structure encountered along the seismic ray paths (Zerva and Zervas, 2002) that introduce random variations of the wave passage effect. These random variations are sources of random phase variations and are represented in the lagged coherency function, which is not taken into account by assumption (ii).

However, in the absence of such information, the apparent propagation velocity of the motions needs to be evaluated analytically from the source-site geometry and the characteristics of the soil profile. It can be clearly seen from Eqs. (5.23) and (5.23) that uncertainties in the estimated apparent propagation velocity of the waveforms will directly affect the value of the seismic ground strain. Additionally, any strain estimate based on the traveling-wave assumption will only be an approximation for the actual strains, as Eq. (5.22) does not consider the effect of the change in the shape of the motions (dispersion, amplitude variability, and loss of coherency) on the seismic ground deformation. Just the consideration of the apparent propagation of the motions would provide a lower bound for actual seismic ground strains. Indeed, Bodin *et al*. (1997), from their analysis of seismic strains in the Valley of Mexico, suggest that Eq. (5.22) may, in certain cases, be uncertain within a factor of 2 to 3. Additional differential displacements and strains are caused by changes in the amplitudes and phases of the motions as well as the above-cited arrival time perturbations of the waveforms at the various locations on the ground surface. These effects are those of the spatial variability of seismic ground motions.

The last assumption (iii), considers that the site can be approximated by horizontal layers extending to infinity. Lateral variations in the site's subsurface topography, however, can significantly amplify seismic ground strains. In addition, assumption (iii) implies that the soil properties within each layer can be considered deterministic. In reality, they are uncertain, a fact that will invariably affect the value of the strain estimate. It is noted that the spatial variation of the seismic ground motions incorporates the effect of the variability in the soil properties at a site into the local scattering effect.

The significance of incoherence versus that of apparent propagation in the evaluation of surface seismic strains is analyzed herein. It is assumed that the cross-spectral density of the seismic ground motions is described by Eq. (5.14), which incorporates the effects of both the incoherence evaluated for strong motion shear waves (incident motion incoherence and layer stochasticity) and the apparent propagation. For this, we adopt the analytical approach developed by Zerva and Harada (1997), already used in the previous section on the evaluation of surface seismic motions. It allows for the analytical estimation of horizontal strains of a soil site having stochastic characteristics and also for analyzing the contribution of incoherence and wave propagation in seismic ground strains.

In this analytical methodology, it is necessary to represent, in addition to the spatial correlation function, $R_{\omega\omega}(\xi)$, in Eq. (5.19), the coherency function, $\gamma(\xi,\omega)$, of the total ground surface motions by an analytical model. For the latter, and from its definition given in Eq. (5.17), only the term of the loss of coherency of the incident base rock motion $\gamma_{b,coh}(\xi,\omega)$ remains to be described by the existing parametric lagged coherency models from

the literature. The wave passage effect and the layer stochasticity contribution to the coherency function and are already incorporated earlier through analytic expressions and by Eqs. (2.45) and (5.19), respectively. Because of the analytic random vibration evaluation of certain response quantity of lifelines, e.g. the variance of the horizontal seismic strains, it is required that the random field resulting from the selected spatial incoherence model $\gamma_{coh}(\xi,\omega)$ in Eq. (5.21) is mean-square differentiable. Therefore, its term $\gamma_{b,coh}(\xi,\omega)$, should be selected according to this condition. For this purpose, from the previous three parametric lagged coherency models with the parameter values found in Sect. 3.3, only the Luco and Wong (1986) model respects this condition and might be used with its value incoherence parameter α in this type of development in the case of small to medium separation distance.

The behavior of the sample spatial correlation function, $R_{\omega\omega}(\xi)$, is approximated by the analytical expression:

$$R_{\omega\omega}(\xi)=\sigma^2_{\omega\omega}\, f_{\omega\omega}(\xi) \tag{5.24}$$

in which, $f_{\omega\omega}(\xi)$, the normalized spatial correlation function, ought to be consistent with the variability of the data at the site and satisfy the following conditions: (i) it ought to be symmetric around $\xi=0$ (homogeneity requirement); (ii) its first and second derivatives ought to exist and assume finite values at $\xi=0$, so that the evaluation of strains based on the expression is feasible. It is noted that these two conditions impose $f'_{\omega\omega}(0)=0$. For the present example, the mathematical expression used for $f_{\omega\omega}(\xi)$ is:

$$f_{\omega\omega}(\xi)=\left[1-2\left(\frac{\xi}{b_\omega}\right)^2\right]e^{-\left(\frac{\xi}{b_\omega}\right)^2} \tag{5.25}$$

in which b_ω is the scale of correlation. Alternative expressions for the normalized autocorrelation function can be found in, e.g., Harada and Shinozuka (1986).

Seismic strains resulting on the surface of the stochastic layer are evaluated as follows. The cross correlation function of the seismic motions on the ground surface is defined as:

$$R_{uu}(\xi,\tau)=\int_{-\infty}^{+\infty} S_{uu}(\xi,\omega)e^{i\omega\tau}\, d\omega \tag{5.26}$$

From the above expression, the variance of the horizontal seismic strains $\left(\varepsilon(x,t)=\dfrac{\partial u(x,t)}{\partial x}\right)$ along the X-direction (direction of wave propagation on the ground surface) becomes:

$$\sigma_{\varepsilon\varepsilon}^2 = [-\frac{\partial^2 R_{uu}(\xi,\tau)}{\partial \xi^2}]\Big|_{\substack{\xi=0\\ \tau=0}} = -[\int_{-\infty}^{+\infty} \frac{\partial^2 S_{uu}(\xi,\omega)}{\partial \xi^2}\, d\omega]\Big|_{\xi=0} \tag{5.27}$$

and that of the seismic ground velocities $\left(\upsilon(x,t) = \frac{\partial u(x,t)}{\partial t}\right)$ (particle velocities):

$$\sigma_{vv}^2 = [-\frac{\partial^2 R_{uu}(\xi,\tau)}{\partial \tau^2}]\Big|_{\substack{\xi=0\\ \tau=0}} = [\int_{-\infty}^{+\infty} \omega^2 S_{uu}(\xi,\omega)\, d\omega]\Big|_{\xi=0} \tag{5.28}$$

The square-root of the variance (root-mean-square) of a random quantity provides information on its mean maximum value, since rms values are proportional to the mean maximum ones (Cranswick, 1988).

The evaluation of seismic ground strains (Eq. 5.27) requires the integration of the second derivative with respect to ξ of the cross correlation of the motions at $\tau = 0$, which becomes (Eqs. 5.14, 5.18, and 5.26):

$$R_{uu}(\xi,\tau=0) = \int_{-\infty}^{+\infty} [H_1(\beta,\omega_0,\zeta_0,\omega) + R_{\omega\omega}(\xi) H_2(\beta,\omega_0,\zeta_0,\omega)] e^{-\alpha^2\omega^2\xi^2} e^{-i\omega\frac{\xi}{c}} S_{u_b u_b}(\omega)\, d\omega \tag{5.29}$$

in which $H_1(\beta,\omega_0,\zeta_0,\omega)$ and $H_2(\beta,\omega_0,\zeta_0,\omega)$ are given by Eq. (5.20). Since both the value and the derivatives of the spatial correlation function $R_{\omega\omega}(\xi)$ are needed at $\xi = 0$ in Eqs. (5.27) and (5.29), its analytical approximation (Eq. 5.24) is required. These derivatives, for any assumed correlation function expression $f_{\omega\omega}(\xi)$, take the form:

$$R_{\omega\omega}(0) = \sigma_{\omega\omega}^2;\ R_{\omega\omega}'(0) = 0;\ R_{\omega\omega}''(0) = \sigma_{\omega\omega}^2 f_{\omega\omega}''(0) \tag{5.30}$$

The substitution of Eq. (5.30) into Eqs. (5.27) and (5.29) yields the variance of the seismic ground strains:

$$\sigma_{\varepsilon\varepsilon}^2 = \int_{-\infty}^{+\infty} [\omega^2(2\alpha^2 + (1/c)^2)(H_1 + \sigma_{\omega\omega}^2 H_2) - \sigma_{\omega\omega}^2 f_{\omega\omega}''(0) H_2]\, S_{u_b u_b}(\omega)\, d\omega \tag{5.31}$$

in which, the dependence of H_1 and H_2 on β, ω_0, ζ_0 and ω has been omitted for simplicity. With the assumption that $S_{\ddot{u}_b\ddot{u}_b}(\omega)$, the power spectral density of the incident motion acceleration, is a slowly varying function of frequency, and noting that both $|H(\omega_0,\zeta_0,\omega)|^2$

and $\left|H(\omega_0,\zeta_0,\omega)\right|^4$ peak close to $\omega=\omega_0$, an approximation for the variance of the ground strains is found to be :

$$\sigma_{\varepsilon\varepsilon}^2=\left\{\omega_0^2(2\alpha^2+(1/c)^2)(\beta^2(1+\frac{\sigma_{\omega\omega}^2}{2\zeta_0^2})+4\zeta_0^2)-\frac{\beta^2\sigma_{\omega\omega}^2 f_{\omega\omega}{}''(0)}{2\zeta_0^2}(1+4\zeta_0^2)\right\}\frac{\pi}{2\zeta_0\omega_0^3}S_{\ddot{u}_b\ddot{u}_b}(\omega_0) \quad (5.32)$$

The variance of the seismic velocity at the ground surface can also be evaluated through a similar procedure. Eqs. (5.20), (5.28) and (5.30) lead to:

$$\sigma_{vv}^2=\int_{-\infty}^{+\infty}\omega^2(H_1+\sigma_{\omega\omega}^2H_2)S_{u_bu_b}(\omega)\,d\omega \quad (5.33)$$

which, with the same approximations used to evaluate of the seismic strains, yields

$$\sigma_{vv}^2=\left\{\omega_0^2[\beta^2(1+\frac{\sigma_{\omega\omega}^2}{2\zeta_0^2})+4\zeta_0^2]\right\}\frac{\pi}{2\zeta_0\omega_0^3}S_{u_bu_b}(\omega_0) \quad (5.34)$$

Eqs. (5.32) and (5.34) then result in the following estimate for the rms seismic ground strain in terms of the rms ground velocity:

$$\frac{\sigma_{\varepsilon\varepsilon}}{\sigma_{vv}}=\sqrt{[2\alpha^2+(1/c)^2]-\frac{3\beta^2\sigma_{\omega\omega}^2 f_{\omega\omega}{}''(0)}{2\zeta_0^2\omega_0^2}\frac{(1+4\zeta_0^2)}{[\beta^2(1+\sigma_{\omega\omega}^2/2\zeta_0^2)+4\zeta_0^2]}} \quad (5.35)$$

The normalized spatial correlation function of the present example (Eq. 5.25) yields $f_{\omega\omega}{}''(0)=-6/b_\omega^2$, and Eq. (5.35) takes the form of:

$$\frac{\sigma_{\varepsilon\varepsilon}}{\sigma_{vv}}=\sqrt{[2\alpha^2+(1/c)^2]+\frac{3\beta^2\sigma_{\omega\omega}^2}{\zeta_0^2\omega_0^2b_\omega^2}\frac{(1+4\zeta_0^2)}{[\beta^2(1+\sigma_{\omega\omega}^2/2\zeta_0^2)+4\zeta_0^2]}} \quad (5.36)$$

which presents the rms seismic strain, $\sigma_{\varepsilon\varepsilon}$, normalized with respect to the rms ground velocity, σ_{vv}, as a function of the apparent propagation velocity of the motions on the ground surface. It incorporates the effects of propagation, loss of coherency of the incident motion at bedrock, and stochasticity in the local site conditions.

If the soil has deterministic characteristics, equation (5.36) becomes:

$$\frac{\sigma_{\varepsilon\varepsilon}}{\sigma_{vv}} = \sqrt{[2\alpha^2 + (1/c)^2]} \tag{5.37}$$

In the two extreme cases, i.e., when $c \to 0$ and $c \to \infty$, the seismic ground strains of Eq. (5.36) assume the value:

$$c \to 0 : \frac{\sigma_{\varepsilon\varepsilon}}{\sigma_{vv}} = 1/c \tag{5.38}$$

i.e., the apparent propagation velocity of the motions controls the strains. It is noted that Eq. (5.38) is in complete agreement with the commonly used assumption of Eq. (5.22), and

$$c \to \infty : \frac{\sigma_{\varepsilon\varepsilon}}{\sigma_{vv}} = \sqrt{2\alpha^2 + \frac{3\beta^2\sigma_{\omega\omega}^2}{\zeta_0^2\omega_0^2 b_\omega^2} \frac{(1+4\zeta_0^2)}{[\beta^2(1+\sigma_{\omega\omega}^2/2\zeta_0^2)+4\zeta_0^2]}} \tag{5.39}$$

i.e., the random characteristics of the ground contributes in the shear strains.

In the next section a numerical example is presented to illustrate the effect of the spatial-random-variable soil profiles on the coherency loss function of the surface motions and seismic ground strains.

5.1.5 Numerical example

Stochastic characteristics of the ground

The parameters of the proposed model, ζ_0, ω_0, $\sigma_{\omega\omega}$ and $R_{\omega\omega}(\xi)$, depend on the soil properties and they need to be estimated. The mean value and standard deviation can be determined using standard techniques. In the present study, we consider the Sogedia site in El-Asnam city, with the soil conditions, shown in Figs. 5.2a, 5.2b and Table 5.1, over a length of 1200m.

The thicknesses and material properties given in Fig. 5.2a and Table 5.1, respectively, represent the mean values (expected values) estimated by Petrovski and Milutinovic (1981) of the properties of our one-dimensional, spatial random variable soil profile. For reasons of the limited availability of information (data from only one borehole is available at the Sogedia site) about spatial variation of soil properties in each layer and the measurement errors, it is assumed that the stochasticity in soil characteristics is due to variabilition in the depths of the

layers, i.e., the soil characteristics given in Table 5.1 are constant within each sub layer. The statistical variations of most soil properties follow a normal distribution (Wang and Hao, 2002). In this case, a same distribution is assumed for soil layer thickness and is accounted for by the coefficient of variation $cov_H = \sigma_{HH}/H$, with $cov_H = 20\%$ for each soil layer, j, j = 1, 2. Therein, the model ground (1200m x 33m x 1m) consists of two different layers (M = 2) with the material properties shown in Table 5.1. The bedrock is assumed to be rigid. The ground is divided into sixty sections in the horizontal direction, and each section has a horizontal length of 20m (20=1200/60). From the layer thickness and soil material data shown in Fig. 5.2b and Table 5.1, the predominant ground frequency $\omega^*(x_n)$ (n = 1, 2,..., 60) may be computed by Eq. (5.40), an extension of Okamoto's (1984) equation, for each vertical soil section. The mean predominant frequency value is $\omega_0 = 9.6\pi$ rad/s ($f_0 = 4.8$ hz) with a corresponding standard deviation of $\sigma_{\omega\omega} = 0.06$.

$$\omega^*(x_n) = \frac{\pi}{2}\frac{1}{\sum_{j=1}^{M} H_j(x_n)/v_{S_j}(x_n)} \tag{5.40}$$

Table 5.1 - Material properties of the site profile in Fig. 5.2.

Soil type	Mass density (gr/cm^3)	Poisson's ratio	Shear modulus (kgf/cm^2)	Shear wave velocity (m/s)	Damping ratio (%)
1- Clayey mixture	1.90	0.48	3040	400	5
2- Sandstone clay and sand	2.30	0.48	18630	900	3
3- Bedrock	2.4	0.49	96000	2000	1.25

For the value of the damping ratio, ζ_0, it is well-known that the response of a soil system subjected to strong earthquake motions is connected with significant, nonlinear effects that have to be taken into account in an appropriate manner. The site response in terms of the cross-spectral density function (Eq. 5.14) was derived using the soil columns at two stations separated by ξ as two linear systems. The derivation makes us of stationary random vibration theory, involving the frequency response function of the soil $H(\omega_0, \zeta_0, \omega)$. By definition, this function is the steady-state response of a linear system to a complex harmonic excitation of the form $\exp(i\omega t)$. Of course, behavior under strong earthquake motions is not linear. We need to define this function for some sort of an equivalent linear soil system. The model of the response function given by Equation (5.15) considers the soil column at the site as a single-degree-of-freedom system with viscous damping, where ω_0 and ζ_0 are the parameters of the

equivalent soil system. This, however, is a very crude model for several reasons, including the fact that soil damping is not viscous (Wang and Hao, 2002), and deep soil columns usually possess several significant modes of vibration. Additionally, it is not easy to determine the parameters ω_0 and ζ_0 on a rational basis. Nevertheless, this model is a simple alternative when other options are not practical. It is noted that this model is consistent with the well-known Kanai-Tajimi model (Kanai, 1957; Tajimi, 1960) for ground motions on soil sites. Typical ranges of the parameter values for that model are $\omega_0 = 2\pi - 5\pi$ rad/s and $\zeta_0 = 0.2 - 0.6$.

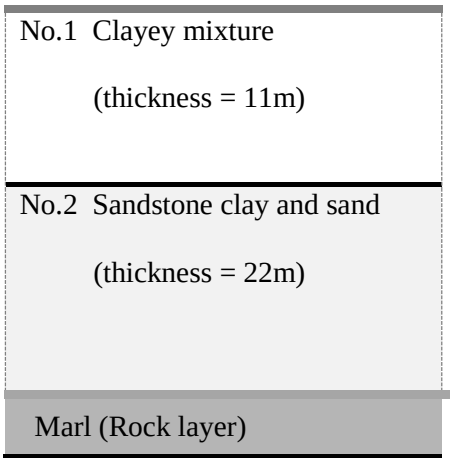

(a)

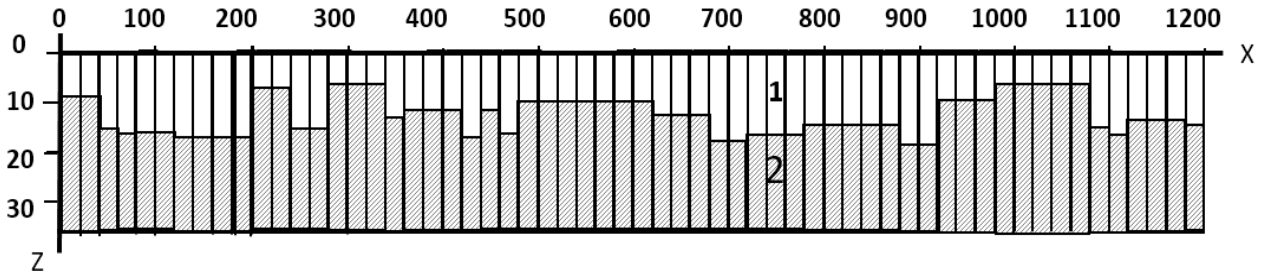

(b)

Fig. 5.2 - (a) Site profile at Sogedia Factory in northwest Algeria with mean layer thicknesses as shown (from Petrovski and Milutinovic (1981)), and **(b)** a realization of the soil profile (bedrock not shown) with stochastic layer thickness.

For a better representation of the frequency response function, one must model the site itself, not the frequency response function directly. Once such a model is developed, one can use existing soil response analysis, e.g., the program SHAKE (Idriss *et al*., 1992), to compute the frequency response function. The analysis would require computing the response of the soil column to a complex harmonic excitation for a long period in order to achieve the steady-

state response, as required by the definition of that function. Naturally, such an approach can account for the non-viscous and nonlinear behavior of soils, albeit in an approximate, equivalent, linear sense. This analysis must be repeated for each frequency, ω, to obtain a complete description of $H(\omega_0, \zeta_0, \omega)$. In this study, damping in each layer was estimated by using equivalent, linear, one-dimensional site response analysis. The bedrock motion is used as input motion, and an iterative procedure is used to estimate the damping ratio of an equivalent linear system. Therefore, it is considered to model hysteretic energy dissipation in the soil layers. The algorithm for the damping ratio and transfer function is SHAKE 91 (Idriss *et al*., 1992). Using the average properties (Fig. 5.2a and Table 5.1), the numerical values found of the damping ratio for each soil layer are given in Table 5.1. They are in accord with those estimated by Petrovski and Milutinovic (1981), whose values were found to be in the range of 1.0 - 4.5%.

We note that this approach is different from the one commonly used in investigating of the effects of lateral ground heterogeneities in ground-motion coherency. For example, for a firm site (high predominant frequency ω_0) in the present example, a damping ratio of 60% has been used by Zerva and Harada (1997), based on observations that the average power spectral density functions of recorded ground motion at firm sites match the so-called modified Kanai-Tajimi model with the parameter ζ_0 equal to 0.6. This parameter from the Kanai-Tajimi model can be interpreted to represent ground damping, but is not necessarily related to it. In particular, when power spectral density functions of ground motion recorded at different sites (all relatively firm but with slightly different predominant frequencies) are averaged, the averaging operation smooths the peaks of the spectra of individual ground motions. The resulting average spectrum has a broader peak with a width that is not representative of the widths of the individual spectra. Estimating damping (which controls the width of the peak) from the average spectra may not be reliable because of this. In any case, damping values as high as 60% are not realistic for firm soils. It is interesting to note that damping ratios of soft and firm sites estimated from average Kanai-Tajimi spectra are not consistent with common geotechnical engineering practice. For example, in studies such as Zerva and Harada (1997), soft soils are assumed to have a much lower damping ratio than firm sites. It is well known that soft soils dissipate more energy during inelastic deformations and, therefore, exhibit higher damping than firm sites.

The 5% of the damping ratio of the top layer (in Fig. 5.2a) is assumed for the damping coefficient, ζ_0, for the Sogedia soil site, because the values of the developed shear maximum strains occurred in all the thickness of this layer are significantly higher than those developed in the second layer.

The participator factor determined from Eq. (5.10) is $\beta = 4/\pi$. The sample spatial correlation function, $R_{\omega\omega}(\xi)$ of $\omega(x)$, is calculated by interpreting the sample, $\omega^*(x_n)$, as a realization of the homogeneous stochastic process, $\omega^*(x)$, using the following equation (Jenkins and Watts, 1969):

$$\tilde{R}_{\omega\omega}(\xi_k) = \frac{1}{N-k}\sum_{n=1}^{N-k}\left[\left(\frac{\omega^*(x_n+\xi_k)-\omega_0}{\omega_0}\right)\cdot\left(\frac{\omega^*(x_n)-\omega_0}{\omega_0}\right)\right] \tag{5.41}$$

where *N* is the total number of soil sections (60). To avoid a small averaging number, *N-k* in Eq. (5.41), $\xi_k = 600m$ is used as the longest separation distance.

The resulting normalized spatial correlation function, $\tilde{R}_{\omega\omega}(\xi_k)/\tilde{R}_{\omega\omega}(0)$ ($\tilde{R}_{\omega\omega}(0) = \sigma^2_{\omega\omega}$), is plotted in Fig. 5.3. The analytical spatial correlation function (Eqs. 5.24 and 5.25), normalized by the layer frequency variance, is also plotted in Fig. 5.3. The value of b_ω is determined in such a way that $R_{\omega\omega}(\xi)$ (Eq. 5.24) becomes zero for the same value of the separation distance, ξ, that produces a zero value for $\tilde{R}_{\omega\omega}(\xi)$ (Eq. 5.41); in this study case, $\xi = 60$ m for $\tilde{R}_{\omega\omega}(\xi) = 0$ (Fig. 5.3) and, thus, $b_\omega = 84.85$ m.

The power spectral density of the total surface motions (Eq. 5.16), normalized with respect to that of the incident motion PSD ratio, is shown in Fig. 5.5. As expected, its power is contained in the vicinity of the mean value of the layer predominant frequency, and its shape resembles that of the Kanai-Tajimi spectrum (Kanai, 1957; Tajimi, 1960). The high level of amplification is related to the low value of 5% selected for the damping, ζ_0. This high level is in accord with that found using SHAKE 91 for the absolute transfer function, $|H(\omega)|$, (also given in Fig. 5.5) between the surface and the top of the rock boundary of the soil at the Sogedia site, in regards to the other relation of the PSD ratio, $S_{uu}(\omega) = |H(\omega)|^2 \; S_{u_b u_b}(\omega)$ (Der Kiureghian, 1996). It is interesting to observe that the site has multiple resonant frequencies. Obviously, if a single-degree-of-freedom soil model, as in (Eq. 5.15), is used, one can model one resonant frequency at best. However, one should not discard this simple model too soon, since there are many structures, e.g., long-span bridges, for which the high-frequency components of ground motion are not significant. Even this simple model may be adequate if it captures the first resonant frequency well, as is the case for this site.

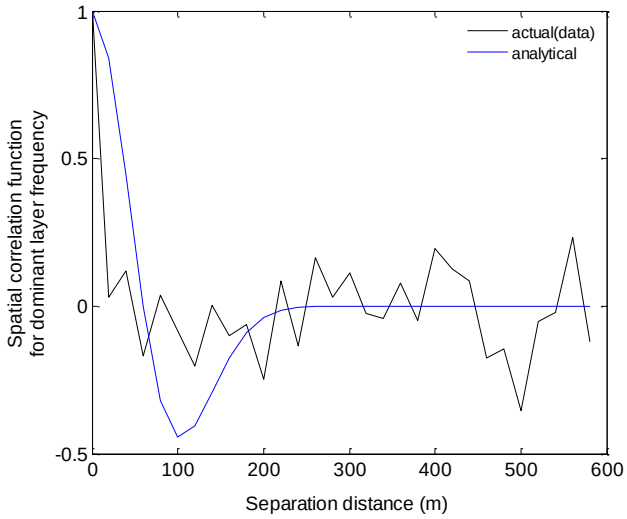

Fig. 5.3 - Spatial correlation functions for the predominant ground frequency of the stochastic layer using actual soil data (Sogedia soil profil shown in Fig. 5.2) and an analytical approximation.

From the individual stationary PSD of simulated acceleration at each station at the bedrock, the point spectrum, $S_{\ddot{u}_b\ddot{u}_b}(\omega)$, of the assumed incident random field can be obtained by simple averaging over all stations. In order to compensate for slight intensity variations from station to station, it is advisable to normalize each auto spectrum by dividing by the variance of the corresponding acceleration prior to averaging. Also, since averaging reduces the variance of the final point spectral estimates, each, individual auto spectrum can be estimated using a window with a small bandwidth in order to achieve good resolution (Harichandran, 1991).

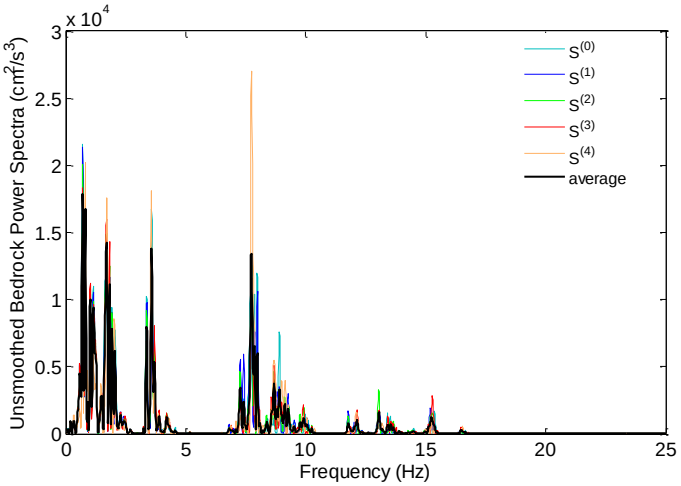

Fig. 5.4 - Power spectral density functions of simulated ground accelerations at bedrock (around Sogedia site) at the five stations (around Sogedia Factory site) corresponding to the 1980 El-Asnam Earthquake, and their average spectrum.

In the present study, we made a simple averaging because, as shown in Fig. 5.4, PSD's frequency content follows the same trend, and, exhibits insignificant differences (which are purely numerical as stations are located on uniform rock conditions) in the amplitudes. The average, $S_{\ddot{u}_b\ddot{u}_b}(\omega)$, of the unsmoothed (raw) PSD functions of the incident acceleration motions and their corresponding acceleration at the surface, $S_{\ddot{u}\ddot{u}}(\omega)$, computed using Eq. (5.16), are given in the Fig. 5.5. The function, $S_{\ddot{u}\ddot{u}}(\omega)$, will be utilized in Section 5.2 for the simulation of the SVGMs on the ground surface required for the nonlinear structural response history analysis.

The contribution of the layer stochasticity to lagged coherency at the ground surface (Eq. 5.19) at separation distances of 40, 100, 200, and 500 m are presented in Fig. 5.6. The correlation structure in Fig. 5.6 is different from that expected in spatial variability (i.e. exponential decay with both separation distance and frequency). The site contribution to the coherency is exactly equal to one, except for a drop at the stochastic layer predominant frequency (at approximately $f_0 = 4.8$ Hz) that is caused by the random variability around its mean value for the different soil columns from the site. The explanation of Zerva and Harada (1997) for this realistic phenomenon was that the soil layer responds to the incident excitation as a series of single-degree-of-freedom systems with slightly varying, correlated natural frequencies. For input motion frequencies close to the mean natural frequency of the oscillators, the response of the systems is affected by the variability in the value of this natural frequency and results in a loss of correlation. As the exciting frequencies increase past the natural frequency of the systems, the actual value of the natural frequency (for small variabilities) ceases to affect the response significantly.

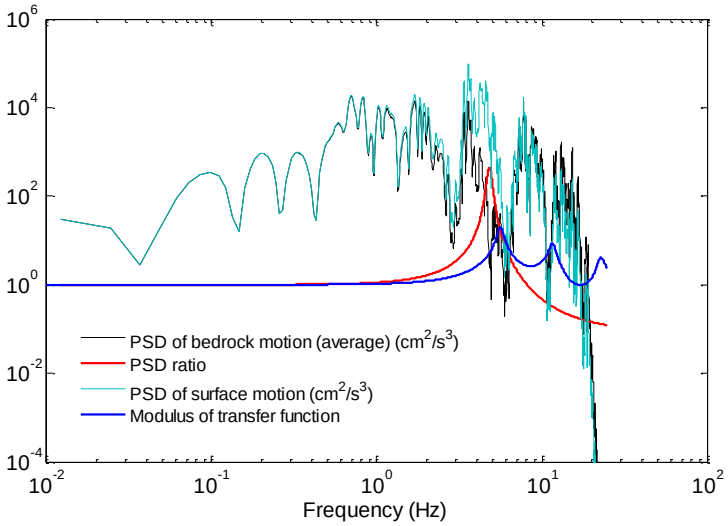

Fig. 5.5 - Power spectral density of ground acceleration at bedrock and the ground surface, their ratio, and equivalent linear transfer function of the site (see legend for units and descriptions).

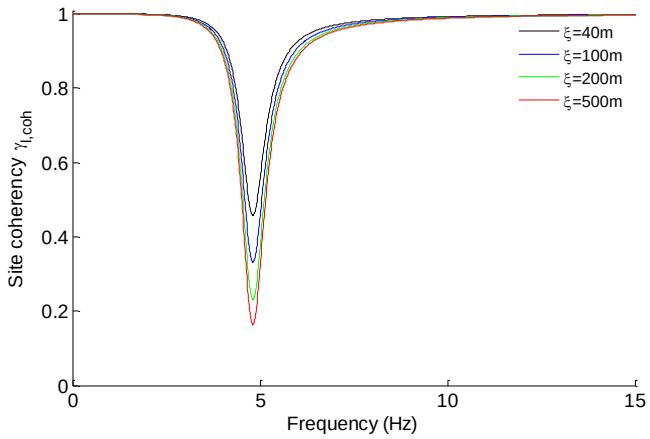

Fig. 5.6 - Contribution of layer stochasticity to the lagged coherency of surface motion (see Eq. 5.16).

Through this numerical example, it is clear that the effects of soil heterogeneity are to significantly decrease lagged coherency at frequencies close to the fundamental frequency of the firm site. The decrease is, as expected, proportional to the separation distance. At a short separation distance, 40m, soil heterogeneity results in significantly incoherent motion, and results in greatly incoherent motion for medium to large separation distances, even for the firm soil condition when its damping ratio is low. On the other hand, it is important to stress that the decrease of the coherency is significant even for the relatively low coefficient of variation, 20%, considered in this study. Zerva and Harada (1997) adopted larger coefficients of variation (in the range of 30-90%), but observed a less pronounced loss of coherency than that presented in Fig. 5.6. This is due to the high damping ratio adopted by Zerva and Harada as discussed previously. The results indicate that the loss of coherency is very sensitive to damping in soil. Therefore, a proper estimation of the soil damping ratio is very important studying the soil effects in ground-motion incoherence. From the analytic expression of $\gamma_{l,coh}(\xi,\omega)$ in Eq. (5.19), it is clear that the soil damping ratio has a direct effect on the loss of coherency. On the other hand, the effect of the coefficient of variation of layer thickness, cov_H, is indirect through its effect on the autocorrelation function of the predominant site frequency, which depends also on the horizontal fluctuation of values of the material soil property, $q(x,z)$, such as the shear wave velocity.

In Eq. (5.21), for the overall incoherence, the incident motion incoherence, $\gamma_{b,coh}(\xi,\omega)$, is obtained from simulated ground motion using the extended EGF method. The details of simulation are explained in Section 3.2. The lagged coherency functions at the bedrock for four separation distances are shown in Fig. 5.7. The parametric models of Hindy and Novak (1980), Luco and Wong (1986) and Somerville *et al*. (1988), that were described and

discussed in Section 3.3, fitted to the estimated lagged coherency functions are also shown in Fig. 5.7. The Hindy and Novak coherency model, with its two parameter values of $\alpha = 5.87\times10^{-5}$ sec m^{-1} rad^{-1} and $\lambda = 1.52$, is then selected as the preferred model (it exhibits a better fit, as discussed in Sect. 3.3) to idealize and represent the actual incident motion incoherence , $\gamma_{b,coh}(\xi,\omega)$, in Eq. (5.21). On the other hand, because of its respect of the requirement of mean-square differentiable unlike to the Hindy and Novak model, the Luco and Wong model with the value found for its parameter, $\alpha = 9.41\times10^{-5}$ sec m^{-1} rad^{-1}, is selected to idealize the same $\gamma_{b,coh}(\xi,\omega)$ in the ground shear strain estimate resulting from Eq. (5.36) and which is addressed later herein.

Using this parametric model for bedrock, and the site contribution shown in Fig. 5.6, the lagged coherency at the surface was estimated and is presented in Fig. 5.8. The lagged coherency functions exhibit a sharp decrease near the fundamental frequency of the site. Even at a short separation distance of 40m, the effect of soil heterogeneities reduces the lagged coherency near the site fundamental frequency from ~0.95 at bedrock to ~0.4 at the surface.

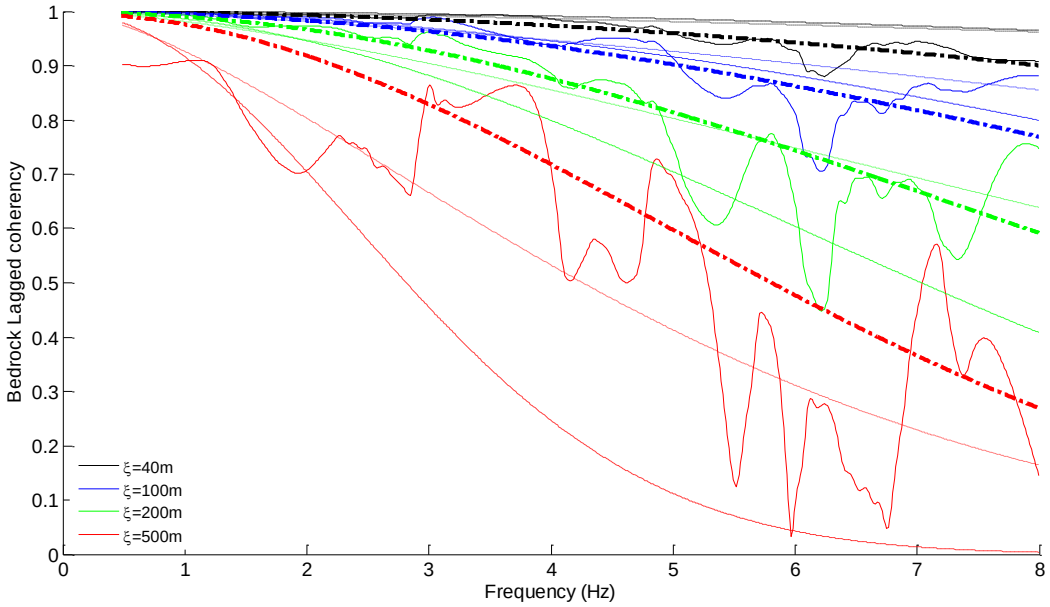

Fig. 5.7 - Lagged coherency function estimated at the bedrock (solid lines, see Fig. 3.8) and the fitted parametric models of Luco and Wong (dashed lines), Hindy and Novak (dotted lines) and Somerville *et al*. (thicker dashed-dotted lines).

Figure 5.9 compares the coherency at distances of 40, 100, 200 and 500 m for incident and surface motions. It is noted from the figure that the overall shape of the total coherency is controlled by that of the incident motion as it decays with separation distance and frequency, following the model of Hindy and Novak, i.e., the loss of coherency due to the finite-source

effect. The layer stochasticity results in a decrease in the correlation close to the mean value of the natural frequency of the layer. This is expected, since the total incoherence of the surface motions is the product of the incident motion incoherence and incoherence resulting from the layer stochasticity.

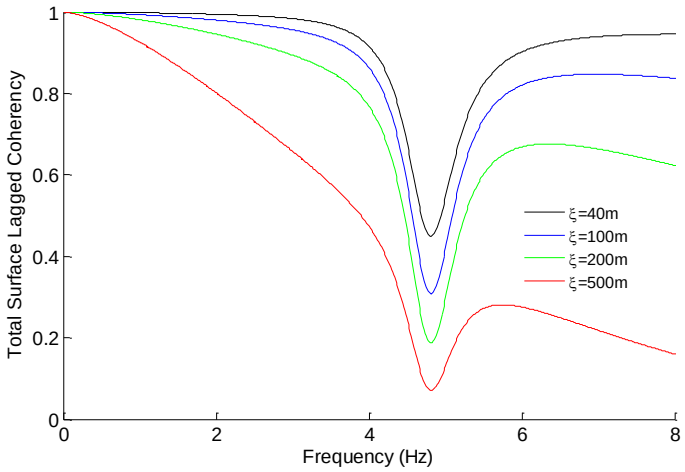

Fig. 5.8 - Lagged coherency function at the surface; obtained from the bedrock coherency function (Hindy and Novak model as shown with dotted lines in Fig. 5.7) and the contribution of stochastic site as shown in Fig. 5.6.

The drop in the correlation at the predominant frequency of the layers is distinguishable. The drop in coherency observed in Figs. 5.6 and 5.9 has also been noted by Kanasevich (1981), who suggested that site resonances can be identified from holes in the coherency spectra of motions at adjacent locations and by Cranswick (1988), who further indicated that perturbations with small deviations in the layer characteristics will produce the greatest changes in the response functions. Since incoherence is a measure of similarity in the motions (i.e., the change in the shape of the motions at different locations), it will be low at the resonant frequencies. Liao and Li (2002) also reached a similar conclusion from their analytical evaluation of wave propagation through media with random variable properties.

The overall agreement of the spatial coherency with and without site effects found by Zerva and Harada in their example of a random, soft soil site with $\zeta_0 = 0.2$ is not the case with the present observations at the firm Sogedia site. These indicate that the site variability may particularly influence the overall correlation structure of the total motion. It also does not justify the use of smoothly decaying spatial coherency models with parameters obtained from surface records (e.g., Luco and Wong, 1986) to describe the coherency of the incident motions.

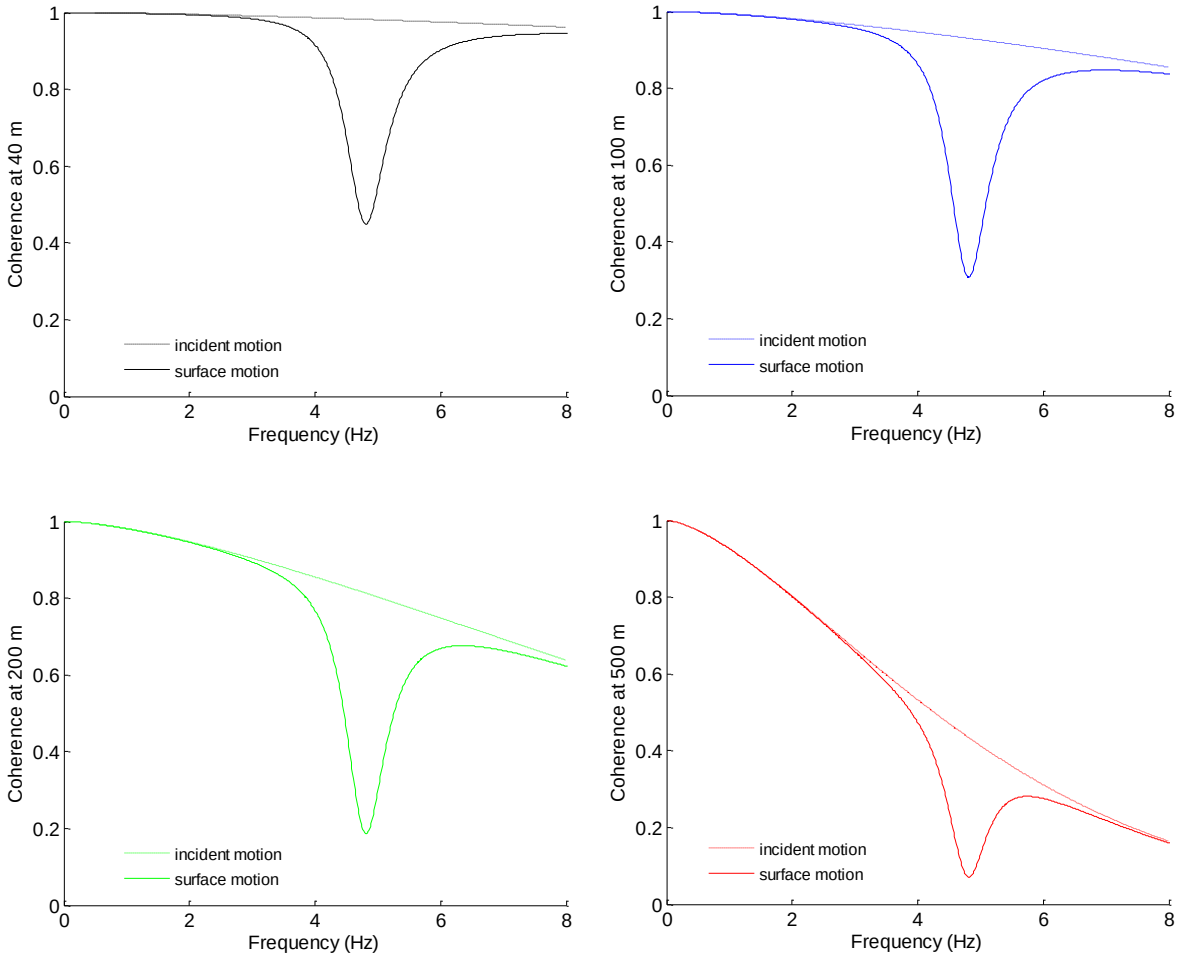

Fig. 5.9 - Variation of the total spatial incoherence (incident motion and layer stochasticity) with frequency at separation distances of 40, 100, 200 and 500 m.

The coherency trough in Fig. 5.9 where the power spectral amplitude is peaked due to the site effects, (see red curve of the PSD ratio in Fig. 5.5) could be seen as not in agreement with observations from recorded data. Abrahamson *et al.* (1991) observed that the peaks of an average Fourier amplitude spectrum (FAS) from surface motions produce high coherency at the same frequencies and spectral troughs at low coherency, that were attributed, respectively, to the direct (coherent) energy that dominates spectral peaks and to the scattered energy that dominates spectral troughs. According to Zerva and Harada's conclusion, if the coherency troughs occurred at the dominant frequencies of the site, they would be associated with amplitude peaks rather than troughs. We think that the contradiction with Abrahamson *et al.*'s conclusion is not evident. A comparison between them should be based on the analysis of the spectral ratio (i.e. modulus of the ratio of transfer functions) between the two considered sites, wave paths, or soil columns. This is a more reliable and appropriate parameter to measure the local site effects on incoherence of spatial surface ground motions, according to the approach

of Bi and Hao (2011), explained in the beginning of this chapter and the above rational interpretation of this type of coherency-drop given by Cranswick (1988). Indeed, the PSD ratio expression taken from the Eq. (5.16) of Zerva and Harada uses the mean values of soil properties and not those corresponding to each soil column. The FAS in Abrahamson *et al.*'s research is that of surface motion and not a FAS ratio with respect to the bedrock motion, in addition to the fact that it is an average taken over several stations having different wave paths through the considered site.

Of course, there are additional considerations that need to be taken into account for the proper evaluation of local coherency at a specific site. The seemingly reasonable and simplifying approximations in the analytical derivations of coherency models do not capture the complex physical causes underlying (the complex geologic conditions underneath the arrays and the complexity of the incoming waves) the spatial variation of seismic ground motions. In other words, such models do not take into consideration the lateral coupling of the wave propagation at the site.

The present methodology of Zerva and Harada (1997) incorporates site effects in the spatial correlation structure of the motions that are consistent with observations, but have not been taken into account before, in its estimates through a simple approach. Generally, it is assumed that the site contribution results from the response of the individual, statistically independent soil columns with different characteristics. Accordingly, the site contribution does not affect incoherence but produces a deterministic phase difference in the surface motion correlation (Der Kiureghian, 1996). Clearly, the deterministic phase difference is caused by the delays in the arrival of the waves from the bedrock to the ground surface due to their propagation through different layers.

The present approach approximates the soil columns transmitting the bedrock excitation to the ground surface by single-degree-of-freedom systems with similar, correlated characteristics. The time delay in the arrival of the waves from the interface to the ground surface is incorporated in the model through the layer predominant frequency (Eq. 5.8). An incident impulse acceleration at the bedrock-layer interface at $t=0$ would produce a maximum response on the ground surface at approximately $t=(1/4)(2\pi/\omega_0)$, with $(2\pi/\omega_0)$ representing the period of oscillation. The layer stochasticity causes random fluctuations in the arrival of the waves from the bedrock to the surface. Thus, it affects the lagged coherency random phase variability of the motions. The apparent propagations (deterministic phase) of the surface motions are controlled by that of the incident motion, since vertical propagation is considered within the layer.

It is emphasized that the present methodology is applicable to sites with no dramatic changes in their topography, for which the homogeneity assumption for the layer variability is

valid. For sites with spatial characteristics that deviate significantly from constant mean values, the spatial homogeneity assumption ought to be waived. In this case, the layer stochasticity would affect both the incoherence and the apparent propagation (deterministic phase) of the motions.

Figure 5.10 presents the estimate of the ratio of the rms ground strain, $\sigma_{\varepsilon\varepsilon}$, at the site over the rms of particle velocity, $\sigma_{\upsilon\upsilon}$, (Eq. 5.36) of the seismic motion at the surface of our spatial-random-variable Sogedia soil profile as function of the apparent propagation velocity of the motions. In addition to the variation in Eq. (5.38) due to the apparent propagation effects only and which is the basic assumption of the single-station strain estimates, three others variations of seismic strains are presented in the figure. The first, termed incidence motion incoherence in the figure, corresponds to incident wave effects only (Eq. 5.37) (i.e., ground motions exhibiting loss of coherency according to the Luco and Wong model, $\alpha = 9.41\times10^{-5}$ sec m^{-1} rad^{-1}, and propagating on the ground surface, but the random variability in the layer properties is not considered). The second, termed site incoherence, corresponds to site effects only, i.e., the incident motions are fully coherent, $\alpha = 0$ in Eq. (5.36), and loss of coherency results only from the variability in the layer properties while motions still propagate on the ground surface. The third estimate, termed total incoherence, incorporates the contributions of both the incident motion variability ($\alpha = 9.41\times10^{-5}$ sec m^{-1} rad^{-1}) and the surface layer stochasticity (Eq. 5.36).

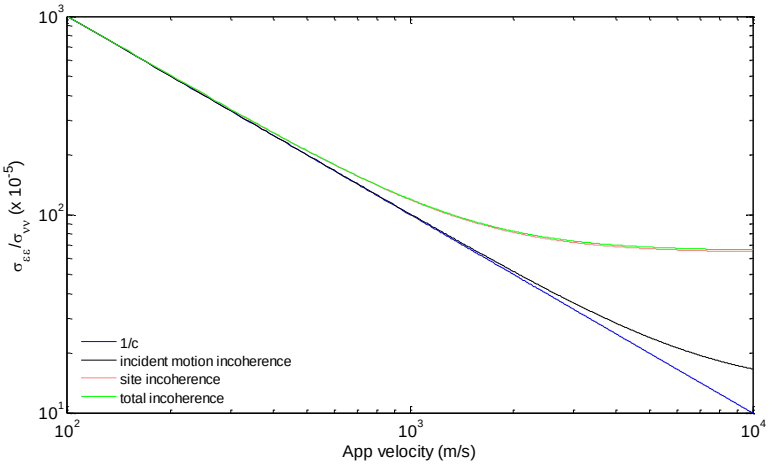

Fig. 5.10 - Variation of rms strain over rms ground velocity ($\sigma_{\varepsilon\varepsilon}/\sigma_{\upsilon\upsilon}$) with the apparent propagation velocity of the motions, *c*.

Figure 5.10 shows that, for low values of the apparent propagation velocity, $c \prec 500\,m$, that are the case for surface, rather than body, wave propagation, the apparent propagation

effects overshadow those of loss of coherency, and Eq. (5.22) is valid. For higher values of the apparent propagation velocity, which are more appropriate in near-source regions for the shear waves considered in the analysis (in these regions, more realistic values for *c* would be greater than 1500 m/s, since the strong shaking part of the seismic motion generally propagates on the ground surface with the apparent velocity of the body waves at the bedrock-surface layer interface, and the angle of incidence of such waves could be as high as 90° ($c \to \infty$)), loss of coherency starts become important and fully controls the values of the seismic ground strains, which in turn control the seismic response of buried pipelines, as is reflected by the essentially constant value of the ratios in Fig. 5.10, at the apparent propagation velocity of $c \succ 3500$ m/s. This constant value should increase with increasing total incoherence. In this region, the estimate of the commonly used assumption from Eq. (5.22) significantly underestimates the actual values of the seismic strains. For $c \prec 3500$ m/s, there is transition region where the propagation effects start contributing to the strains, which start increasing until, eventually, they become proportional to the inverse propagation velocity. Again, in this range of velocities, Eq. (5.22) underestimates the seismic strains. Figure 5.10 confirms that higher strain occurs are obtained at low propagation velocities, i.e., that wave effects may be more significant for the response of pipelines in regions where surface waves dominate (low propagation velocities) rather than in near-source regions where body waves dominate (significant incoherence effects from extended sources and/or from scatterers and/or from random soil properties).

It should be noted at this point that a similar pattern for the variation of the seismic strains with the apparent propagation velocity of the motions was observed by O'Rourke et *al*. (1980) from their analysis of the recorded data during the 1971 San Fernando earthquake. The epicentral distance of the 1980 El-Asnam earthquake, Ms=7.2, from the Sogedia site under consideration was around 5Km, i.e. the area would be considered a near-source region (according to Table A3 in the Appendix), in which body waves should dominate. The value of *c* at the Sogedia bedrock-layer interface, evaluated analytically from the source-site geometry as explained in Section 5.2, is 5200 m/s. Then, we can see from the Fig. 5.10 that when $c = 5200$ m/s, the relative strain estimate, $1/c$, produces only 1/5 of the value of the strain due to total incoherency effects, suggesting that strain estimates as they are currently used for design produce nonconservative results in regions where incoherence effects are important.

This incoherence effect was not obvious from the spatial variability of the surface ground motions (Fig. 5.9). Although, it is not altogether unexpected, since the layer stochasticity contribution to seismic strains occurs around the dominant soil frequency (Eq. 5.32). Figure 5.10 further suggests that the effects of the site stochasticity contribute more to the total values of seismic ground strains than those of the incident motion variability. As expected, the combined effect of the bedrock motion and layer stochasticity yields higher strains (Fig.

5.10). The Zerva and Harada (1997) analysis used for the Sogedia site suggests that the effect of layer stochasticity cannot be neglected in the evaluation of the spatial variation of seismic ground motions, and a simple approach may suffice for the site-specific evaluation of seismic ground strains.

The spatially variable seismic ground motion model described in the previous section (the coherency model given in Eq. (5.17) using the Hindy and Novak or Luco and Wong coherency models) can be used directly as input motions at the supports of lifelines in random vibration analyses. The nonlinear response evaluation of the structural systems, however, requires a time history analyses. Such analyses, in turn, necessitate the generation of spatially variable time histories to be used as input excitations at the structures. Spatially variable seismic ground motions can be generated either from the description of the random field through a power spectral density (or a response spectrum) and a spatial variability coherency model or from a predefined seismic ground motion time history (e.g., a recorded accelerogram) and a spatial coherency model. The former, which is the most common approach, is referred to as an unconditional simulation of spatially variable seismic ground motions (Hao *et al*., 1989; Deodatis, 1996), whereas the latter is referred to as a conditional simulation of spatially variable seismic ground motions (Abrahamson, 1992).

5.2 Spatial ground motion time histories simulation at spatial-random-variable soil

We propose, in this section to simulate the horizontal, in-plane, spatially variable acceleration motions on the surface of the Sogedia layered stochastic soil profile by applying the stochastic methodology given by Hao *et al*. (1989) and Olievera *et al*. (1991), which is a spectral decomposition simulation scheme utilizing a sequential approach and random phase variability and which needs to predefine the random field through a power spectral density and a spatial variability model. According to Hao *et al*. (1989), a spectral representation based simulation algorithm is first used to generate stationary time histories that are compatible with a prescribed power spectral density and lagged coherency functions and constant apparent propagation velocity, but not with the prescribed response spectrum. After multiplying these stationary time histories by an appropriate envelope function to introduce non-stationary ground motions and to control the duration of strong ground motions, Hao *et al*. adjust each non-stationary time history independently to make it compatible with the prescribed response spectrum. This adjustment is performed by Fourier transforming each non-stationary time history to the frequency domain, multiplying its frequency domain Fourier transform by the ratio of the prescribed response spectrum over the computed response spectrum of the non-stationary time history, and then inverse transforming the product back to the time domain. This adjustment procedure is usually repeated a few times. Many later developments, such as

of Deodatis (1996) for generating non-stationary, non-homogeneous and response-spectrum-compatible spatially variable seismic ground motions, are based on this method.

The surface motions at different locations are assumed to be stationary, random processes with zero mean values and have the same two-sided power spectral density $S_{ii}(\omega)$ or $S_0(\omega)$ of ground motion u (this assumption is reasonable, see in Section 5.1.2). The two-side cross power spectral density function, $S_{ij}(i\omega)$, between ground surface motions at *n* locations in a site can be expressed in terms of $S_0(\omega)$ and the complex spatial coherency functions, $\gamma_{ij}(i\omega)$, $i, j = 1, 2, ..., n$, which includes the wave passage effect, as :

$$\boldsymbol{S}(\omega) = \begin{bmatrix} \gamma_{11}(\omega) & \gamma_{12}(i\omega) & \dots & \gamma_{1n}(i\omega) \\ \gamma_{21}(i\omega) & \gamma_{22}(\omega) & \dots & \gamma_{2n}(i\omega) \\ \dots & \dots & \dots & \dots \\ \gamma_{n1}(i\omega) & \gamma_{n2}(i\omega) & \dots & \gamma_{nn}(\omega) \end{bmatrix} S_0(\omega) \qquad -\omega_N \le \omega \le \omega_N \tag{5.42}$$

Since the matrix, $\boldsymbol{S}(\omega)$, given by Eq. (5.42) is Hermitian and a positive definite, it can always be decomposed into the multiplication of a complex lower triangular matrix, $\boldsymbol{L}(i\omega)$, and its Hermitian $\boldsymbol{L}^H(i\omega)$, as shown by:

$$\boldsymbol{S}(\omega) = \boldsymbol{L}(i\omega)\boldsymbol{L}^H(i\omega)\, S_0(\omega) \tag{5.43}$$

where

$$\boldsymbol{L}(i\omega) = \begin{bmatrix} l_{11}(\omega) & 0 & \dots & 0 \\ l_{21}(i\omega) & l_{22}(\omega) & \dots & 0 \\ \dots & \dots & \dots & \dots \\ l_{n1}(i\omega) & l_{n2}(i\omega) & \dots & l_{nn}(\omega) \end{bmatrix} \tag{5.44}$$

and where l_{ij} $(i = 1, 2, ..., n,\ j = 1, 2, ... i)$ can be calculated by the Cholesky method. After obtaining $\boldsymbol{L}(i\omega)$, the stationary time series at all points, $u_i(t)$ $i = 1, 2, ..., n$, that reflect the effects of time delay and loss of coherency, can be simulated in the time domain directly :

$$u_i(t) = \sum_{m=1}^{i} \sum_{k=1}^{N} A_{im}(\omega_k) \times \cos\left[\omega_k t + \beta_{im}(\omega_k) + \phi_{mk}(\omega_k)\right] \tag{5.45}$$

where

$$A_{ij}(\omega) = \sqrt{4S_0(\omega)\Delta\omega}\ \left|l_{ij}(i\omega)\right| \qquad 0 \le \omega \le \omega_N \tag{5.46}$$

$$A_{ij}(\omega) = \sqrt{4S_0(\omega)\Delta\omega}\ \left|l_{ij}(i\omega)\right| \qquad 0 \le \omega \le \omega_N \tag{5.47}$$

$$\beta_{ij}(\omega) = \tan^{-1}\left(\frac{\mathrm{Im}\left[l_{ij}(i\omega)\right]}{\mathrm{Re}\left[l_{ij}(i\omega)\right]}\right) \qquad 0 \le \omega \le \omega_N \tag{5.48}$$

are the amplitudes and phase angles of the simulated time histories that ensure the spectrum of the simulated time histories are compatible with those given in Eq. (5.42). $\phi_{mk}(\omega_k)$ is the random phase angles, uniformly distributed over the range of [0, 2π], ϕ_{mk} and ϕ_{rs}, and should be statistically independent unless $m = r$, and $k = s$. ω_N represents an upper cut-off frequency beyond which the elements of the cross power spectral density matrix given in Eq. (5.42) is assumed to be zero (i.e., insignificant) for either mathematical or physical reasons. $\Delta\omega$ is the resolution in the frequency domain. $\omega_k = k\Delta\omega$ is the *k*th discrete frequency, *k* = 1 to *N* and where *N* is the total number of frequencies under analysis, $\omega_N = N\Delta\omega$. The time series generated by Eq. (5.45) are stationary processes. In order to obtain the non-stationary time histories, the envelope (intensity modulating) function, $\zeta(t)$, is applied to $u_i(t)$. The non-stationary time histories at different locations are obtained by:

$$f_i(t) = \zeta(t).u_i(t), \qquad i = 1,\ 2,...,\ n \tag{5.49}$$

In the present example of the Sogedia soil profile, we generate the horizontal component of accelerations on the ground surface at five (*n* = 5) locations (stations), namely $S'^{(0)}$, $S'^{(1)}$, $S'^{(2)}$, $S'^{(3)}$, and $S'^{(4)}$. Station $S'^{(0)}$, which corresponds to the projection on the surface of the previous station, $S^{(0)}$, at the rock, is considered as the reference station and is located at X=0 in the Fig. 5.1. The other stations are separated from it by 40 m, 100 m, 200 m, and 500 m. The epicentral distance of the surface reference station is 5 km.

The power spectral density function, $S_{ii}(\omega)$, of the surface motions is modelled by the Eq. (5.16) (displacement) that was plotted (acceleration) in Fig. 5.5. The spatial coherency function, $\gamma_{ij}(i\omega)$, at any two locations, i and j, on ground surface separated by a distance, ξ, is modeled by the complex spatial coherency function, $\gamma(\xi,\omega)$, given in Eq. (5.17), in which the bedrock coherency loss, $\gamma_{b,coh}(\xi,\omega)$, is represented by the previously selected Hindy and Novak (1980) lagged coherency. $\gamma_{b,prop}(\xi,\omega)$ represents the wave passage effect at the bedrock. For the Sogedia base rock with a shear wave velocity of, $v_s = 2000$ m/s and considering the location chosen for the five stations relative to the El-Asnam fault, we

estimate analytically the value of the angle of incidence for waves at the interface of $\pi - i_\xi$ = 180-157.38°. c is the apparent wave velocity $\left(c = v_s / \sin(\pi - i_\xi)\right)$ at the bedrock-surface layer interface. This is 5200 m/s, according to the base rock property and the specified incident angle. $\gamma_{l,coh}(\xi, \omega)$ is the contribution of the Sogedia layer stochasticity to the coherency modeled by Eq. (5.19) and plotted in Fig. 5.6. The overall incoherence, $\gamma_{coh}(\xi, \omega)$ (incident motion incoherence and layer stochasticity), in the spatial variation of the surface motions is plotted in Fig. 5.8. To model the temporal variation of the simulated ground motions, the simulated stationary time histories are multiplied by the Jennings *et al*. (1968) envelope function with the following form:

$$\zeta(t) = \begin{cases} (t/t_0)^2 & 0 \le t \le t_0 \\ 1 & t_0 \le t \le t_n \\ \exp\left[0.155(t - t_0)\right] & t_n \le t \le T \end{cases} \tag{5.50}$$

$t_0 = 2$ sec and $t_n = 15$ sec were used, so that the flat part of the envelop function, or, equivalently, the strong motion duration of the series, is $t_n - t_0 = 13$ sec. This assumed value of 13 sec corresponds to the same strong duration of motions on the Sogedia bedrock generated by the EGF method in the Section 3.2.

In the simulation, the time increments between discrete points in a time series is Δt = 0.02 sec. The total number of points in the series is Npts = 4096 (=2^{12}), which gives a total duration of T = $(N\text{pts-1}) \cdot \Delta t$ =81.90 sec. The sampling frequency, f_s ($f_s = 1/\Delta t$), and the Nyquist folding frequency, f_N ($f_N = 1/2\Delta t$), for such a sample are 50 Hz and 25 Hz. That is, the highest frequency that can be investigated if one samples a time series at intervals of length Δt is $1/2\Delta t$. Otherwise, the power spectrum will be aliased. The usual frequency increment for FFT data analysis is $df = 1/T$ = 0.0122 Hz ($\Delta\omega$ = 0.0767 rad/s) and $N = N\text{pts}/2+1$ = 2049, which implies that $\omega_N = N\Delta\omega$ = 24.997 Hz (157.065 rad/s).

The five, generated, horizontal surface motions are shown in Fig. 5.11 from t = 0 up to t = 50 sec rather than the simulated, full duration of 81.90 sec. The PGAs of the simulated motions are around 1000 m/s². The high level of the PGAs is related to the high value of the PSD ratio, or equivalently, that of the absolute transfer function of the soil (shown in Fig. 5.5), which is due to the -low value of 5% of the equivalent ratio damping, ζ_0, found for the firm Sogedia soil profile.

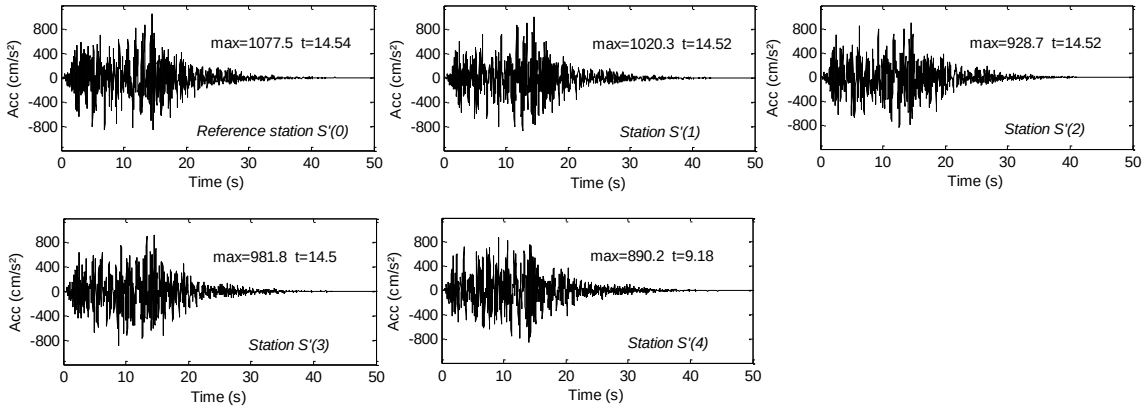

Fig. 5.11 - Generated horizontal, in-plane acceleration motions at five stations on ground surface over a length equal to 81.90 sec.

Fig. 5.12 shows the comparison of the power spectral densities (acceleration) of the generated time histories with the target spectral density function model (Eq. 5.16). It shows that power spectral densities of the simulated motions match well with the target spectrum. Fig. 5.13 shows the coherency loss functions computed (as described in Sect. 2.5) between the generated time histories and the overall incoherence model, $\gamma_{coh}(\xi,\omega)$, (Eq. 5.21). A good match can also be observed. It is then proven that the simulated, spatial ground motion time histories are compatible with the model of power spectral density individually and the model coherency loss function between stations. In the absence of recorded data, the generated time histories can be used as input to multiple supports of long span structures crossing a random site.

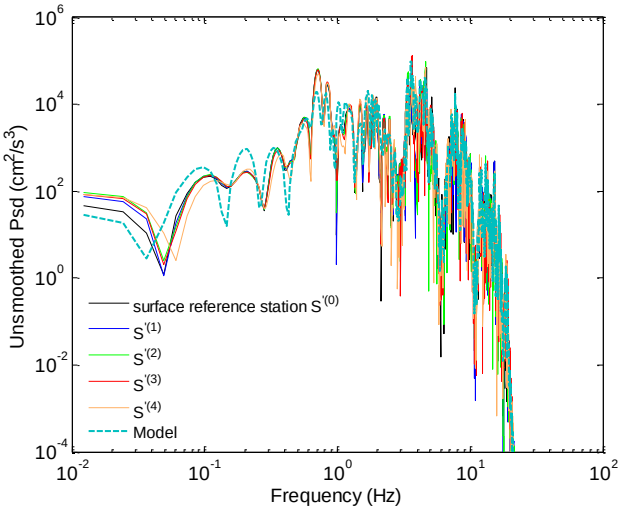

Fig. 5.12 - Comparison of power spectral density of the generated surface acceleration with model power spectral density.

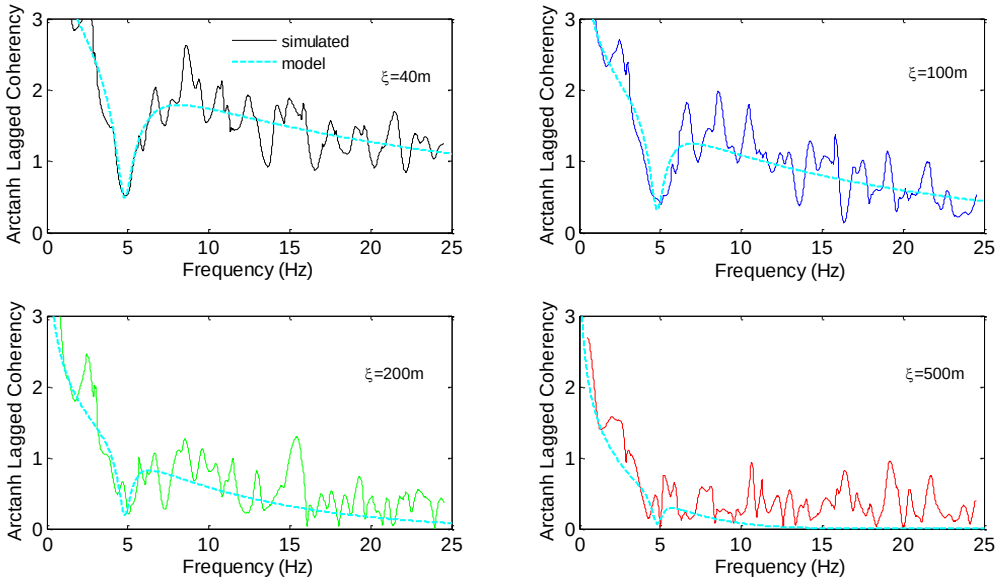

Fig. 5.13 - Comparison of coherency loss between the generated surface accelerations with model coherency loss function.

SUMMARY AND CONCLUSIONS

Summary and conclusion:

The main contribution of this work is to present an approach to simulate spatially variable ground motions using the empirical Green's function method. This method has been extensively used in the literature to simulate point estimates of strong ground motion. In this work, we test whether it is suitable for simulating a ground bedrock motion field within a relatively small spatial extent, thereby modelling incoherence effects. The case study and parametric study presented herein suggest that the approach is suitable for simulating incoherence due to finite source effects. In particular, plane wave coherency estimates can be obtained through such simulations. Although loss in coherency is due to source scattering and local site effects, the present methodology captures only the effects from finite sources. This is a limitation of the method. Nevertheless, in the absence of recorded data, the method can be useful in modelling spatially variable ground motion at bedrock, in that the simulated coherencies can be considered as upper bounds of what is expected in the presence of scattering and local site effects. In a practical sense and in the absence of strong motion array data in the study region, the results presented could provide a rough approximation of ground motion coherency that can be used in a random vibration analysis of lifeline structures or simulating spatially variable ground motion for a time history analysis of such structures. To facilitate such modelling, a parametric model of lagged coherency was presented. The parametric model follows the same functional form as that of Hindy and Novak (1980), and the model parameters are calibrated using simulated lagged coherency functions. The presented model should be considered representative of plane wave coherency when scattering effects in the simulated ground motion are lacking, as is the case of Hindy and Novak (1980) model.

A parametric study investigating sensitivity of lagged coherency showed that shear wave velocity, earthquake magnitude, and epicentral distance are all important factors that contribute to plane wave coherency. Larger shear wave velocity was found to produce more coherent motion in general. Larger earthquakes were found to produce more incoherent motion. In the near-field, the finite source effect seems to be significant for producing incoherent motion. While in the far-field, plane wave coherency was found to be almost equal to one up to a frequency of 8 Hz. Because structures in the near-field are more severely affected by earthquakes, the practical significance of the presented methodology is justified in because it provides a first approximation, and possibly an upper bound, on lagged coherencies.

From the seismic engineering viewpoint where the simulations of SVGMs are desirable on the ground surface, a method of accounting for stochastic, local site effects in estimating total loss incoherence of surface motions at the El-Asnam Sogedia site was used. The study shows that the layer stochasticity can significantly reduce, and greatly for medium to large separation distances, the lagged coherency near the site's resonant frequency, even for firm soil conditions with a low damping ratio. It was also shown that, for these soil conditions, the layer stochasticity controls the seismic ground strains. A stochastic generation of time histories at various locations on the ground surface of the El-Asnam Sogedia site, compatible with our estimations of the target power spectral densities and the spatial coherency functions, was presented. These resulted in spatial surface ground motion time histories that can be used as multiple inputs for the nonlinear seismic response analysis of multi-supported structures.

Further study on the effect of other relevant parameters, such as geometry of the fault, location of stations on the hanging or foot wall, directivity of stations with respect to rupture propagation, and geometry of the rupture source, would be valuable in understanding their effects in plane wave coherency. In addition, investigating scattering effects (near the earth's surface, near the array, and elsewhere along the propagation path at increasing distances) would be valuable. For example, randomness in rupture velocity and rise time on the fault can enrich the frequency content of ground motion (Zerva and Shinozuka, 1991). The effects of fault geometry and the size of sub-events could also have significant effects on ground-motion coherency (see, for example, Ding and Song, 2010). Bilateral rupture propagation and source directivity effects can also influence ground-motion coherency (see, Spudich, 1994). Source asperities may generate highly coherent energy in a narrow frequency band (Abrahamson et al., 1991) thereby altering the spectral nature of lagged coherency functions. These effects, and others, need to be investigated in detail, preferably using well recorded past earthquakes.

REFERENCES

References:

Abrahamson NA (1992) Generation of spatially incoherent strong motion time histories. Proceedings of the 10th World Conference on Earthquake Engineering, Madrid, Spain.

Abrahamson N, Schneider JF, Stepp JC (1991) Spatial coherency of shear waves from the Lotung, Taiwan large-scale seismic test. Structural Safety, 10: 145-162.

Abrahamson N, Schneider JF, Stepp JC (1991a) Empirical Spatial Coherency Functions for Application to Soil-Structure Interaction Analyses. Earthquake Spectra, 7(1): 1-27.

Afif Chaouch K, Tiliouine B, Hammoutene M (2003) Simulation stochastique d'accelerogrammes à partir d'un model sismologique de source, Colloque International: Risque, Vulnérabilité et Fiabilité dans la Construction, 11 et 12 Octobre, Alger.

Afif Chaouch K, Tiliouine B, Hammoutene M (2013) Estimation of coherency functions of spatially variable seismic ground motions in the El-Asnam region (N.W. Algeria), SE-50EEE 1963-2013 International Conference on Earthquake Engineering, Skopje, 29-31 May.

Afif Chaouch K, Tiliouine B, Hammoutene M (2014) Effects of layered stochastic soil profile on the coherency functions of spatially variable seismic ground motions: case study of the El-Asnam region (NW Algeria). Proceedings of the 8th European Conference on Numerical Methods in Geotechnical Engineering: Probabilistic methods and neural networks, Netherland, 2: 441-446.

Afif Chaouch K, Rupakhety R, Tiliouine B, Hammoutene M, Sigbjörnsson R (2016) Estimating ground motion incoherence through finite source simulation: a case study of the 1980 El-Asnam Earthquake. Bulletin of Earthquake Engineering, 14: 1195-1217.

Afif Chaouch K, Rupakhety R, Ólafsson S, Tiliouine B, Hammoutene M (2017) The october 1980 El-Asnam earthquake in N.W. Algeria: modelling incoherence of ground motion. Proceedings of the 16th World Conference on Earthquake Engineering, Santiago, Chile.

Afif Chaouch K, Rupakhety R, Ólafsson S, Tiliouine B, Hammoutene M (2017) Effects of stochastic soil layers on ground-motion incoherence: a case study in N.W. Algeria. Proceedings of the 16th World Conference on Earthquake Engineering, Santiago, Chile.

Aki K, Richards PG (2002) Quantitative seismology, Second Edition, University Science Books, Sausalito, CA.

Ancheta TD, Stewart JP (2015) Conditional simulation of spatially variable motions on 2D grid. 12th International Conference on Applications of Statistics and Probability in Civil Engineering, ICASP12 Vancouver, Canada, July 12-15.

Bi K, Hao H (2011) Influences of irregular topography and random soil properties on coherency loss of spatial seismic ground motions. Earthquake Engineering and Structural Dynamics, 40(9): 1045-1061.

Bielak J, Ghattas O, Kim EJ (2005) Parallel octree-based finite element method for large-scale earthquake ground motion simulation. Computer Modeling in Engineering and Science, 10: 99-112.

Bodin P, Gomberg J, Singh SK, Santoyo M (1997) Dynamic deformations of shallow sediments in the valley of Mexico. Part I: Three dimensional strains and rotations recorded on a seismic array. Bulletin of the Seismological Society of America, 87: 528-539.

Bolt BA, Herraiz M (1983) Simplified estimation of seismic moment from seismograms. Bulletin of the Seismological Society of America, 73: 735-748.

Boore DM (1983) Stochastic simulation of high-frequency ground motions based on seismological models of the radiated spectra. Bulletin of the Seismological Society of America. 73: 1865-1894.

Boore DM (2003) Simulation of ground motion using the stochastic method. Pure and Applied Geophysics, 160: 635-676.

Chapellier D, Mari JL (2011) Cours de géophysique, Université de Lausanne. Institut français du pétrole.

Cisternas A, Dorel J, Gaulon R (1982) Models of the complex source of the El-Asnam earthquake. Bulletin of the Seismological Society of America, 72: 2245-226.

Cranswick E (1988) The information content of high-frequency seismograms and the near surface geologic structure of hard rock recording sites. Pure and Applied Geophysics, 128: 333-363.

Dechamps A, Gaudemer Y (1981) Etude d'ondes telesismiques longues périodes. Journées Scientifiques d'Alger sur le séisme d'El-Asnam du 10 octobre 1980, 15 et 16 Juin, 132-138.

Dechamps A, Gaudemer Y, Cisternas A (1982) The El-Asnam, Algeria, earthquake of 10 october 1980: multiple-source mechanism determined from long-period records. Bulletin of the Seismological Society of America, 72: 1111-1128.

Deodatis G (1996) Non-stationary stochastic vector processes: seismic ground motion applications. Probabilistic Engineering Mechanics, 11(3): 149-67.

Der Kiureghian A (1996) A coherency model for spatially varying ground motions. Earthquake Engineering and Structural Dynamics, 25: 99-111.

Despeypoux (1984) Some lessons to be drawn from the El-Asnam earthquake of 10 october 1980. Proceedings of the 8th World Conference on Earthquake Engineering, San Francisco, California, USA.

Ding H, Song Z (2010) Effects of source parameters on coherency function of ground motion. Journal of Vibration and Shock, 29 (7): 16-18.

Gao Y, Wu Y, Li D, Liu H, Zhang N (2012) An improved approximation for the spectral representation method in the simulation of spatially varying ground motions. Probabilistic Engineering Mechanics, 29: 7-15.

Geller RJ (1976) Scaling relations for earthquake source parameters and magnitudes. Bulletin of the Seismological Society of America, 66: 1521-1523.

Graves RW, Pitarka A (2010) Broadband ground-motion simulation using a hybrid approach. Bulletin of the Seismological Society of America, 100: 2095-2123.

Hammoutene M, Tiliouine B, Bard PY (1992) A two dimensional nonstationary optimized accelerogram scaled for magnitude, distance and soil conditions. Proceedings of the 10th World Conference on Earthquake Engineering, Madrid, Spain.

Hao H (1993) Input seismic motions for use in the seismic structural response analysis. Proceedings of the 6th International Conference on Soil Dynamics and Earthquake Engineering, 6: 87-100.

Hao H, Oliveira CS, Penzien J (1989) Multiple-station ground motion progressing and simulation based on SMART-1 array data. Nuclear Engineering and Design, 111: 293-310.

Harada T, Shinozuka M (1986) Ground deformation spectra. Proceedings of the 3rd US-National Conference on Earthquake Engineering, Charleston, SC.

Harichandran RS (1991) Estimating the spatial variation of earthquake ground motion from dense array recordings. Structural Safety, 10: 219-233.

Harichandran RS, Vanmarcke E (1986) Stochastic variation of earthquake ground motion in space and time. Journal of Engineering Mechanics, ASCE, 112(2): 914-925.

Hartzell SH (1978) Earthquake aftershocks as Green functions. Geophysical Research Letters, 5: 1-4.

Hindy A, Novak M (1980) Pipeline response to random ground motion. Journal of Engineering Mechanics, ASCE, 106 (2): 339-360.

Idriss IM, Sun and Joseph I (1992) SHAKE91: A computer program for conducting equivalent linear seismic response analyses of horizontally layered soil deposits, Center for Geotechnical Modeling, Department of Civil and Environmental Engineering, University of California, Davis, California.

Irikura K (1983) Semi empirical estimation of strong ground motions during large earthquakes. Bulletin of Disaster Prevention Research Institute, Kyoto University, Japan, 33: 63-104.

Irikura K (1986) Prediction of strong acceleration motions using empirical Green's function. Proceedings of the 7th Japan Earthquake Engineering Symposium, 7: 151-156.

Irikura K, Kagawa T, Sekiguchi H (1997) Revision of the empirical Green's function method by Irikura (1986), Programme and Abstracts. The Seismological Society of Japan, 2: B25.

Jenkins GW, Watts DG (1969) Spectral Analysis and its Applications. Holden Day, San Francisco, CA.

Jennings PC, Housner GW, Tsai NC (1968) Simulated earthquake motions. Technical Report, Earthquake Engineering Research Laboratory, California Institute of Technology, Pasadena, CA.

Jin X, Chen C, Zhang Mi-yu (2000) Far-field analysis of effects of unilateral rupturing fault on the space correlation of strong ground motion. Acta Seismologica Sinica, 13(5): 544-551.

Joshi A, Midorikawa S (2004) A simplified method for simulation of strong ground motion using finite rupture model of the earthquake source. Journal of Seismology, 8: 467-484.

Joshi A, Mohan K (2008) Simulation of accelerograms from simplified deterministic approach for the 23rd October 2004 Niigata-ken Chuetsu, Japan earthquake. Journal of Seismology, 12: 35-51.

Karmakar D, Ray-Chaudhuri S, Shinozuka M (2012) Seismic response evaluation of retrofitted Vincent Thomas bridge under spatially variable ground motions. Soil Dynamics and Earthquake Engineering, 42: 119-127

Kamae K, Irikura K, Pitarka A (1998a) A technique for simulating strong ground motion using hybrid Green's function. Bulletin of the Seismological Society of America, 88: 357-367.

Kamae K, Bard PY, Irikura K (1998b) Prediction of strong ground motion at EURO-SEISTEST site using the empirical Green's function method. Journal of Seismology, 2: 193-207.

Kanai K (1957) Semi empirical formula for the seismic characteristics of the ground. Bulletin of the Earthquake Research Institute, University of Tokyo, Japan, 35: 309-325.

Kanamori H, Anderson DL (1975) Theoretical basis of some empirical relations in seismology. Bulletin of the Seismological Society of America, 65: 1073-1095.

Kanasewich ER (1981) Time Sequence Analysis in Geophysics, University of Alberta Press, Edmonton, Alberta.

Liao S, Li J (2002) A stochastic approach to site-response component in seismic ground motion coherency model, Soil Dynamics and Earthquake Engineering, 22: 813-820.

Liao S, Zerva A, Stephenson WR (2007) Seismic spatial coherency at a site with irregular subsurface topography. Proceedings of Sessions of Geo-Denver, Geotechnical Special Publication, No. 170: 1-10.

Luco JE, Wong HL (1986) Response of a rigid foundation to a spatially random ground motion. Earthquake Engineering and Structural Dynamics, 14: 891-908.

Lupoi A, Franchin P, Pinto PE, Monti G (2005) Seismic design of bridges accounting for spatial variability of ground motion. Earthquake Engineering and Structural Dynamics, 34: 327-348.

Martinellia L, Domaneschia M, Shib C (2016) Submerged Floating Tunnels under Seismic Motion: Vibration Mitigation and Seaquake effects. Procedia Engineering 166: 229 - 246.

Mazzieri I, Stupazzini M, Guidotti R, Smerzini C (2013) SPEED: Spectral Elements in Elastodynamics with Discontinuous Galerkin: a con-conforming approach for 3D multi-scale problems. International Journal of Numerical Methods in Engineering, 95(12): 991—1010.

Menke W, Lerner Lam AL, Dubendorff B, Pacheco J (1990) Polarization and coherence of 5 to 30 Hz seismic wave fields at a hard rock site and their relevance to velocity heterogeneities in the crust. Bulletin of the Seismological Society of America, 80: 430-449.

Motazedian D, Khaheshi Banab K, Hunter JA, Sivathayalan S, Crow H, Brooks G (2011) Comparison of Site Periods Derived from Different Evaluation Methods. Bulletin of the Seismological Society of America, 101(6): 2942-2954

National Research Council of Canada -NRCC- (2010). National Building Code of Canada 2010, Ottawa, Canada.

Newland DE (1984) An introduction to random vibrations and spectral analysis, 2nd edition, Longman, London.

Newmark NM & Rosenblueth E (1971) Fundamentals of Earthquake Engineering, Prentice Hall, Englewood Cliffs, NJ.

Novak M, Hindy A (1979) Seismic response of buried pipelines, Proceedings of the 3rd Canadian Conference on Earthquake Engineering, Montreal, Canada, Jun, 1: 177-203.

Okamoto S (1984) Introduction to Earthquake Engineering, Tokyo: University of Tokyo Press.

O'Rourke MJ, Bloom MC, Dobry R (1982) Apparent propagation velocity of body waves. Earthquake Engineering and Structural Dynamics, 10: 283-294.

O'Rourke MJ, Castro G & Centola N (1980) Effects of seismic wave propagation upon buried pipelines. Earthquake Engineering and Structural Dynamics, 8, 455-467.

O'Rourke MJ, Castro G, Hossain I (1984) Horizontal soil strain due to seismic waves. Journal of the Engineering Mechanics Division, ASCE, 110: 1173-1187.

Petrovski J, Milutinovic Z (1981) Deconvolution analysis of surface accelerogram records in El-Asnam region. Actes des journées scientifiques sur le séisme d'El-Asnam du 10.10.80, Alger, 15-16 Juin, 373-401.

Pitarka A (1999) 3D elastic finite-difference modelling of seismic motion using staggered grids with nonuniform spacing. Bulletin of the Seismological Society of America, 89: 54-68.

Roumelioti Z, Kiratzi A, Thcodulidis N, Papaioannou C (2000) A comparative study of a stochastic and deterministic simulation of strong ground motion applied to the Kozani-Grevena (NW Greece) 1995 sequence. Annals of Geophysics, 43(5): 951-966.

Rupakhety R, Sigbjörnsson R (2012) Spatial variability of strong ground motion: novel system-based technique applying parametric time series modelling. Bulletin of Earthquake Engineering, 10: 1193-1204.

Rupakhety R, Halldorsson B, Sigbjörnsson R (2010) Estimating coseismic deformations from near source strong motion records: methods and case studies. Bulletin of Earthquake Engineering, 8(4): 787-811.

Rupakhety R, Sigbjörnsson R (2014) Rotation-invariant formulation of strong ground-motion parameters. Proceedings of the 2nd European Conference on Earthquake Engineering and Seismology, Istanbul, Aug 25-29.

Schneider JF, Abrahamson NA, Stepp JC (1992) The spatial variability of earthquake ground motion and effects of local site conditions. Proceedings of the 10th World Conference on Earthquake Engineering, Madrid, Spain.

Shrestha B, Hao H, Bi K (2014) Effectiveness of using rubber bumper and restrainer on mitigating pounding and unseating damage of bridge structures subjected to spatially varying ground motions. Engineering Structures, 79:195-210.

Smerzini C, Villani M (2012) Broadband numerical simulations in complex near field geological configurations: the case study of the Mw 6.3 2009 L'Aquila earthquake. Bulletin of the Seismological Society of America, 102: 2436-2451.

Somerville PG, McLaren JP, Saikia CK, Helmberger DV (1988) Site-specific estimation of spatial incoherence of strong ground motion. Proceedings of Earthquake Engineering and Soil Dynamics II Conf., ASCE, Geotechnical Special Publication, 20: 188-202.

Somerville PG, Mclaren JP, Sen MK, Helmberger DV (1991) The influence of site condition on the spatial incoherence of ground motions. Structural Safety, 10: 1-13.

Soyluk K, Sicacik EA (2012) Soil–structure interaction analysis of cable-stayed bridges for spatially varying ground motion components. Soil Dynamics and Earthquake Engineering, 35 : 80-90.

Spudich P (1994) Recent seismological insights into the spatial variation of earthquake ground motions. in New Developments in Earthquake Ground Motion Estimation and Implications for Engineering Design Practice, ATC 35-1, Redwood City, CA.

Tajimi H (1960) A statistical method of determining the maximum response of a building structure during an earthquake. Proceedings of the 2nd World Conference on Earthquake Engineering, Tokyo and Kyoto, Japan.

Tiliouine B, Zermout S (2003) Génération de spectre de puissance pour l'analyse stochastique de la réponse sismique des structures. AFPS. 6ème Colloque AFPS , Jul 2003, Palaiseau, France, 1-8.

Walling M, Abrahamson N (2007) Spatial coherency of ground motions for embedded structures. 4th International Conference on Earthquake Geotechnical Engineering, Thessaloniki, Greece.

Wang S, Hao H (2002) Effects of random vibrations of soil properties on site amplification of seismic ground motions. Soil Dynamics and Earthquake Engineering, 22(7): 551-64.

Wolf JP (1985) Dynamic soil–structure interaction. Englewood Cliffs (NJ): Prentice Hall.

Yielding G, Jackson JA, King GCP, Sinvhal H, Vita-Finzi C, Wood RM (1981) Relations between surface deformation, fault geometry, seismicity, and rupture characteristics during the E1-Asnam (Algeria) earthquake of 10 October 1980. Earth and Planetary Science Letters, 56: 287-304.

Zerva A (1994) On the spatial variation of seismic ground motions and its effects on lifelines. Engineering Structures, 16(7)**:** 534-546.

Zerva A (2009) Spatial Variation of Seismic Ground Motions. Modeling and Engineering Applications. CRC Press, Taylor&Francis Group, 978-0-8493-9929-9.

Zerva A, Harada T (1997) Effect of surface layer stochasticity on seismic ground motion coherence and strain estimates. Soil Dynamics and Earthquake Engineering, 16**:** 445-457.

Zerva A, Shinozuka M (1991) Stochastic differential ground motion. Structural Safety, 10: 129-143.

Zerva A, Zervas V (2002) Spatial variation of seismic ground motions: An overview. Applied Mechanics Reviews, ASME, 55: 271-297.

Zhang D, Liu W, Xie WC, Pandey MD (2013) Modeling of spatially correlated, site-reflected, and nonstationary ground motions compatible with response spectrum. Soil Dynamics and Earthquake Engineering, 55: 21-32.

APPENDIX

Appendix:

Table A1 Input parameters for the application of the EGF method

Parameter	Simulation of the El-Asnam mainshock	
	Target Event	**Small Event**
M_s	7.3	5.6
M_0 (*dyne.cm*)	540×10^{24} from Dechamps and Gaudemer (1981)	1.55×10^{24} estimated from the Bolt and Herraiz (1983) equation: $\log M_0 = (17.92 \pm 1.02) + (1.11 \pm 0.15) M_L$ for $3 \le M_L \le 6.2$
Epicenter coordinates	36°17N 01°41E	36°14N 01°40E
Hypocentral depth (*km*)	12	12
Strike angle (°)	220	220
Dip angle (°)	60 calculted by Dechamps	60
Rake angle (°)	78 and Gaudemer (1981)	78
Fault length (*km*)	40	5.714 from scaling relations :
Fault width (*km*)	15	2.142 Eq. (4.4)
Rise time τ (*sec*)	1.4	0.2
Coordinates of the reference station point $S^{(0)}$:		
Hypocentral distance $r_{i_0 j_0}$ (*km*)	12.96	
Radiation pattern $R_s(\theta_{i_0 j_0}, \varphi_{i_0 j_0})$	0.868	

Table A2 Geotechnical characteristics of generic rocks used in parametric study (Petrovski and Milutinovic, 1981; Yielding *et al*., 1981; Chapellier and Mari, 2011)

Rock type	Sogedia El-Asnam	Medium(a)	Hard(b)	Very Hard (c)
ρ (density)	2.4 gr/cm^3	2.2	2.5	2.8
Vs (S-wave velocity)	2000 m/s	1500	2500	3500
Vp (P-wave velocity)	3460 m/s	3100	4500	5300
Qs (Quality factor)	45	125	230	300

Table A3 Classes of magnitude and the field of distances (from Hammoutene *et al*., 1992).

Magnitude	d1 (Near-field)	d2 (Intermediate-field)	d3 (Far-field)
M < 4.5	≤10 Km	10-20 Km	≥20 Km
4.5 ≤ M < 5.5	≤15	15-30	≥30
5.5 ≤ M < 6.5	≤20	20-40	≥40
4.5 ≤ M < 7.5	≤25	25-50	≥50
M > 7.5	≤30	30-60	≥60